JPTM

Journal of Pathology and Translational Medicine

November 2020
Vol. 54 / No.6
jpatholtm.org
pISSN: 2383-7837
eISSN: 2383-7845

Recommendations for Pathologic Practice Using Digital Pathology

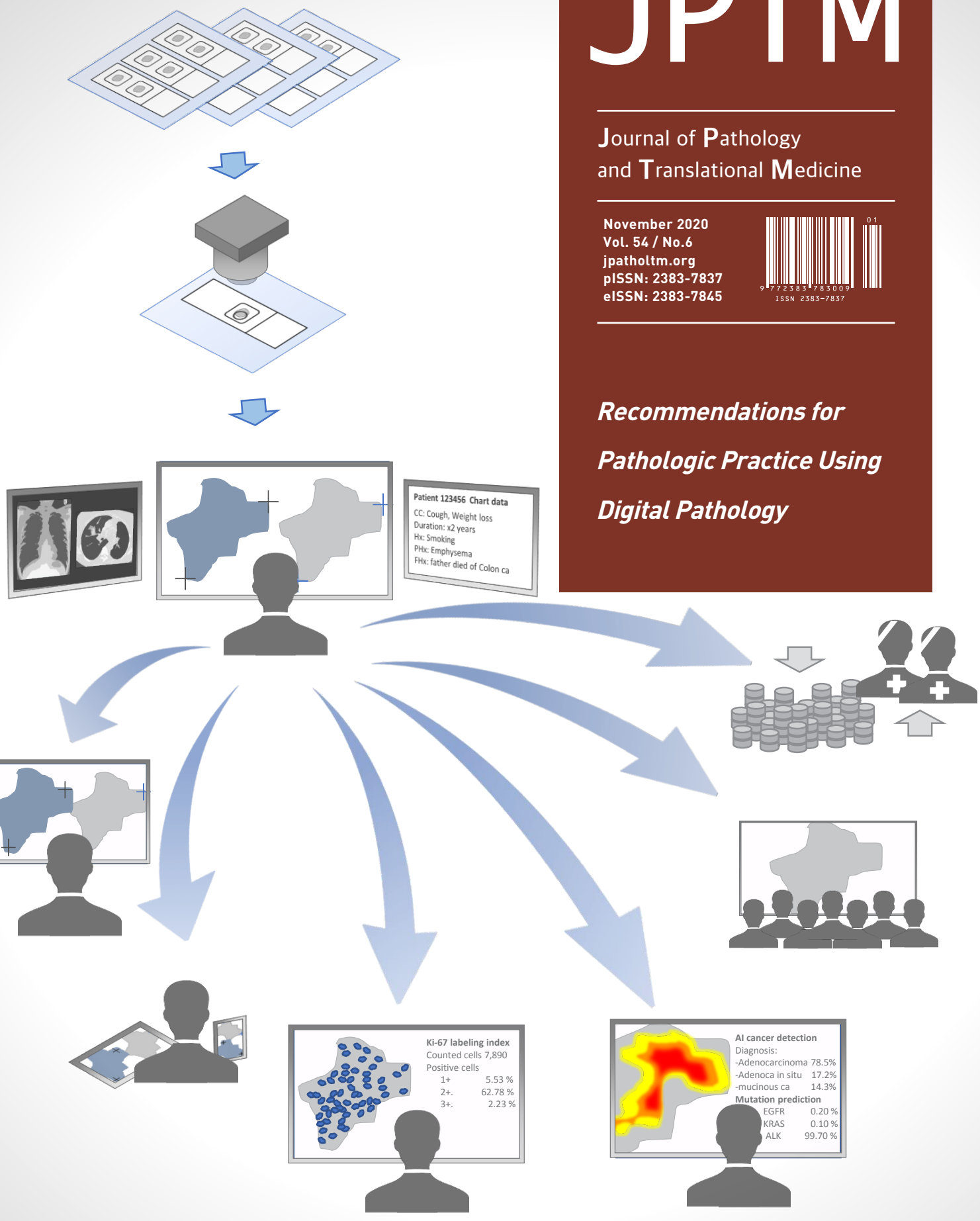

Journal of Pathology and Translational Medicine

Volume 54 • Number 6 • November 2020 (bimonthly)
Published since 1967
Printed on 11 November 2020 Published on 15 November 2020

J Pathol Transl Med
pISSN: 2383-7837
eISSN: 2383-7845

Aims & Scope

The Journal of Pathology and Translational Medicine is an open venue for the rapid publication of major achievements in various fields of pathology, cytopathology, and biomedical and translational research. The Journal aims to share new insights into the molecular and cellular mechanisms of human diseases and to report major advances in both experimental and clinical medicine, with a particular emphasis on translational research. The investigations of human cells and tissues using high-dimensional biology techniques such as genomics and proteomics will be given a high priority. Articles on stem cell biology are also welcome. The categories of manuscript include original articles, review and perspective articles, case studies, brief case reports, and letters to the editor.

Subscription Information

To subscribe to this journal, please contact the Korean Society of Pathologists/the Korean Society for Cytopathology. Full text PDF files are also available at the official website (http://jpatholtm.org). *Journal of Pathology and Translational Medicine* is indexed by Emerging Sources Citation Index (ESCI), PubMed, PubMed Central, Scopus, KoreaMed, KoMCI, WPRIM, Directory of Open Access Journals (DOAJ), and CrossRef. Circulation number per issue is 50.

Contact the Korean Society of Pathologists/the Korean Society for Cytopathology

Publishers: Choi, Chan, MD, Hong, Soon Won, MD
Editors-in-Chief: Jung, Chan Kwon, MD, Park, So Yeon, MD
Published by the Korean Society of Pathologists/the Korean Society for Cytopathology

Editorial Office
Room 1209 Gwanghwamun Officia, 92 Saemunan-ro, Jongno-gu, Seoul 03186, Korea
Tel: +82-2-795-3094 Fax: +82-2-790-6635 E-mail: office@jpatholtm.org

#1508 Renaissancetower, 14 Mallijae-ro, Mapo-gu, Seoul 04195, Korea
Tel: +82-2-593-6943 Fax: +82-2-593-6944 E-mail: office@jpatholtm.org

Printed by iMiS Company Co., Ltd. (JMC)
Jungang Bldg. 18-8 Wonhyo-ro 89-gil, Yongsan-gu, Seoul 04314, Korea
Tel: +82-2-717-5511 Fax: +82-2-717-5515 E-mail: ml@smileml.com

Manuscript Editing by InfoLumi Co.
210-202, 421 Pangyo-ro, Bundang-gu, Seongnam 13522, Korea
Tel: +82-70-8839-8800 E-mail: infolumi.chang@gmail.com

Front cover image: Pathologic practice using digital pathology (p437-452).

Journal of Pathology and Translational Medicine

J Pathol Transl Med
pISSN: 2383-7837
eISSN: 2383-7845

Volume 54, Number 6, November 2020

CONTENTS

REVIEWS

ORIGINAL ARTICLES

CONTENTS CONTINUED

CASE REPORTS

Instructions for Authors for *Journal of Pathology and Translational Medicine* are available at http://jpatholtm.org/authors/authors.php

JPTM
Journal of Pathology and Translational Medicine 2020; 54: 437-452
https://doi.org/10.4132/jptm.2020.08.27

REVIEW

Recommendations for pathologic practice using digital pathology: consensus report of the Korean Society of Pathologists

Yosep Chong[1], Dae Cheol Kim[2], Chan Kwon Jung[1], Dong-chul Kim[3], Sang Yong Song[4], Hee Jae Joo[5], Sang-Yeop Yi[6], Medical Informatics Study Group of the Korean Society of Pathologists

[1]Department of Hospital Pathology, College of Medicine, The Catholic University of Korea, Seoul;
[2]Department of Pathology, Dong-A University College of Medicine, Busan;
[3]Department of Pathology, Seoul Clinical Laboratories, Yongin;
[4]Department of Pathology, Samsung Medical Center, Sungkyunkwan University School of Medicine, Seoul;
[5]Department of Pathology, TCM Laboratory, Seongnam;
[6]Department of Pathology, Catholic Kwandong University College of Medicine, Gangneung, Korea

Digital pathology (DP) using whole slide imaging (WSI) is becoming a fundamental issue in pathology with recent advances and the rapid development of associated technologies. However, the available evidence on its diagnostic uses and practical advice for pathologists on implementing DP remains insufficient, particularly in light of the exponential growth of this industry. To inform DP implementation in Korea, we developed relevant and timely recommendations. We first performed a literature review of DP guidelines, recommendations, and position papers from major countries, as well as a review of relevant studies validating WSI. Based on that information, we prepared a draft. After several revisions, we released this draft to the public and the members of the Korean Society of Pathologists through our homepage and held an open forum for interested parties. Through that process, this final manuscript has been prepared. This recommendation contains an overview describing the background, objectives, scope of application, and basic terminology; guidelines and considerations for the hardware and software used in DP systems and the validation required for DP implementation; conclusions; and references and appendices, including literature on DP from major countries and WSI validation studies.

Key Words: Digital pathology; Guideline; Recommendations; Whole slide image; Quality; Validation

Received: July 14, 2020 **Accepted:** August 27, 2020
Corresponding Author: Sang-Yeop Yi, MD, PhD, Department of Pathology, Catholic Kwandong University College of Medicine, 25 Simgok-ro 100beon-gil, Seo-gu, Incheon 22711, Korea
Tel: +82-32-290-2972, Fax: +82-32-290-3440, E-mail: pathysy@naver.com

Digital pathology (DP) refers to the use of a digital scanner to convert and save pathologic slides as digital images and the use of those images for pathologic diagnosis [1,2]. DP includes various processes of pathologic diagnosis, including primary diagnosis based on whole slide imaging (WSI) that enables diagnosis through display devices such as monitors instead of a microscope; telepathology that allows opinions to be obtained and digital images to be shared with experts at different locations over a network connection; and computer-aided diagnosis based on quantitative and morphometric analyses made using image analysis software [1].

Because the implementation of DP is based on automatic sample tracking systems, it can prevent sample contamination and switching caused by human error and play an important role in patient safety [3,4]. Moreover, DP allows easier and faster consultation between experts, which could minimize problems such as overtreatment and loss of treatment opportunity due to differences in diagnosis [3-5]. Furthermore, the permanent storage of high-resolution digital images as data eliminates the risks of discoloration, damage, and loss of glass slides over time while also enabling efficient, accurate, and comprehensive reading by allowing pathologists to easily compare current results with past pathologic examinations [3,4]. In addition, the future development of digital image sharing systems among medical institutions could significantly reduce the healthcare costs associated with the production of additional slides and duplicate tests when a patient transfers to another hospital [3,4].

Recent advances in relevant technologies and equipment

pISSN 2383-7837
eISSN 2383-7845

have led many countries to implement DP systems for primary diagnosis using WSI. Based on the results of recent studies showing high concordance between primary WSI-based diagnosis and conventional pathologic diagnosis using a microscope [5,6], the United States, European Union, and Japan are already accepting the use of DP for medical practice in clinical settings, with the US Food and Drug Administration (FDA) approving the registration of WSI equipment as medical devices in 2017 [5,6]. Moreover, teleconsultation and telediagnosis using DP have been approved, with Japan creating charges associated with DP systems in its insurance system in 2018 [7].

However, because the associated technologies are still maturing, more data and experience are required to determine whether and to what extent primary diagnoses based on WSI can safely replace conventional pathologic diagnoses using a microscope.

Accordingly, the United States, Japan, and European countries, including the United Kingdom, Spain, and Germany, have released national-level guidelines for the safe implementation and quality assessment of DP to promote the active application of this technique (Table 1) [2,3,5-30]. Those guidelines suggest detailed principles to inform primary diagnosis based on WSI, teleconsultation, and telepathology; considerations regarding hardware, such as digital scanners, medical image archiving and communication systems, and image display systems; considerations for image acquisition, viewing, archiving, and analysis software; strategies for connection to laboratory information systems; and basic principles for the validation and quality assessment of DP systems.

As of 2019, several university hospitals, including the Catholic University of Korea Seoul St. Mary's Hospital, Seoul National University Hospital, and Samsung Medical Center, have introduced DP systems and started making primary diagnoses based on WSI, although it has not yet fully replaced conventional microscopic diagnoses [3].

To keep pace with these domestic and international trends, the Korean Society of Pathologists (KSP) launched a research project in June 2019 by which the members of the Medical Informatics Study Group (MISG) were asked to develop a recommendation for pathologic practices using DP. Accordingly, the MISG spent 5 months conducting a literature search and comprehensive review, proposing recommendation principles, and establishing a draft recommendation through 4 rounds of discussion and solicitation of expert opinions. On November 20, 2019, the MISG held an open public forum to hear from relevant corporations, stakeholders, and regulatory authorities and then revised the draft recommendations accordingly.

This recommendation was prepared based on DP guidelines released by the U.S. Digital Pathology Association [29], College of American Pathologists (CAP) [30], U.K. British Royal College of Pathologists (RCP) [6], Canadian Association of Pathologists [11], Royal College of Pathologists of Australia [25], Federal Association of German Pathologists (FAGP) [10], Japanese Society of Pathology (JSP) [5,7,26], and Spanish Society of Anatomic Pathology [9] and the final report of the "Preparation of Reimbursement Assessment Guidelines for AI-based Medical Technology (Pathology)" research project funded by the Health Insurance Review and Assessment Service and carried out and published by the KSP Committee of Informatics in August 2019 [3].

The goal for this recommendation is to include only the most critical and fundamental principles suitable for the current situation and environment in Korea based on the opinions of the experts in the MISG and various stakeholders. DP will be broadly applied only after rationalization of the implementation costs, additional technical advances, the establishment of an adequate reimbursement policy within the domestic health insurance system, and the resolution of technical issues in clinical practice. Accordingly, it will be necessary to regularly update this recommendation to promptly integrate relevant knowledge and additional considerations as they evolve along with the DP environment.

The Korean version of this report is also provided separately as Supplementary Material 1.

MATERIALS AND METHODS

This study was approved by the Institutional Review Board of the Catholic University of Korea, College of Medicine (SC19ZCSI0173). We searched major electronic databases from January 1, 2000, to May 31, 2019, for relevant literature on DP guidelines, recommendations, and position papers published or officially announced from major countries. In addition, all the relevant studies validating DP and WSI, including original articles and reviews, were searched. The searched databases included MEDLINE (PubMed) and Google Scholar. After reviewing the relevant articles, more references were added by cross-referencing (Tables 1, 2) [2,3,5-51]. We next selected a dozen references, mostly recent versions of DP guidelines and recommendations from the major countries and recent reviews of DP and WSI, to extract relevant opinions applicable to the current Korean environment. Synthesizing them, we prepared a draft of this recommendation and revised it through 4 rounds of discussion among

 https://doi.org/10.4132/jptm.2020.08.27

Table 1. Digital pathology guidelines, position papers, and relevant instructions in leading countries

Country	Guideline and instruction
Canada	Canadian Association of Pathologists (CAP-ACP)
	2014: Guidelines from the Canadian Association of Pathologists for establishing a telepathology service for anatomic pathology using whole-slide imaging [11]
United States	College of American Pathologists (CAP)
	2013: Validating whole-slide imaging for diagnostic purposes in pathology [30]
	2011: Anatomic pathology checklist: CAP accreditation program [12]
	American Telemedicine Association (ATA)
	2014: Clinical guidelines for telepathology [13]
	Digital Pathology Association (DPA)
	2019: Computational pathology definitions, best practices, and recommendations for regulatory guidance: a white paper from the Digital Pathology Association [29]
	2011: Validation of digital pathology in a healthcare environment [14]
	2011: Archival and retrieval in digital pathology systems [15]
	2011: Interoperability between anatomic pathology laboratory information systems and digital pathology systems [16]
	2011: Validation of digital pathology systems in the regulated nonclinical environment [17]
	Food and Drug Administration (FDA)
	2015: Technical performance assessment of digital pathology whole-slide imaging devices: draft guidance for industry and Food and Drug Administration staff [18]
	Centers for Medicare & Medicaid Services (CMS)
	2015: Clinical Laboratory Improvement Amendments (CLIA) [19]
	Centers for Disease Control and Prevention (CDC)
	2013: Clinical Laboratory Improvement Advisory Committee (CLIAC) [20]
	Society of Toxicologic Pathology
	2013: Validation of digital pathology systems in the regulated nonclinical environment [17]
	2007: Pathology position paper on pathology image data [22]
European Union	European Commission (EC)
	2012: Guidelines on the qualification and classification of stand alone software used in healthcare within the regulatory framework of medical devices [23]
Spain	Spanish Society of Anatomic Pathology (SEAP-IAP)
	2015: Practical guidelines for digital pathology implementation [9]
United Kingdom	The Royal College of Pathologists (RCP)
	2018: Best practice recommendations for implementing digital pathology [6]
	2013: Telepathology: guidance from The Royal College of Pathologists [24]
Germany	Federal Association of German Pathologist (FAGP-BDP)
	2018: Guidelines digital pathology for diagnosis on (and reports of) digital image [10]
Australia	The Royal College of Pathologists of Australasia (RCPA)
	2014: Position statement: telepathology [25]
Japan	Japanese Society of Pathology (JSP)
	2019: Guidelines for pathologic diagnosis using digital pathology image (clinical questions and answers) [5]
	2018: Technical standards for digital pathology system for pathologic diagnosis ver. 3 [7]
	2016: Guidelines for pathologic diagnosis using digital pathology image [26]
	2016: Technical standards for digital pathology system for pathologic diagnosis ver. 2 [26]
	2015: Technical standards for digital pathology system for pathologic diagnosis ver. 1 [28]
Korea	Korean Society of Pathologists (KSP)
	2019: Preparation of reimbursement assessment guidelines for AI-based medical technology (pathology) [3]

experts. On November 20, 2019, the MISG of the KSP held an open forum to present the draft to the public and hear from interested parties, including companies, industry and academic associates, and stakeholders. The draft recommendation was also released on the KSP webpage, and opinions and suggestions from KSP members were accepted and considered. After this hearing, relevant revisions were made based on the submitted opinions.

Objectives

This recommendation suggests that the following objectives should be recognized and considered when implementing and operating DP systems in pathology labs.

1) To define the standard terminology generally used for DP.

2) To regulate the scope and boundaries of DP application and suggest its evidentiary foundation.

3) To present institutional-level considerations regarding the hardware and software needed to implement DP systems.

4) To provide relevant guidelines and considerations for the validation and in-house quality control (QC) of DP systems during implementation and operation.

That information is expected to provide background knowledge about DP and serve as a reference for preparing checklists

Table 2. List of whole-slide imaging validation studies

Year	Author	Journal	No. of samples /observers	Results	Evidence level	Reference No.
2006	Gilbertson et al.	BMC Clin Pathol	25 Mixed/3	32% Discordancy	IV	[31]
2011	Jukic et al.	Arch Pathol Lab Med	101 Mixed/3	3%–7% discordancy	III	[32]
2012	Al-Janabi et al.	J Clin Pathol	100 Breast	Kappa = 0.92	IV	[33]
2012	Al-Janabi et al.	Hum Pathol	100 GI	5% Discordancy (minor)	IV	[34]
2012	Al-Janabi et al.	J Clin Pathol	100 Skin	6% Discordancy (minor)	IV	[35]
2013	Al-Janabi et al.	J Clin Pathol	100 Pediatric	WSI: 10% discordancy Glass: 7% discordancy	IV	[36]
2013	Bauer et al.	Arch Pathol Lab Med	607 Mixed	WSI: 1.65% discordancy Glass: 0.99% discordancy	III	[37]
2013	Krishnamurthy et al.	Arch Pathol Lab Med	100 Breast	WSI: 9.5% discordancy Glass: 7.9% discordancy	III	[38]
2013	Pantanowitz et al.	Arch Pathol Lab Med	Meta-analysis of 27 papers	-	III	[30]
2014	Al-Janabi et al.	J Renal Inj Prev	100 GU	13% Discordancy	III	[39]
2014	Buck et al.	J Pathol Inform	150 Mixed/6	WSI: 2.1%–10.1% discordancy Glass: 3.3%–13.3% discordancy	III	[40]
2014	Reyes et al.	J Pathol Inform	103 Breast /3	WSI: 1%–4% discordancy Glass: 0%–7% discordancy	III	[41]
2015	Ordi et al.	J Clin Pathol	452 GYN/2	5.8% Discordancy	III	[42]
2016	Pekmezci et al.	J Pathol Inform	97 neuro/2	5.1%–12% Discordancy	III	[43]
2016	Snead et al.	Histopathology	3,017/17 (2,666 biopsy, 340 surgery, 11 frozen, 10 organs)	1.3% Discordancy	III	[44]
2016	Wack et al.	J Pathol Inform	33 Mixed/16	WSI: 20.9% discordancy Glass: 23.5% discordancy	III	[45]
2017	Kent et al.	JAMA Dermatol	499 Skin/3	WSI: 6% discordancy Glass: 6% discordancy	III	[46]
2017	Saco et al.	Dig Liver Dis	176 Liver/2	3.4%–9.7% discordancy	III	[47]
2017	Tabata et al.	Pathol Int	1,070 Mixed/9	4.4% discordancy	III	[48]
2018	Araujo et al.	Virchow Arch	70 Oral/2	3% Discordancy	III	[49]
2018	Lee et al.	Am J Dermatopathol	77 Skin/2	0.3% Discordancy	III	[50]
2018	Mukhopadhyay et al.	Am J Surg Pathol	1,992 Mixed/16	WSI: 4.9% discordancy Glass: 4.6% discordancy	III	[51]

Evidence level in the table is as follows.
I, Systematic review or meta-analysis; II, At least one randomized controlled study; III, Non-randomized clinical trial (NRCT); IV, Analytic epidemiological study (cohort or case-controlled study); V, Descriptive study (case report or case series); VI, Expert opinion.
GI, gastrointestinal; WSI, whole slide imaging; GU, genitourinary; GYN, gynecopathology.

for the Quality Control Program of the KSP (The Red Book), the external QC program (proficiency tests), and resident training programs regarding DP. Furthermore, this recommendation also provides basic information toward establishing an appropriate reimbursement system, including incorporation into the coverage of the National Health Insurance System.

Scope of application

This recommendation includes guidelines and considerations for the implementation and operation of the hardware, systems, and software listed below, which can be used in DP systems for WSI-based diagnosis.

1) Whole slide scanner (WSS) used to generate and acquire digital images from glass slides and image acquisition software used to operate this scanner.

2) Pathology picture archiving and communication system (PACS) and image storage systems for saving, archiving, managing, and preserving the digital images acquired by image input devices.

3) Image viewing software that allows the observation of DP images through image display devices and records measurements or annotations.

4) Image display devices used for image observation (monitors and displays).

5) Network or data sharing systems used for transmitting images.

This recommendation does not cover the acquisition, transmission, observation, and annotation of microscopic images acquired with digital cameras set up on microscopes, smartphones, or tablets (digitizer pen tablets).

https://doi.org/10.4132/jptm.2020.08.27

In terms of staining methods and sample types applicable to WSI-based diagnosis using DP systems, most basic tissue slides stained with hematoxylin and eosin (H&E), most special stains, immunohistochemical stains, and frozen section slides are expected to be applicable, though they will require appropriate validation studies followed by trial periods until the users reach a stable learning level [30]. However, for the few special cases listed below, a higher level of validation and longer period of trial operation are recommended.

1) Cytology slides: In most cases with cell smears, liquid-based cytology, or blood smears, the results are similar to those from microscopic diagnoses made using glass slides with appropriate focus stacking (Z-stacking) during scanning and sufficient validation [52]. However, the optimal focus stacking method must be carefully selected for certain sample types (e.g., samples with many 3-dimensional structures, such as thyroid gland fine-needle aspirates [53]), staining conditions, and smear conditions. Excessive focus stacking and the acquisition of higher-magnification images (60× 100× or higher) could lead to over-scaling of the WSI files, which could negatively affect the operation of the entire system [6]. Therefore, the determination of optimal scanning conditions during the implementation of DP for cytology slides is essential and should be based on a balance between desirable scan quality and file size. Partial image acquisition of the slides is not recommended because it can severely impair diagnostic integrity and accuracy. In conclusion, importing cytology slides into a DP system requires a more extensive validation and trial operation period than is needed for other types of slides, including simultaneous comparison periods of diagnostic results using both WSI- and microscope-based diagnosis.

2) Samples clinically or morphologically suspected of lymphoreticular neoplasms: Lymphoreticular neoplasms have similar morphology at low magnification and similar nuclear features, such as chromatin patterns and nucleoli features, that are important for histologic diagnosis [5,37,48,54]. Accordingly, the acquisition of high-magnification images is generally recommended. Although evidence is lacking about diagnostic agreement at different scanning magnifications, results to date have shown less than 1% of major discordance between WSI-based and microscopic diagnoses using a basic 20× scan [54]. Moreover, the recorded 6.25% of minor discordance was mostly due to differences in grading follicular lymphoma and was similar to the inter- and intra-observer diagnostic discordance in microscopic diagnosis [54]. Because pathologic diagnosis of lymphoreticular neoplasms is almost always made in combination with the results of additional tests, such as immunohistochemical staining, diagnostic differences in the findings of H&E slide images alone do not seem to significantly affect diagnostic accuracy. On the other hand, the image comparison function available in the image viewing software of DP systems might offer the benefit of improved accuracy in the interpretation of immunohistochemical staining. Carefully designed validation studies and trial operations based on those considerations are needed.

3) Detection of microorganisms such as *Helicobacter pylori*: The detection of *H. pylori* infections through the microscopic examination of gastric biopsy tissue samples, especially when special staining such as the Giemsa stain is used, showed specificity and sensitivity comparable to that in other *H. pylori* tests [5]. However, concerns remain about whether microorganisms such as *H. pylori* can be detected successfully in the 40×-scanned WSI most commonly used today [5,44,55]. A recent study demonstrated that increasing the number of focus stacking layers provided results similar to those obtained via microscopic examination [56]. Without focus stacking, WSI-based detection showed an impaired sensitivity of 0.562 and specificity of 0.818 [57]. Therefore, when detecting microorganisms, special care is required, such as using appropriate focus stacking for assessment and mentioning the limitations of such examination results in the report.

Basic terminology

– Digital pathology (DP): Dynamic imaging environment (or academic field related to this environment) that involves the acquisition and management of pathologic information by converting microscopic glass slides into digital files and the pathologic diagnosis and interpretation of those images by means of an image display device. The scope of application includes education, research, image analysis, archiving, retrieval, connection to laboratory information systems, consultations among specialists, and image sharing.

– Digital pathology system (DPS): Image data–based computer system that enables the collection, management, and interpretation of pathologic information by digitalizing glass slides. It includes a scanner that contains an optical microscope and digital camera connected to a computer, software, and a network connection.

– Digital image analysis: Analytical method for quantifying or detecting the unique features of enhanced or processed digital images using a computer, such as chromosomal and morphometric analyses of fluorescence in situ hybridization or immunohistochemical staining images.

– Computer-aided diagnosis: Computerized assistance in the

interpretation of medical images, such as providing differential diagnoses or detecting lesions by means of a digital image analysis.

– Telepathology: Digital or real-time pathologic image communication environment using wired or wireless networks or a related academic field. Telepathology could be used widely for consultation with specialists in other areas or the diagnosis of samples in a remote facility [11]. Generally two methods are available: the conventional method uses a remote-controlled microscope for the real-time transmission of glass slide images, and the DP method transmits WSIs over a wired or wireless network [11].

– Whole slide image/imaging (WSI): A single high-resolution glass slide image file or associated technology that has been scanned and converted from a single glass slide using a whole slide scanner. With this high-resolution copy or mirrored image of a glass slide with equivalent quality, image viewing software can create a virtual environment for pathologic diagnosis that mimics the conventional pathology environment of microscopic diagnosis. WSIs are also referred to as virtual slides or virtual microscopy.

– Image input device: The initial processing device for converting actual images, including glass slides, into electronic signals and recording them as digital data.

– Whole slide scanner (WSS): Device used to scan glass slides and digitally convert them to WSIs. A WSS is generally run by image acquisition (operating) software, and a WSI is generated by combining multiple small, continuously acquired, high-resolution image tiles or strips at various magnifications, such as 20×, 40×, 60×, or 100× (corresponding to 200, 400, 600, or 1,000 times magnification under a general light microscope). The digital image data can be saved using a variety of compression methods.

– Focus stacking (Z-stacking): Image processing techniques combine digital images acquired at varying focus levels to obtain a much greater depth of field than that in the individual original images. When obtaining images of samples with many 3-dimensional microstructures and cell clusters, such as cytology slides, it is difficult to obtain the appropriate depth of field with a single focus. Thus, multiple images at slightly different levels of the Z-axis are combined using various image processing methods to convert them into a single image file.

– Image acquisition software: Computer software that operates and controls the WSS device to allow images to be acquired and saved using the appropriate format, compression rate, and compression method.

– Image viewing software: Computer software that makes acquired image data viewable through an image display device such as a monitor. This software can also provide observation functions to compare two or more images, pan the image laterally, or zoom in and out of areas of interest, along with other functions such as making basic length and area measurements, saving screenshots in compatible image file formats, and recording user annotations during review.

– Image database system: Computer system and software used for the compression, management, and mass storage of acquired image data.

– Picture archiving and communication system (PACS): A system that archives, processes, and transmits digital medical images in accordance with the international standard Digital Imaging and Communications in Medicine (DICOM) format. A PACS comprises image viewing and archiving software, a mass storage device, and a computer hardware system. Its typical functions include data archiving and transfer, including text data such as interpretation reports and data acquired by medical imaging devices (computed tomography, magnetic resonance imaging, etc.). Systems based on a similar concept include a pathology PACS that manages pathologic images.

– Laboratory information management system (LIMS): Also referred to as a laboratory information system (LIS), this software-based system is designed to manage information related to the overall operation of a laboratory.

– Electronic medical record (EMR): An EMR contains a patient's digital medical information, all the data obtained during diagnosis and treatment. The EMR and order communication system constitute a hospital information system (HIS), which is vital in the digitalization of medicine.

– Quality assurance (QA): Activities performed by a QC manager to ensure that certain material, data, products, or services (in this recommendation draft, QA refers to examination services inside a laboratory) have functions or results that comply with or satisfy established technical requirements.

– Quality control (QC): QC, also referred to as quality management, refers to laboratory analysis activities designed to improve the quality of test results by detecting and correcting defects that can occur during the experimental processes of all tests conducted within a laboratory. QC can be divided into internal QC, standard operating procedures and regulations set by the laboratory itself, and external QC, verified and approved by the FDA, member organizations of the International Laboratory Accreditation Cooperation, or agencies that operate proficiency assessment programs in accordance with international standards.

– Validation: Validation describes the process of confirming

 https://doi.org/10.4132/jptm.2020.08.27

whether equipment, reagents, and test methods that have already been verified can be appropriately applied to the individual laboratory in question according to certain standards before they are implemented. Validation should be established by documents that provide a high level of assurance.

GUIDELINES AND CONSIDERATIONS

Considerations for the hardware and software used in DP systems

This recommendation combines the essence of various research articles and guidelines, position papers, and instructions announced by major countries to present the functional requirements for DP hardware and software, along with related information to be considered when implementing a DP system. Using this information, each institution can select an appropriate system suitable for its particular circumstances when implementing a DP system, training experts to manage the DP system, and educating the pathologists and residents who will be using the DP system.

Considerations and recommended functional requirements for a WSS

Considerations for a WSS

The process of scanning to acquire images might be the most significant aspect of the DP system. When implementing a DP system using a WSS, it is important to understand that a WSI is a high-resolution copy of a glass slide image [6]. In other words, the actual glass slide image might not be 100% accurately replicated into a digital image due to various factors involved in image acquisition using a scanner. During the scanning process, some image data can be missed or inadvertently omitted because of inappropriately set scan parameters or tissue samples that are too thin or too small (e.g., fine needle aspirate of breast fat tissue or highly necrotic tissue) or an automatic tissue detection system error [6,10]. Therefore, the person in charge must verify that all important areas of interest are included in the scan range and prepare a plan to prevent errors that can occur for those reasons. Commercially available WSSs are listed in Supplementary Table S1 organized by manufacturer.

Recommended functional requirements for a WSS

The WSS requires an optical system that can illuminate glass slides using a bright field method as well as appropriate luminous intensity to scan the entire area [7,58]. Users should have detailed information about the light source, color temperature, and mode of illumination in the optical system [7].

The scanner is recommended to have an optical system capable of at least 40× magnification [6,7,58]. Resolutions of 500 and 250 nm per pixel can be achieved with 20× and 40× scans, respectively; thus, the scan magnification should be set based on the type of sample and purpose of the test.

The scanner must be designed such that the glass slide is safely maintained without being damaged, dislodged, or shifted during the slide exchange process as a scanned glass slide is removed and the next glass slide to be scanned is mounted [58]. A slide that is not firmly secured could shift slightly during this exchange, potentially creating artifacts in the scanned digital image [6].

The scanner must have an identification function, such as the ability to scan and recognize the labels of glass slides or identification information such as barcodes or QR codes to match the information from a slide to its digital image [4,7,58]. Scanners that support an identification function using a barcode or QR code play an important role in the automation of pathology laboratories and could help to reduce errors such as switched samples [4].

In addition to acquiring magnified images, the scanner should provide overview images (also called preview or macro-images) to allow users to observe the entire tissue on a glass slide in a single view [7,58]. During image acquisition, the horizontal and vertical resolution must be the same, and the color range and gradation of color images must satisfy the quality standard designated by the manufacturer [6,58].

The scanner must have an auto-focus function that satisfies the quality standard designated by the manufacturer, and it must be able to tell the user whether the image was successfully scanned with the normal auto-focus function [7,58].

The scanner must provide a function that allows users to check whether the digital image was scanned satisfactorily [7,58]. The manager who evaluates the quality of scanned images must carefully examine whether faint stains, pen marks, foreign objects, air bubbles during sealing, or damage to the cover slide affected the quality of scanned digital images and whether errors such as misalignment of strips or tiles when combining have occurred [6]. A work process enabling screening for those and similar factors must be established.

When implementing a DP system, the scanner type, performance, and quantity must be selected based on the scale of testing at the institution, sample size, sample type, tests being applied, required turn-around time (TAT), and amount of labor required to carry out the scan work [4]. The number of scanners appro-

priate for each institution can be calculated by determining the total time needed for scanning, available time for scanning, and scanner utilization rate [4]. The total time needed for scanning can be calculated by multiplying the number of samples to be scanned and average scan time per slide of the equipment; however, other factors, such as the time required to mount and dismount slides, time required for maintenance and repair, changes in workflow, and available labor, must also be considered [4]. Moreover, even digital images acquired from the same glass slide can show slight differences in saturation, color density, and color temperature depending on the scanner manufacturer [59]; thus, comparison tests of suitable equipment from various vendors should be performed before system implementation [55].

Considerations and recommended functional requirements for image database systems

Considerations for image database systems

An image database system comprises a computer system to manage image data, a storage device such as a server, and image-archiving software related to the database that manages data storage [6,7,58]. Data can also be stored on a hard disk drive managed by the computer operating system (OS) without image archiving software [10]. In the case of an image database system, a pathology PACS using an independent server is recommended to accommodate the size of digital pathologic image data and the amount of data transmitted. However, depending on the situation and needs of each individual institution, data storage could also be integrated and use the same server as the general institutional PACS [6,7].

Each institution should determine how long digital image data should be preserved. The guidelines by CAP (USA), RCP (UK), and FAGP (Germany) recommend data preservation for at least 10 years, whereas the guidelines from the JSP (Japan) recommend permanent preservation, with a minimum of 5 years [6,10,26,30]. The JSP guidelines also recommend that data from the past 5 years be preserved in hot storage, meaning that they are available for immediate use [26]. For reference, the preservation period recommended by the Medical Act of South Korea for glass slides containing pathological tissue is 5 years, which is the requirement for test records or findings among general medical records.

Each institution must set a preservation period based on its particular situation and the relevant laws.

During implementation of an image database system, institutional IT specialists should be consulted because their cooperation is required for integration with the LIMS, connection to electronic health records that include clinical information, compliance with the institution's information security policies, and seamless interconnection and integration with existing PACS [6,7,10].

Recommended functional requirements for image database systems

The image database system must be able to guarantee that the identification information of the glass slide matches that of the digital image [26]. Moreover, even if the version of the image archiving software changes, using a preserved image should not be problematic, and the possibility that digital images could be damaged by overheating of the storage device or recording medium should be eliminated [7].

The type of storage method must include the concept of backup or mirroring to ensure that data are safely preserved (e.g., using network attached storage or a redundant array of inexpensive disks) [10].

The image database system (or software) could support the DICOM format, the standard file format for medical imaging designated by the American College of Radiology and National Electrical Manufacturers Association, to ensure compatibility with other scanners or PACS [7,10]. This is an important function that must be considered when implementing image database systems to enable future data exchange or transmission to other institutions and combined use with other image acquisition/storage devices within the institution [7,10].

Considerations and recommended functional requirements for image display devices and image viewing software

Considerations for image display devices and image viewing software

Image display devices include flat-screen monitors, occasionally with touch-input function. The devices can be portable, such as a tablet PC, for telepathology [7,58]. The image viewing software should run on various platforms suitable for the image display devices used by an institution and should support operation over a network connection [58].

Image display devices, including monitors, are part of an imaging chain (also called a visualization pipeline), as are optical components such as scanner lenses and image acquisition components such as a charge-coupled device, an electronic component for data processing [6,10]. Consideration should be given to the following factors that determine the quality of image display devices: the type of display (such as the size of the device), the

 https://doi.org/10.4132/jptm.2020.08.27

structure of the light source (light-emitting or light-receiving), the liquid crystal alignment mode (in-plain switching or vertical alignment), and the structure of the liquid-crystal display and flat panel; the mechanical characteristics of the device, including the resolution (dots per inch), luminance, contrast ratio and contrast, color temperature, color profile of the monitor, viewing angle, response rate, image retention, and burn-in [6,7,10]; the mechanical characteristics of the image display system associated with the speed and capacity of the graphic memory in the computer system; and environmental factors such as room lighting, window placement, distance from the observer eye level, and differences in user heights [6,10].

When making diagnoses using a DP system, it is often necessary to check clinical information from the patient EMR or radiologic data from the PACS, for which multiple monitors can be used. When comparing or observing two or more DP images using multiple monitors, the monitors should have been manufactured in the same year and should be the same model to minimize differences in the images caused by the different monitors [6,10]. Moreover, the performance of an image display device can degrade after extended use in terms of decreased luminance, decreased contrast ratio, and burn-in. Therefore, each device must be regularly validated by appropriate methods, or actions must be taken to maintain its performance [6,7,10,58]. For reference, examples of displays used in current DP deployments and the largest validation studies presented in best-practice recommendations by the RCP for implementing DP are listed in Supplementary Table S2 [6].

Recommended functional requirements for image display devices and image viewing software

Because technologies for image display devices such as monitors are advancing rapidly, it is difficult to define the minimum requirements for a DP system based simply on numeric values [7,58]. Moreover, it is difficult to define the absolute requirements because the luminance, luminance ratio, and contrast can change depending on the office environment. Therefore, optimal functional conditions should be defined according to the situation and needs of each institution [58].

Various international DP guidelines present minimum functional requirements with slightly different specifications that all gradually increased depending on when they were announced (Table 3) [7,9,10,55,58].

These guidelines generally recommend the following: horizontal resolution ≥1,280–2,560 pixels, screen size (diagonal) ≥17–27 inches, luminance ≥170–300 cd/m^2, luminance ratio ≥250–1,600:1, pixel pitch ≤0.33 mm, and minimum luminance ≥0.5 cd/m^2. However, certain guidelines do not specify values and recommend that each laboratory select suitable monitors at their discretion, with validation of the overall performance [2,6]. Increasing the monitor resolution does not enable digital images acquired by a scanner to be viewed at a resolution higher than the original resolution. However, if the monitor resolution is too low, original digital images acquired at higher resolutions might not be accurately displayed [2,6].

Image viewing software can include the following functions: an observation field display that shows overview images (also referred to as preview or macro-images), with the part of the total overview image being observed indicated within a square; an annotation function that displays the object magnification and length scale (accumulation) on the images and allows users to insert figures or words to mark areas of interest; a function to screen-capture partial or entire images of interest displayed on the monitor; a function that allows side-by-side comparison of DP images from different tests performed on the same patient, such as immunohistochemical or special stains, or DP images from similar cases for reference; and basic morphometric functions, such as measuring the length and area of certain microstructures [7,10]. Whether these functions can be adequately performed in the workflow of real practice should be determined in advance

Table 3. Minimum requirements for image display devices recommended by international guidelines

	CAP[a] (US) [55]	SEAP (Spain) [9]	FAGP (Germany) [10]	JSP (Japan) [7]
Published year	2015	2015	2018	2019
Screen resolution (pixels)	1,280×1,024	1,920×1,080	2560×1600	1,280×1,024
Screen size (inch)	17 or 19	22	27	19.3
Pixel pitch (mm)	-	-	-	≤0.33
Luminance (cd/m^2)	-	≥100	≥300	≥170
Luminance ratio (contrast ratio)	-	1,000–1,600:1	-	≥250:1
Minimum luminance (cd/m^2)	-	-	≥0.5	-

CAP, College of American Pathologists; SEAP, Society of Anatomic Pathology; FAGP, Federal Association of German Pathologist; JSP, Japanese Society of Pathology.
[a]Results of validation studies conducted based on U.S. CAP guidelines [55].

[4,6,10]. The image viewing software can also include additional functions such as morphological classification, morphometry, tumor grading, and tumor diagnosis and detection with the aid of machine- or deep-learning computer algorithms [1,3]. It is necessary to determine whether sufficient evidence, based on the results of comparative analyses with conventional microscopy, supports the use of those functions within the diagnostic process [1,3].

Other considerations

Issues related to integration/links with LIS and EMR systems

The DP system must be linked appropriately to the LIS that stores and manages test records from the pathology laboratory and the HIS or EMR system that manages clinical patient records inside the hospital [7,10,58]. The ATA (US), Canadian, and European guidelines recommend linkage and management using standard methods such as HL7 [9-11,60]. The DP system must include metadata associated with the digital images [58; i.e., overview images (preview, macro-images), scan parameters, and data on the scanned area. When the system is linked to the LIS, data such as the test number, tissue information, block number, and staining information must be appropriately linked. Moreover, the linked systems must be checked to confirm the smooth operation of both systems and the link between them under actual workflow conditions [4].

The DP system must also be linked to the institutional PACS and EMR or HIS so that the patient clinical and radiologic image data needed for diagnosis are easily accessible [7,10,61,62]. It is best to follow the international standard DICOM. When linking to other information systems within an institution, IT specialists within that institution should be consulted in advance so that they can ensure safety by minimizing the effects of those links on network or information security [61-64].

Issues related to telepathology, firewalls, protection of personal information, and mobile device use

Rapid advances in wired/wireless networks and mobile technologies are expected to increase WSI diagnosis by means of remote systems or portable devices such as tablet PCs [6]. Diagnostic systems once used real-time images acquired by remotely controlled microscopes [13,60,65]. In South Korea, which has a relatively small territory with a highly developed wireless network environment and equally distributed access to healthcare, transmitting and sharing WSIs through a wired/wireless network is more likely than using the older telepathology system [1,3]. Moreover, rapid advances in the wireless network environment are likely to accelerate diagnosis or consultation using portable devices.

In both cases, strict technical measures must be in place to ensure information security and protect personal information regardless of the type of terminal being used [6,10]. Therefore, measures are needed to ensure that transmitted data are not easily released outside the network and that transmitted metadata do not contain personal information to minimize the risk to personal data even if a data leak were to occur.

When diagnoses are made using portable terminals such as a tablet PC, the use of a relatively small screen is a major concern. The results of a recent study suggest that diagnosis using portable terminals should be limited to special cases that require relatively low accuracy but rapid reporting of results, such as frozen section tests [1,53,65]. These terminals are generally not reliable for routine diagnostic work. Appropriate caution and considerations are deemed necessary.

Portable terminals run on different OSs, usually iOS (Apple) or the Android OS (Google). Image viewing software for portable terminals must be built to run smoothly on each OS. Cross-platform software that can run on any OS could be built based on HTML5 [58].

Guidelines and considerations for validation needed for the implementation of DP systems and internal QC needed during operation

For primary pathologic diagnosis by WSI, the DP system must undergo appropriate validation by the managing personnel before implementation. Moreover, internal QC must be performed regularly while the system is in operation to ensure that the system is operating normally and that the test results are reliable. Upon the identification of a system defect that could cause serious errors in the test results, immediate action must be taken to resolve the issue.

This recommendation is based on guidelines related to the validation of DP systems published by CAP (US) (Table 4) [30] and FAGP (Germany) (Supplementary Table S3) [10] and contains general principals and instructions that could be referenced for internal QC during operation, validation of the DP system during implementation at each institution, and the development of QA items related to DP systems for the KSP QC program.

Laboratory QA includes verification and validation. Verification refers to the approval of equipment or the production of reagents by regulatory authorities, such as the Ministry of Food and Drug Safety, before the implementation of a specific test or

 https://doi.org/10.4132/jptm.2020.08.27

Table 4. College of American Pathologists guidelines for validating whole slide imaging systems for diagnostic purposes in pathology [30]

Guideline statement	Grade of evidence
1. All pathology laboratories implementing WSI technology for clinical diagnostic purposes should carry out their own validation studies.	Expert consensus opinion
2. Validation should be appropriate for and applicable to the intended clinical use and clinical setting of the application in which WSI will be used. Validation of WSI systems should involve specimen preparation types relevant to the intended use (e.g., formalin-fixed paraffin-embedded tissue, frozen tissue, immunohistochemical staining, cytology slides, hematology blood smears). Note: If a new intended use for WSI is contemplated and this new use differs materially from the previously validated use, a separate validation for the new use should be performed.	Recommendation Grade A
3. The validation study should closely emulate the real-world clinical environment in which the technology will be used.	Recommendation Grade A
4. The validation study should encompass the entire WSI system. Note: It is unnecessary to separately validate each individual component of the system (e.g., computer hardware, monitor, network, scanner) or the individual steps of the digital imaging process.	Recommendation Grade B
5. Revalidation is required whenever a significant change is made to any component of the WSI system.	Expert consensus opinion
6. At least one pathologist adequately trained to use the WSI system must be involved in the validation process.	Recommendation Grade B
7. The validation process should include a sample set of at least 60 cases for one application (e.g., H&E stained sections of fixed tissue, frozen sections, cytology, or hematology) that reflects the spectrum and complexity of specimen types and diagnoses likely to be encountered during routine practice. Note: The validation process should include another 20 cases for each additional application (e.g., immunohistochemistry, special stains).	Recommendation Grade A
8. The validation study should establish diagnostic concordance between digital and glass slides for a single observer (i.e., intra-observer variability).	Suggestion Grade A
9. Digital and glass slides can be evaluated in random or nonrandom order (as to which is examined first and second) during the validation process.	Recommendation Grade A
10. A washout period of at least 2 weeks should occur between viewing digital and glass slides.	Recommendation Grade B
11. The validation process should confirm that all of the material present on a glass slide to be scanned is included in the digital image.	Expert consensus opinion
12. Documentation recording the method, measurements, and final approval of the validation results for the WSI system should be maintained.	Expert consensus opinion

WSI, whole slide imaging; H&E, hematoxylin and eosin.

experiment. Validation is an institutional-level testing process before implementation in a laboratory. Validation can be divided into internal validation performed in-house by each laboratory, which is the case for DP systems, and external validation performed by third-party institutions. During DP operation after implementation, a quality management program should be performed continuously and routinely. This program also includes internal quality management programs carried out in-house according to internal instructions and an external quality management program performed by independent institutions. A typical example of an external quality management program is the KSP Quality Control Program (proficiency test). Because that program does not currently include quality assessment items related to DP systems, appropriate items should be developed and included soon; in doing so, the following rules should be considered. The following recommendation statements are summarized in Table 5.

1. All pathology laboratories operating WSI-based DP systems for clinical diagnosis must conduct in-house validation studies (Expert consensus)

Variable factors in the testing process could influence DP system performance and validity; thus, a validation study before system implementation is essential. Simply because the DP system has already been approved by relevant authorities through a verification process and is being operated according to the manufacturer's recommended operating protocol does not guarantee the validity of the system for the samples and environment at each institution. The validation results must be appropriately documented and maintained accordingly [6,10,30].

2. The validation study should be conducted under conditions that are consistent with the clinical use intended by the DP system manufacturer (Recommendation)

Validation is intended to prove that the WSI system is operating as expected according to its intended purpose [6,10,30]. Therefore, the specific methods and design of the validation must be consistent with the purpose at the time that the WSI system was

Table 5. Recommendation statements from the Medical Informatics Study Group (MISG) of the Korean Society of Pathologists (KSP) for validation of digital pathology systems for primary diagnosis during implementation

Recommendation statement	Grade of evidence
1. All pathology laboratories operating whole slide image–based digital pathology systems for clinical diagnosis must conduct in-house validation studies.	Expert consensus
2. The validation study should be conducted under conditions that are consistent with the clinical use intended by the digital pathology system manufacturer.	Recommendation
3. The validation study should be designed to be as similar as possible to the actual clinical settings in which the technology will be used.	Recommendation
4. The validation study should cover the entire digital pathology system.	Recommendation
5. Significant changes in the composition of the digital pathology system necessitate re-validation.	Expert consensus
6. Validation is intended to be conducted by at least one pathologist who has been acclimated to the digital pathology system.	Recommendation
7. The validation must be performed on at least 60 samples for a single applicable field (e.g., histopathologic H&E-stained slides, frozen sections, cytology slides, blood smear slides) according to the type of sample or test. For additional applicable fields (e.g., immunohistochemical staining, special staining), validation could be performed by adding 20 or more samples.	Recommendation
8. Validation must be carried out using a comparative analysis of diagnostic concordance between microscopic and WSI-based diagnoses by a single observer (intra-observer variability assessment).	Suggestion
9. Validation can be performed using either randomly or sequentially arranged samples.	Recommendation
10. During the validation, a washout period of at least 2 weeks is needed to minimize the influence of recall bias.	Recommendation
11. During validation, data integrity during image acquisition must be assessed by verifying whether all tissues on the glass slide have been properly scanned to form the digital image.	Expert consensus
12. Pathology laboratories must maintain documentation regarding the validation of the digital pathology system, including the methods, results, and final approval.	Expert consensus

H&E, hematoxylin and eosin; WSI, whole slide imaging.

manufactured. For example, even if a DP system that was manufactured to run gynecological liquid-based cytology slides has been successfully validated using gynecological liquid-based cytology samples before implementation, it would not be safe to assume that this system would demonstrate the same quality for centrifuged urine cytology samples. Therefore, separate testing must be conducted when the DP system is to be used for purposes other than originally planned. However, if the overall process of sample preparation and interpretation is the same, then a single validation study could be sufficient [6,10,30]. For example, when testing immunohistochemical stain slides, having the sample preparation process would obviate the need to individually test all antibodies.

3. The validation study should be designed to be as similar as possible to the actual clinical settings in which the technology will be used (Recommendation)

It is not advisable to conduct the validation study by selecting samples that show "typical" pathologic findings for each diagnosis favorable for testing [6,10,30]. The validation must represent common cases and should include a sufficient number of borderline cases that could be difficult to diagnose using the DP system, such that the spectrum of diagnostic complexity and difficulty found in actual workflow is adequately represented. In addition to a comparison of diagnostic accuracy, the validation must also include an assessment of its performance with respect to cases that are expected to be more difficult than by microscopy, such as dysplasia grading, calcium oxalate crystal detection, mitosis counting, eosinophil counting, microorganism detection, and viral inclusion detection. This process can be used to facilitate user training and learning, as well as proper validation. For frozen section cases, whether the TAT from scanning to diagnosis is similar to that of microscopic diagnosis must also be assessed [6,10,30]. If the system is used in a single institution, comparative assessment with other laboratories is not necessary. However, if samples prepared in other institutions are used, then advanced testing of the method is necessary to simulate the same workflow.

4. The validation study should cover the entire DP system (Recommendation)

The validation study is a QA process intended to test the entire process; thus, separate testing of individual system components (e.g., the computer system, monitor, and scanner) or processes is unnecessary [6,10,30].

5. Significant changes in the composition of the DP system necessitate re-validation (Expert consensus)

Validation must be repeated whenever significant changes are made to the composition of the DP system, such as the use of a new type of scanner or hardware or software upgrades [6,10,30]. The validation could be performed with a smaller number of samples (i.e., 20 samples) if the new scanner was manufactured

 https://doi.org/10.4132/jptm.2020.08.27

by the same manufacturer; is the same model as the previously validated scanner; and is used with the same network, image database system, image viewing software, and image display device. Minor changes can be managed according to internal guidelines [6,10,30].

6. Validation is intended to be conducted by at least one pathologist who has been acclimated to the DP system (Recommendation)

The validation process assumes that a pathologist who has been acclimated to the DP system will make a diagnosis [6,10,30]. Therefore, validation should be performed by someone familiar with using the DP system, rather than inexperienced individuals, to eliminate results biased by the tester's level of education and training. Moreover, although the system does not need to be validated by every pathologist who uses it, the validation could include other laboratory personnel (e.g., laboratory managers, histo- or cytotechnicians, and residents), IT managers, or technical advisors. The validation should also include personnel who perform slide scanning [6,10,30].

7. The validation must be performed on at least 60 samples for a single applicable field (e.g., histopathologic H&E-stained slides, frozen sections, cytology slides, blood smear slides) according to the type of sample or test. For additional applicable fields (e.g., immunohistochemical staining, special staining), validation could be performed by adding 20 or more samples (Recommendation)

The number of people involved in the validation and the scale of the validation could vary significantly between institutions [6,10,30]. Moreover, it is difficult to accurately calculate the minimum number of samples needed to guarantee 100% validity. The manager of the DP system at each institution must fully consider the scale and characteristics handled by the institution as well as the relevant personnel and include samples with varying degrees of diagnostic difficulty when selecting the appropriate number of samples needed to ensure reliable operation of the DP system [4,6,10,30]. A prospective validation process during 1–3 months of actual operation, as well as a retrospective validation study using prior tests, could be also considered.

8. Validation must be carried out using a comparative analysis of concordance between microscopic and WSI-based diagnoses made by a single observer (intra-observer variability assessment) (Suggestion)

Validation is intended to assess the diagnostic concordance between microscopic and WSI-based diagnoses; thus, it must be conducted as an intra-observer variability assessment with repeated assessments by the same observer [4,6,10,30]. The degree of diagnostic concordance can be assessed using a 3-tier system according to the clinical implications (i.e., major discordance that could drastically affect patient prognosis and treatment; minor discordance that could affect the diagnosis severity without causing changes in patient prognosis and treatment; and minimal discordance with little or no difference in the diagnosis severity and patient prognosis or treatment) [4,6,10,30]. The goal of comparative analysis should be to identify the cause of problems related to image quality, such as artifacts during digital image scanning, rather than diagnostic variability resulting from interpretational changes by the observer [6].

9. Validation can be performed using either randomly or sequentially arranged samples (Recommendation)

Intuitively, the random arrangement of samples would seem to minimize the influence of recall bias on validation. However, relevant studies have reported no significant difference between random and sequential assessments [2,4,6,10,30].

10. During the validation, a washout period of at least 2 weeks is needed to minimize the influence of recall bias (Recommendation)

An observer remembering tissue slide images previously examined and their corresponding diagnoses can cause recall bias that could affect validation concordance [2,4,6,10,30]. Therefore, it is important to perform the validation with a sufficient washout period between the observations. Previous studies and major guidelines recommend a washout period of at least 2 weeks; however, a longer washout period might be more favorable as long as it does not burden the operation of the institution.

11. During validation, data integrity during image acquisition must be assessed by verifying whether all tissues on the glass slide have been properly scanned to form the digital image (Expert consensus)

In addition to assessing the diagnostic concordance, the assessment of data integrity during image acquisition is also important with respect to the QA of the DP system [2,4,6,10,30]. Slides with poor staining quality, images of very small tissues that are out-of-focus, and errors or scan failure during image acquisition should be checked and appropriate measures taken during validation. In addition, it is important to check whether the metadata of the digital images and the slide identification numbers

(slide labels) match [2,4,6,10,30].

12. Pathology laboratories must maintain documentation regarding the validation of the DP system, including the methods, results, and final approval (Expert consensus)

Pathology laboratories must keep and manage the documents demonstrating their successful validation of their DP systems, including the methods used, results, and final approval [2,4,6,10,30]. During the validation, system users should be educated and trained to operate the system, and supporting documents showing that this education has been conducted must be prepared and maintained. The final document must contain the signature of the DP system manager or designated representative. In addition, the inclusion of a statement in the pathologic report that a DP system was used for diagnosis is recommended [26].

CONCLUSION

The technical innovations in the past decade have advanced DP enough for it to replace conventional microscopic diagnosis [1]. However, caution is still needed in certain situations that require specific pathologic determination, such as microbial infection assessment [1]. Ultimately, accumulating experience and data could lead to solutions to these current technical limitations.

The successful implementation of DP systems provides a foundation from which pathology laboratories can enhance their services and create innovative workflows. DP could change the daily lives of pathologists in the next 20–30 years. The convergence of DP with various cutting-edge scientific fields, such as computing based on big data and artificial intelligence, would be a game-changer in the upcoming 4th Industrial Revolution. Therefore, government-led planning and systemic support for the timely implementation of DP systems is needed. KSP-MISG continues to introduce relevant and timely technologies to meet demand and strives to provide standards and advice on their safe implementation in actual clinical practice.

Supplementary Information

The Data Supplement is available with this article at https://doi.org/10.4132/jptm.2020.08.27.

Ethics Statement

This work was reviewed and approved by the Institutional Review Board of The Catholic University of Korea (SC19ZCSI0173).

ORCID

Yosep Chong https://orcid.org/0000-0001-8615-3064
Dae Cheol Kim https://orcid.org/0000-0002-9404-0366
Chan Kwon Jung https://orcid.org/0000-0001-6843-3708
Dong-chul Kim https://orcid.org/0000-0002-4710-6449
Sang Yong Song https://orcid.org/0000-0001-5540-6823
Hee Jae Joo https://orcid.org/0000-0002-6706-4397
Sang-Yeop Yi https://orcid.org/0000-0003-2875-1263

Author Contributions

Conceptualization: YC, DCK (Dae Cheol Kim), CKJ, DCK (Dong-chul Kim), SYS, HJJ, SYY. Data curation: YC, DCK (Dae Cheol Kim), DCK (Dong-chul Kim). Funding acquisition: SYY. Investigation: YC, DCK (Dae Cheol Kim), CKJ, DCK (Dong-chul Kim), SYS, HJJ, SYY. Methodology: YC, DCK (Dae Cheol Kim), SYY. Project administration: DCK (Dae Cheol Kim), CKJ, SYS, HJJ, SYY. Resources: YC, DCK (Dae Cheol Kim), CKJ, DCK (Dong-chul Kim). Supervision: SYS, HJJ, SYY. Validation: YC, DCK (Dae Cheol Kim), CKJ, DCK (Dong-chul Kim), SYS, HJJ, SYY. Visualization: YC, DCK (Dae Cheol Kim). Writing—original draft: YC, DCK (Dae Cheol Kim), SYY. Writing—review & editing: YC, DCK (Dae Cheol Kim), CKJ, DCK (Dong-chul Kim), SYS, HJJ, SYY. Approval of final manuscript: all authors.

Conflicts of Interest

C.K.J., the editor-in-chief and Y.C., contributing editor of the *Journal of Pathology and Translational Medicine*, were not involved in the editorial evaluation or decision to publish this article. All remaining authors have declared no conflicts of interest.

Funding Statement

This research was supported by The Korean Society of Pathologists Grant (KSPG2019-03).

Acknowledgments

We appreciate Prof. Se Jin Jang from Asan Medical Cencer, University of Ulsan, College of Medicine, Seoul, the Chairman of the KSP, Prof. Kyoung Bun Lee from Seoul National University, Seoul, the Executive Director of the Committee of Informatics of the KSP, Prof. Ho-Chang Lee from Chungbuk National University College of Medicine, Cheongju, the Executive Director of the Committee of Scholarship of the KSP, Prof. Ju Han Lee from Korea University Ansan Hospital, the Executive Director of the Committee of Insurance of the KSP, and Prof. Dong Hoon Kim from Kangbuk Samsung Hospital, Sungkyunkwan University School of Medicine, Seoul, the Executive Director of the Committee of General Affairs of the KSP for generously providing practical advice during the project.

References

1. Nam S, Chong Y, Jung CK, et al. Introduction to digital pathology and computer-aided pathology. J Pathol Transl Med 2020; 54: 125-34.
2. Hanna MG, Pantanowitz L, Evans AJ. Overview of contemporary guidelines in digital pathology: what is available in 2015 and what still needs to be addressed? J Clin Pathol 2015; 68: 499-505.
3. Lee K, Jang S, Kim D, Lee J. Preparation of reimbursement assessment guidelines for AI-based medical technology (pathology). Seoul: Health Insurance Review and Assessment Service (HIRA), 2019.
4. Treanor D, Williams B. The leeds guide to digital pathology. Leeds: The Leeds Teaching Hospitals NHS, University of Leeds, 2019.
5. Japanese Society of Pathology. Digital Pathology Assessment Committee: guidelines for pathologic diagnosis using digital pathology images (clinical questions and answers). Tokyo: Japanese Society of Pathology, 2019.
6. Cross S, Furness P, Igali L, Snead DR, Treanor D. Best practice rec-

ommendations for implementing digital pathology. London: The Royal College of Pathologists, 2018; 1-43.
7. Japanese Society of Pathology. Digital Pathology Assessment Committee: technical standards for digital pathology system for pathologic diagnosis. Tokyo: Japanese Society of Pathology, 2018.
8. College of American Pathologists. Validating whole slide imaging for diagnostic purposes in pathology. Northfield: College of American Pathologists, 2013.
9. Garcia Rojo M, Conde A, Ordi J, et al. Guia practica para la implantacion de la patologia digital. In: Guerra Merino I, ed. Libro Blanco de la Anatomia Patologica en Espana 2015. Vitoria: Sociedad Espanola de Anatomia Patologica, 2015; 247-78.
10. Federal Association of German Pathologists Bundesverband Deutscher Pathologen (FAGP-BDP). Guidelines digital pathology for diagnosis on (and reports of) digital images, 2018. Berlin: Federal Association of German Pathologists Bundesverband Deutscher Pathologen (FAGP-BDP), 2018.
11. Canadian Association of Pathologists Telepathology Guidelines Committee; Bernard C, Chandrakanth SA, et al. Guidelines from the Canadian Association of Pathologists for establishing a telepathology service for anatomic pathology using whole-slide imaging. J Pathol Inform 2014; 5: 15.
12. College of American Pathologists. Anatomic pathology checklist: CAP accreditation program. Northfield: College of American Pathologists, 2011.
13. Pantanowitz L. Clinical guidelines for telepathology. Arlington: American Telemedicine Association, 2014.
14. Lowe A, Chlipala E, Elin J, Kawano Y, Long RE, Tillman D. Validation of digital pathology in a healthcare environment. San Diego: Digital Pathology Association, 2011.
15. Chlipala E, Elin J, Eichhorn O, Huisman A, Krishnamurti M, Sabata B. Archival and retrieval in digital pathology systems. Madison: Digital Pathology Association, 2011.
16. Ellin J, Haskvitz A, Premraj P, et al. Interoperability between anatomic pathology laboratory information systems and digital pathology systems. Madison: Digital Pathology Association, 2010.
17. Cann J, Chlipala E, Ellin J, et al. Validation of digital pathology systems in the regulated nonclinical environment. Madison: Digital Pathology Association, 2013.
18. US Food and Drug Administration. Technical performance assessment of digital pathology whole slide imaging devices: draft guidance for industry and food and drug administration staff. Silver Spring: US Department of Health and Human Services, 2015.
19. Centers for Medicare and Medicaid Services. Clinical laboratory improvement amendments (CLIA). Baltimore: Centers for Medicare and Medicaid Services, US Department of Health and Human Services (HHS), 2015.
20. US Department of Health and Human Services. Clinical Laboratory Improvement Advisory Committee. Summary report. Washington, DC: US Department of Health and Human Services, 2013.
21. Long RE, Smith A, Machotka SV, et al. Scientific and Regulatory Policy Committee (SRPC) paper: validation of digital pathology systems in the regulated nonclinical environment. Toxicol Pathol 2013; 41: 115-24.
22. Tuomari DL, Kemp RK, Sellers R, et al. Society of Toxicologic Pathology position paper on pathology image data: compliance with 21 CFR Parts 58 and 11. Toxicol Pathol 2007; 35: 450-5.
23. European Commission, DG Health and Consumer, Directorate B, Unit B2 'Health Technology and Cosmetics. Guidelines on the qualification and classification of stand alone software used in healthcare within the regulatory framework of medical devices. Brussels: European Commission, 2012.
24. Rashbass J, Furness P. Telepathology: guidance from The Royal College of Pathologists. London: The Royal College of Pathologists, 2005.
25. The Royal College of Pathologists of Australasia (RCPA). The Royal College of Pathologists of Australasia (RCPA): position satement: telepathology. Sydney: The Royal College of Pathologists of Australasia, 2014.
26. Japanese Society of Pathology. Digital Pathology Assessment Committee: guidelines for pathologic diagnosis using digital pathology images. Tokyo: Japanese Society of Pathology, 2016.
27. Japanese Society of Pathology. Digital Pathology Assessment Committee: technical standards for digital pathology system for pathologic diagnosis. Tokyo: Japanese Society of Pathology, 2016.
28. Japanese Society of Pathology. Digital Pathology Assessment Committee: technical standards for digital pathology system for pathologic diagnosis. Tokyo:Japanese Society of Pathology, 2015.
29. Abels E, Pantanowitz L, Aeffner F, et al. Computational pathology definitions, best practices, and recommendations for regulatory guidance: a white paper from the Digital Pathology Association. J Pathol 2019; 249: 286-94.
30. Pantanowitz L, Sinard JH, Henricks WH, et al. Validating whole slide imaging for diagnostic purposes in pathology: guideline from the College of American Pathologists Pathology and Laboratory Quality Center. Arch Pathol Lab Med 2013; 137: 1710-22.
31. Gilbertson JR, Ho J, Anthony L, Jukic DM, Yagi Y, Parwani AV. Primary histologic diagnosis using automated whole slide imaging: a validation study. BMC Clin Pathol 2006; 6: 4.
32. Jukic DM, Drogowski LM, Martina J, Parwani AV. Clinical examination and validation of primary diagnosis in anatomic pathology using whole slide digital images. Arch Pathol Lab Med 2011; 135: 372-8.
33. Al-Janabi S, Huisman A, Nap M, Clarijs R, van Diest PJ. Whole slide images as a platform for initial diagnostics in histopathology in a medium-sized routine laboratory. J Clin Pathol 2012; 65: 1107-11.
34. Al-Janabi S, Huisman A, Vink A, et al. Whole slide images for primary diagnostics of gastrointestinal tract pathology: a feasibility study. Hum Pathol 2012; 43: 702-7.
35. Al-Janabi S, Huisman A, Vink A, et al. Whole slide images for primary diagnostics in dermatopathology: a feasibility study. J Clin Pathol 2012; 65: 152-8.
36. Al-Janabi S, Huisman A, Nikkels PG, ten Kate FJ, van Diest PJ. Whole slide images for primary diagnostics of paediatric pathology specimens: a feasibility study. J Clin Pathol 2013; 66: 218-23.
37. Bauer TW, Schoenfield L, Slaw RJ, Yerian L, Sun Z, Henricks WH. Validation of whole slide imaging for primary diagnosis in surgical pathology. Arch Pathol Lab Med 2013; 137: 518-24.
38. Krishnamurthy S, Mathews K, McClure S, et al. Multi-institutional comparison of whole slide digital imaging and optical microscopy for interpretation of hematoxylin-eosin-stained breast tissue sections. Arch Pathol Lab Med 2013; 137: 1733-9.
39. Al-Janabi S, Huisman A, Jonges GN, Ten Kate FJ, Goldschmeding R, van Diest PJ. Whole slide images for primary diagnostics of urinary system pathology: a feasibility study. J Renal Inj Prev 2014; 3: 91-6.
40. Buck TP, Dilorio R, Havrilla L, O'Neill DG. Validation of a whole

slide imaging system for primary diagnosis in surgical pathology: A community hospital experience. J Pathol Inform 2014; 5: 43.
41. Reyes C, Ikpatt OF, Nadji M, Cote RJ. Intra-observer reproducibility of whole slide imaging for the primary diagnosis of breast needle biopsies. J Pathol Inform 2014; 5: 5.
42. Ordi J, Castillo P, Saco A, et al. Validation of whole slide imaging in the primary diagnosis of gynaecological pathology in a University Hospital. J Clin Pathol 2015; 68: 33-9.
43. Pekmezci M, Uysal SP, Orhan Y, Tihan T, Lee HS. Pitfalls in the use of whole slide imaging for the diagnosis of central nervous system tumors: a pilot study in surgical neuropathology. J Pathol Inform 2016; 7: 25.
44. Snead DR, Tsang YW, Meskiri A, et al. Validation of digital pathology imaging for primary histopathological diagnosis. Histopathology 2016; 68: 1063-72.
45. Wack K, Drogowski L, Treloar M, et al. A multisite validation of whole slide imaging for primary diagnosis using standardized data collection and analysis. J Pathol Inform 2016; 7: 49.
46. Kent MN, Olsen TG, Feeser TA, et al. Diagnostic accuracy of virtual pathology vs traditional microscopy in a large dermatopathology study. JAMA Dermatol 2017; 153: 1285-91.
47. Saco A, Diaz A, Hernandez M, et al. Validation of whole-slide imaging in the primary diagnosis of liver biopsies in a University Hospital. Dig Liver Dis 2017; 49: 1240-6.
48. Tabata K, Mori I, Sasaki T, et al. Whole-slide imaging at primary pathological diagnosis: Validation of whole-slide imaging-based primary pathological diagnosis at twelve Japanese academic institutes. Pathol Int 2017; 67: 547-54.
49. Araujo AL, Amaral-Silva GK, Fonseca FP, et al. Validation of digital microscopy in the histopathological diagnoses of oral diseases. Virchows Arch 2018; 473: 321-7.
50. Lee JJ, Jedrych J, Pantanowitz L, Ho J. Validation of digital pathology for primary histopathological diagnosis of routine, inflammatory dermatopathology cases. Am J Dermatopathol 2018; 40: 17-23.
51. Mukhopadhyay S, Feldman MD, Abels E, et al. Whole slide imaging versus microscopy for primary diagnosis in surgical pathology: a multicenter blinded randomized noninferiority study of 1992 cases (pivotal study). Am J Surg Pathol 2018; 42: 39-52.
52. Bongaerts O, Clevers C, Debets M, et al. Conventional microscopical versus digital whole-slide imaging-based diagnosis of thin-layer cervical specimens: a validation study. J Pathol Inform 2018; 9: 29.
53. Canberk S, Behzatoglu K, Caliskan CK, et al. The role of telecytology in the primary diagnosis of thyroid fine-needle aspiration specimens. Acta Cytol 2020; 64: 323-31.
54. Amin S, Mori T, Itoh T. A validation study of whole slide imaging for primary diagnosis of lymphoma. Pathol Int 2019; 69: 341-9.
55. Thrall MJ, Wimmer JL, Schwartz MR. Validation of multiple whole slide imaging scanners based on the guideline from the College of American Pathologists Pathology and Laboratory Quality Center. Arch Pathol Lab Med 2015; 139: 656-64.
56. Kalinski T, Zwonitzer R, Sel S, et al. Virtual 3D microscopy using multiplane whole slide images in diagnostic pathology. Am J Clin Pathol 2008; 130: 259-64.
57. Aoyama H, Daimon Y, Tamaki T, Matsumoto H, Matsuzaki A, Yoshimi N. *H. pylori* infection in gastric biopsy specimens by whole slide image and inflammation assessment. Kure: Japanese Society of Digital Pathology, 2018; 40.
58. Garcia-Rojo M. International clinical guidelines for the adoption of digital pathology: a review of technical aspects. Pathobiology 2016; 83: 99-109.
59. Roy S, Kumar Jain A, Lal S, Kini J. A study about color normalization methods for histopathology images. Micron 2018; 114: 42-61.
60. Evans AJ, Krupinski EA, Weinstein RS, Pantanowitz L. 2014 American Telemedicine Association clinical guidelines for telepathology: another important step in support of increased adoption of telepathology for patient care. J Pathol Inform 2015; 6: 13.
61. Tuominen VJ, Isola J. Linking whole-slide microscope images with DICOM by using JPEG2000 interactive protocol. J Digit Imaging 2010; 23: 454-62.
62. Singh R, Chubb L, Pantanowitz L, Parwani A. Standardization in digital pathology: supplement 145 of the DICOM standards. J Pathol Inform 2011; 2: 23.
63. DICOM Standards Committee. Digital Imaging and Communications in Medicine (DICOM). Supplement 145: whole slide microscopic image IOD and SOP classes. Rosslyn: DICOM, 2010.
64. Zwonitzer R, Kalinski T, Hofmann H, Roessner A, Bernarding J. Digital pathology: DICOM-conform draft, testbed, and first results. Comput Methods Programs Biomed 2007; 87: 181-8.
65. Ribback S, Flessa S, Gromoll-Bergmann K, Evert M, Dombrowski F. Virtual slide telepathology with scanner systems for intraoperative frozen-section consultation. Pathol Res Pract 2014; 210: 377-82.

 https://doi.org/10.4132/jptm.2020.08.27

JPTM
Journal of Pathology and Translational Medicine 2020; 54: 453-461
https://doi.org/10.4132/jptm.2020.08.13

REVIEW

Liquid biopsy using extracellular vesicle–derived DNA in lung adenocarcinoma

In Ae Kim[1,2*], Jae Young Hur[1,3*], Hee Joung Kim[1,2], Seung Eun Lee[3], Wan Seop Kim[3], Kye Young Lee[1,2]

[1]Precision Medicine Lung Cancer Center, Konkuk University Medical Center, Seoul;
Departments of [2]Pulmonary Medicine and [3]Pathology, Konkuk University School of Medicine, Seoul, Korea

Blood liquid biopsy has emerged as a way of overcoming the clinical limitations of repeat biopsy by testing for the presence of acquired resistance mutations to therapeutic agents. Despite its merits of repeatability and non-invasiveness, this method is currently only used as a supplemental test due to a relatively low sensitivity rate of 50%–60%, and cannot replace tissue biopsy. The circulating tumor DNAs used in blood liquid biopsies are passive products of fragmented DNA with a short half-life released following tumor cell death; the low sensitivity seen with liquid blood biopsy results from this instability, which makes increasing the sensitivity of this test fundamentally difficult. Extracellular vesicles (EVs) are ideal carriers of cancer biomarkers, as cancer cells secret an abundance of EVs, and the contents of tumor cell-originated EVs reflect the molecular and genetic composition of parental cells. In addition, EV-derived DNAs (EV DNAs) consist of large-sized genomic DNAs and tumor-specific oncogenic mutant DNAs. For these reasons, liquid biopsy using EV DNA has the potential to overcome issues arising from tissue shortages associated with small biopsies, which are often seen in lung cancer patients, and the biopsy product can be used in other diagnostic methods, such as epidermal growth factor receptor (*EGFR*) mutation testing and next-generation sequencing (NGS). A higher sensitivity can be achieved when EV DNAs obtained from bronchoalveolar lavage fluid (BALF) are used rather than those from blood. BALF, when obtained close to the tumor site, is a promising liquid biopsy tool, as it enables the gathering of both cellular and non-cellular fractions of the tumor microenvironment, and provides increased diagnostic sensitivity when compared to blood.

Key Words: Lung adenocarcinoma; EV-based *EGFR* genotyping; Liquid biopsy; Extracellular vesicles; EV-derived DNA

Received: May 29, 2020 **Revised:** July 22, 2020 **Accepted:** August 13, 2020
Corresponding Author: Kye Young Lee, MD, PhD, Precision Medicine Lung Cancer Center, Konkuk University Medical Center and Department of Pulmonary Medicine, Konkuk University School of Medicine, 120-1 Neungdong-ro, Gwangjin-gu, Seoul 05030, Korea
Tel: +82-2-2030-7521, Fax: +82-2-2030-7784, E-mail: kyleemd@kuh.ac.kr

*These authors contributed equally to this work.

A growing trend in identifying biomarkers in diseases has brought on a dramatic rise in the number of tissue biopsies performed in the era of precision medicine. With advanced non-small cell lung cancer (NSCLC) patients often relying on small biopsies, the clinical need for an established liquid biopsy protocol has become an urgent necessity. Unlike gastrointestinal cancer, where tumor lesions in all locations can generally be visualized, lung cancers can only be approached by bronchoscopy, which limits visualization to central tumors. Even with the use of endobronchial ultrasound, peripheral lung cancers, such as adenocarcinoma before metastasis to the mediastinal lymph node, must rely on the invasive percutaneous needle biopsy (PCNB).

Recent trends have shown a decrease in the incidence of central lung cancers, such as squamous cell carcinoma and small cell carcinoma, with a concomitant increase in the incidence adenocarcinoma, where testing to identify driver oncogenic mutations is essentially useful [1-3]. With the development of target therapy drugs, the clinical need for rebiopsy or even repeated biopsies is increasing in order to identify drug resistance mechanisms in the targeted tissues [4,5]. Lung cancer tumor lesions are often small in size or positioned in a way that makes them difficult to target. In the case of ground-glass nodules (GGNs), a biopsy is not possible until enough of a solid portion develops to obtain tumor tissue by PCNB. For these reasons, "tissue is the issue" is a challenge faced by many clinicians, especially by those treating lung cancers. Liquid biopsy using blood was introduced to over-

pISSN 2383-7837
eISSN 2383-7845

come the difficulties of obtaining a quality solid tumor tissue sample, but remains a secondary diagnostic technique to tissue biopsies due to its low sensitivity [6-8].

Blood liquid biopsy uses circulating tumor DNAs, free-floating DNA fragments found in the blood, has a low sensitivity, as the sample is not from near the tumor site and the DNA is instable due to its nakedness [9]. Since blood is a complex body fluid with many components, there is a need for a different biosource for use in liquid biopsy. Also, the characteristics of cell-free DNAs (cfDNAs) extracted from plasma after the removal of red blood cells have never been properly defined, as these DNAs could have originated from free-floating DNA, DNA-protein complexes, and/or inside of extracellular vesicles (EVs). Extracted cfDNAs are mostly found in fragments of about 180 bp in length, which, in the context of cancer patients, circumstantially indicates that they are passively released byproducts from tumor cell death. The free-floating nature gives cfDNAs a short half-life of 2–2.5 hours, and this instability makes them inadequate as biomarkers [10,11].

EVs, nano-sized vesicles secreted by almost all types of cells, carry bioactive molecules, such as proteins, glycans, lipids, metabolites, RNAs, and DNAs, enclosed by a lipid bilayer, and act as an essential mediator in cell-to-cell communication [12-15]. EVs make an ideal cancer biomarker, as the contents of tumor cell-originated EVs reflect the molecular and genetic composition of parental cells, and are secreted in higher amounts than EVs of normal cells [16]. DNAs inside of an EV have advantages over cfDNAs as a biosource for liquid biopsy. Foremost, EV-derived DNAs (EV DNAs) consist of large-sized genomic DNAs and tumor-specific oncogenic mutant DNAs, unlike the fragmented cfDNAs [17]. However, EVs have yet to be precisely defined and categorized. For the purpose of this review, our main focus will be to classify the exosomes found in EVs and recapitulate the current status of liquid biopsy in lung cancer, focusing on EVs.

BIOSOURCES FOR LIQUID BIOPSY

Most cancers, even when they remain localized to a single primary site, can have a systemic impact by releasing tumor cells and byproducts into various body fluids. Liquid biopsy makes use of these biofluids, such as blood, urine, cerebrospinal fluid, pleural effusion, and glandular secretions, to analyze the characteristics of tumor cells in a continuous and noninvasive matter [18,19]. There are four major biosources used for liquid biopsy: circulating tumor cells (CTCs), cfDNAs, tumor-educated platelets (TEPs), and EVs [20].

CTCs are shed by primary tumors and stay circulating in the bloodstream until they metastasize to various parts of the body, which can happen at any time, even in the early stages of cancer development [21,22]. The advantage of using CTCs over other biosources is that a multi-omics approach evaluating the genomic, transcriptomic, and proteomic profiles of the tumor can be applied [23]. However, due to their minimal presence (there are approximately 1–10 CTCs/mL in blood), identification and characterization of cancer using CTCs is proving to be difficult [24,25], while the heterogeneity of surface markers and size of CTCs makes them challenging for clinical use [22]. The isolation of CTCs is also quite complicated, due to their extreme rarity compared to surrounding blood cells. The CellSearch system is the only U.S. Food and Drug Administration (FDA)–approved commercial product for CTC enumeration, but it is not widely used in a clinical setting because of its shortcomings, such as its high cost, need for manual processing, and high false-positive/false-negative rates [26]. Microfluidic platforms that are affinity-based and that utilize surface markers such as epithelial cell adhesion molecule to distinguish CTCs from surrounding blood cells have been proposed, but the matter of a high false-negative rate remains challenging due to the downregulation of surface epithelial markers driven by the epithelial-mesenchymal transition (EMT) [27,28]. Despite extensive research, CTCs are currently not commonly used in NSCLC mainly due to technical problems.

CfDNAs are the most commonly used biosource for liquid biopsy in lung cancer, because they are easily obtained and their concentration is significantly higher in cancer patients compared to healthy persons, with this increase correlating with cancer stage [22,29,30]. The Cobas EGFR mutation test v2 is clinically used for detecting T790M resistance mutation and in the prescription of osimertinib [31]. In recent years, next-generation sequencing (NGS) using blood-derived cfDNAs has been applied for screening and early diagnosis, treatment selection and prognosis, and residual disease and risk of relapse in NSCLC patients [32]. We are not going to review this area deeply, as many research articles and reviews have already explored blood cfDNA liquid biopsy, especially in epidermal growth factor receptor (*EGFR*)-mutated NSCLC patients [32-36]. The most important thing in blood cfDNA liquid biopsy in NSCLC is that cfDNA has fundamental limitations for liquid biopsy due to the fragmented nature of cfDNA and its instability, which leads to low test sensitivity.

TEP was recently discovered as a potential noninvasive biomarker, as TEPs are involved in the initiation, progression, and metastasis of tumors [37,38]. Cancer cells induce platelet activation

 https://doi.org/10.4132/jptm.2020.08.13

and assist the production of TEPs, which can promote tumor cell invasion through regulation of the p38MAPK-MMP9 pathway, promoting metastasis through EMT and escaping immunity via platelets-coated CTCs [39]. Also, alteration in a panel of RNAs was observed in cancers, which could also be useful as a biomarker [40]. Best et al. [41] reported the development of a TEP algorithm that can predict the presence of *EGFR* mutations, MET amplification, and *KRAS* mutations with high accuracy, which could potentially be used in the diagnosis of NSCLC.

FUNCTIONAL ASPECTS OF TUMOR-DERIVED EXTRACELLULAR VESICLES IN CANCER BIOLOGY

Tumor cells actively produce and release EVs that carry cytoplasmic components, including RNAs, DNAs, and proteins (Fig. 1A) [15,42]. These tumor-derived EVs are found in all bodily fluids, including saliva, blood, urine, and bronchoalveolar lavage fluid (BALF) (Fig. 1B) [43,44]. Mechanisms through which tumor-derived EVs select their cargo, serve the tumor, and affect surrounding cells are under intense investigation. There are multiple hypotheses for the original function of EVs in the context of cancer, from containing toxin and quorum sensing molecules in bacterial EVs to carrying information and conveying genetic messages by the tumor cells [45-47].

Many reports have illustrated that EVs derived from tumors play a significant role in intercellular communication by transmitting signals and transferring their oncogenic contents. These roles include the promotion of oncogenic potential in acceptor cells by increasing their cell proliferation potential [48], modulation of metastatic ability [49], and up-regulation of angiogenesis [50]. Studies have demonstrated that EVs are sufficient to recapitulate the formation of tumors through the neoplastic reprogramming of stem cells using prostate cancer cell-derived EVs [51], and breast cancer cell-derived EVs can promote normal epithelial cells to form tumors in a Dicer-dependent manner [52]. Recent studies have shown that cancer cells secrete immunologically active EVs which mediate immune regulation in the tumor microenvironment (TME) by acting as mediators of intercellular communication [53]. In lung cancers, EVs are shown to act as mediators of intercellular communication and play a vital role in tumor growth, progression, invasion, metastasis, and targeted drug resistance [54-57]. Furthermore, as EVs contain the bioactive molecules of the cells they are derived from, they have great potential as diagnostic biomarkers [14,15,17].

EXTRACELLULAR VESICLES AS IDEAL CANCER BIOMARKERS

In the era of personalized medicine, liquid biopsy is becoming an indispensable method for dealing with medical issues, such as the early detection of diseases, improving the accuracy of diagnosis, predicting responses of patients to drugs, and selecting follow-up of treatments [18,19]. In this sense, the discovery of target bio-molecules that can be used as biomarkers is as important as the advancement of technology used for liquid biopsy.

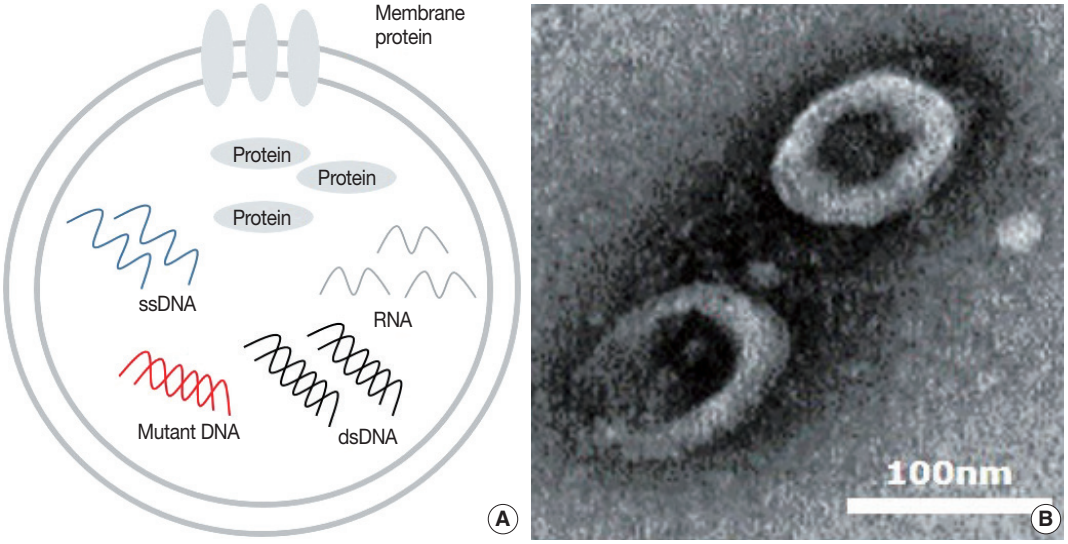

Fig. 1. Contents and image of extracellular vesicle. (A) Diagram of extracellular vesicle (EV) contents. (B) Transmission electron microscopy image of bronchoalveolar lavage fluid EVs.

The EVs secreted by cancer cells, enriched with various proteins, DNAs, and RNAs, have diagnostic value as biomarkers for clinical applications [12,13]. It is well known that EVs carry various types of proteins and RNAs from the cells that originally secreted them, which make them particularly fit as biomarkers for human disease, especially cancer. Many different types of protein, including membrane and cytosolic proteins, involved in various biological functions have been identified in EVs.

In recent years, an increasing number of studies have described the possible use of EV-derived proteins and RNAs as biomarkers. For example, Logozzi et al. [58] developed a method to detect and quantify a tumor-associated marker, a membrane protein called caveolin-1, from EVs. Recent identification of distinct integrin expression patterns in different types of cancer, including through the use of EV proteomics in lung cancer [59], measuring delta-catenin in prostate cancer-derived EVs [60], measuring DEL-1 levels from plasma EVs for early detection of breast cancer [61] and using proteomic profiling to identify subtype-specific protein clusters in breast cancer-derived EVs [62], has revealed the potential to use these expression patterns as cancer detection biomarkers. Many studies have identified elevation or downregulation of specific miRNAs in cancer patients that could be used as markers in the prognosis of NSCLC [63,64]. EV DNAs have been identified in both the double-stranded genomic and mutated fragmented forms [14,16,65].

It is commonly accepted that EV cargo packaging is not a random process, but rather a selective process that represents the cell of origin, which makes EVs and their contents a good representation of cancer. Also, EVs have a long half-life and are well protected in the human body by having an outer membrane. All of these studies indicate that EVs can be used as noninvasive biomarkers. Moreover, from the perspective of liquid biopsy, EVs can offer many advantages.

ADVANTAGES OF EXTRACELLULAR VESICLE DNA IN LIQUID BIOPSY

Unlike the relatively well-characterized proteins and RNAs found in EVs, until recently EV DNAs have not been the center of attention among researchers. Thakur et al. [65] identified tumor-derived EVs carrying double-stranded DNA (dsDNA) and EV DNA that represented the entire genome, including reflecting the mutational status, of parental tumor cells. Several studies also have identified that while EV DNAs exist in short and long sizes, most are 10 kb or longer, and have demonstrated that detection of cancer-related mutations can be done sufficiently with EV DNAs [16,66,67]. A study characterized subpopulations within the EV population with different DNA and RNA content and topology. In addition, they identified two types of DNAs, internally protected and external surface-related DNA, that could be used as a basis for developing diagnostic methods [68,69].

The fragmented nature of cfDNAs makes it difficult to generate a reliable genomic characterization for NGS, which in turn requires barcode and deep sequencing [70,71]. Contrarily, long-stranded and concentrated EV DNA is easy to amplify and therefore makes it a suitable candidate for NGS. In short, the use of EV DNA for NGS requires the same processes as those required in the well-established methods which use a tissue sample [72]. It has been suggested that NGS using EVs isolated from pleural effusions and urine could effectively replace tissue-based NGS in cases where there is a shortage of tissue [73,74]. EV DNAs have several important differences from the more clinically established cfDNA, as shown in Table 1. The encapsulation of DNA within the lipid bilayer of EVs seems to enhance the stability of the DNA by shielding it from the outer environment, unlike the 'naked' cfDNA, which is directly exposed to bodily fluids. The amount of cfDNA released by tumors is normally low, and represents only the fraction of the tumor genomic heterogeneity released by dying tumor cells. By contrast, the process for isolating EVs from fluids increases the final concentration of EV DNAs obtained, and EVs are secreted by both viable and dying tumor cells [44,75]. In a study comparing the use of plasma EV DNAs and cfDNAs of NSCLC patients in liquid biopsies, EV DNA improved the detection sensitivity in *EGFR* profiling of the exon 19 deletion, L858R, and T790M mutations. This study also highlighted the ongoing diagnostic and prognostic ability of EV

Table 1. Comparison of EV DNA and cfDNA

	EV DNA	cfDNA
Origin	Actively shed or secreted by cancer cells	Passive product of cell death
Size	Long (~10 kb)	~200 bp
Stability	High stability due to protection by double layered membrane	Short half-life (2–2.5 hr)
Isolation	Technically sophisticated	Easy and convenient

EV, extracellular vesicle; cfDNA, cell-free DNA.

https://doi.org/10.4132/jptm.2020.08.13

DNA by showing that the mutations identifiable by EV DNA liquid biopsy included the acquired resistance specific mutation T790M. Furthermore, the specificity and sensitivity of liquid biopsy increased even more with the use of BALF EV DNA [16,76]. Similar to NSCLC, analysis of serum EV DNA from pancreatic cancer patients also demonstrated the presence of clinically relevant KRAS-specific mutations [14,77,78].

As previously described, EVs are widely distributed in various body fluids, which make them more easily accessible with less invasive methods than tumor cells. More importantly, the specificity and sensitivity can be significantly increased when EV DNAs are used for liquid biopsy compared to cfDNAs. For these reasons, liquid biopsy of EV DNAs could be a clinically useful means of isolating cancer-specific DNA, while achieving a higher sensitivity and stability than the current diagnostic methods.

LIQUID BIOPSY USING BLOOD

Compared to the relatively invasive and expensive tissue biopsies, liquid biopsies using blood better allows for repeatable evaluation of the disease status of cancer patients, making it an especially useful tool in clinical practice. Recently, many have studied liquid biopsy using cfDNA, which is released into blood through cell death mechanisms, such as necrosis and apoptosis, has a short half-life, and is detected at very low concentrations (5–10 ng/mL). Because of these characteristics, high-sensitivity approaches are needed when using cfDNA. For example, the FDA-approved Cobas tool for detecting mutations with plasma cfDNA has a 69%–86% sensitivity for *EGFR* mutations and a 55–75% sensitivity for T790M mutation [79-81]. Also, the mutation detection rate in intrathoracic metastatic diseases (M1a) is much lower (39% for activation mutations, 27% for T790M) [82]. To overcome this low sensitivity, various high technology platforms, such as droplet digital polymerase chain reaction (PCR) [81] or BEAMing (Beads, Emulsion, Amplification, and Magnetics) technology, were introduced by several research institutes [79,82]. Briefly, the BEAMing assay uses individual DNA molecules that are attached to magnetic beads in water-in-oil emulsions and processed by compartmentalized PCR amplification. However, the cost of these ultra-fast sequencing technologies is too high for use in most clinics.

EV miRNAs have been shown to be promising biomarkers for the diagnosis of NSCLC, because EVs have a large amount of tumor-derived RNA [83], and RNAs within EVs are resistant to the activity of external RNases. MiRNAs are short, non-coding, single-stranded RNA molecules (19–22 nucleotides) that target complementary mRNA sequences and play important roles in regulating gene expression at the post-transcriptional level. For example, miR-660-5p [84], miR-17-5p [85], miR-126 [86], and a multiple miRNAs combination panel [87] are expressed at higher levels in NSCLC patients compared to healthy controls. MiRNAs from circulating EVs seem to be associated with the stage, tumor grade, histology, and prognosis of cancer patients [87,88], but the sensitivity and specificity of these connections remained at only 60%–80%.

The analysis of EV nucleic acids in plasma showed that they are more sensitive in identifying relevant mutations than cfDNAs. Krug et al. [89] showed the EV RNA was significantly more sensitive in detecting activating *EGFR* mutations (98%) and T790M mutation (90%) compared to the matched cfDNA (82% for activating *EGFR* mutations, 84% for T790M). The RNAs from the captured EVs are reverse transcribed to cDNAs, and subsequently analyzed by targeted NGS. These methods increase the sensitivity of detecting *EGFR* mutations but require the high-cost NGS assay. A number of studies on liquid biopsy using EVs isolated from blood have been performed, but the sensitivity of this assay reported in these studies was not yet high enough to replace tissue biopsy. Thus, more sensitive assays must be developed.

LIQUID BIOPSY USING MALIGNANT EFFUSIONS

Malignant pleural effusions are a clinical problem in up to one-third of patients with advanced NSCLC [90,91]. Liquid biopsy of malignant pleural effusions has a relatively low sensitivity for the diagnosis of NSCLC, at approximately 60% [92]. For *EGFR* genotyping, cellular components, including cell block or cytology, are conventionally used, while supernatant fractions are usually discarded. Blind or closed needle pleural biopsy is sometimes indicated, although the diagnostic yield is typically low. Pleuroscopy, also known as medical thoracoscopy, has a higher diagnostic yield and provides better diagnostic sensitivity, but it is a highly invasive procedure. Even with pleuroscopy, adequate tissue biopsies are frequently unavailable due to co-morbidities or for other reasons.

A recent study demonstrated the superiority of using the cell-free supernatant from pleural effusions for *EGFR* mutation detection over using cell pellets [93-95]. *EGFR* genotyping using EV DNAs and cfDNAs from the supernatant of pleural effusions resulted in 100% agreement with tissue *EGFR* genotyping in both EGFR–tyrosine kinase inhibitor (TKI) naïve patients and patients who had acquired resistance to EGFR-TKI [96]. In

addition, it showed that the T790M detection rate using EV DNAs as a biosource was superior to using cell blocks or cfDNAs. These results suggest that the supernatant of pleural effusions is particularly effective for *EGFR* genotyping for patients with pulmonary adenocarcinoma when compared to doing conventional cytology or using cell block samples. Therefore, using EV DNAs from the supernatant of pleural effusions is promising for *EGFR* genotyping, including T790M detection, in pulmonary adenocarcinoma patients who develop pleural effusions.

LIQUID BIOPSY USING BRONCHOALVEOLAR LAVAGE FLUID

Bronchoalveolar lavage (BAL) is a procedure primarily done for diagnostic purposes by which the cellular and non-cellular contents of bronchial and alveolar spaces are obtained [97]. The advantages of BAL are that it is a minimally invasive method and provides access to the disease-located site of diffuse interstitial lung diseases. For lung cancer, BAL can provide a unique gateway to access the TME, where tumor cells are known to shed an abundance of EVs [98]. Correspondingly, the results of liquid biopsy using EVs isolated from the BALF of NSCLC patients have been shown to be superior to liquid biopsy using plasma cfDNAs.

Recent studies have demonstrated that EVs successfully isolated from the BALF of lung cancer patients contain an abundant amount of dsDNAs, and that liquid biopsy for *EGFR* genotyping using BALF is tissue-specific and extremely sensitive compared to using cfDNAs [16,76]. In a study performed with pathologically confirmed NSCLC patients, the sensitivity and specificity of BALF EV-based *EGFR* genotyping were high, and this assay showed an even better mutation detection rate than tissue/cytology-based typing. Also, the sensitivity increased as the stage progressed, reaching 100% with stage IV patient samples [76]. These results seem to suggest BALF EV-based *EGFR* genotyping is a highly promising liquid biopsy method, and particularly efficient for patients that require repeat biopsies throughout progression of the disease.

CONCLUSION

Tissue shortages caused by small biopsy sizes is emerging as a hurdle to the adequate treatment of advanced NSCLC patients in the era of precision oncology. A variety of molecular, genetic, and/or genomic tests, including real-time PCR, reverse transcription polymerase chain reaction, fluorescence in situ hybridization, immunohistochemistry, and NGS, are performed to match the right drugs to the right patients. A second or even third biopsy is frequently performed to investigate the acquired resistance to targeted therapeutic agents, such as *EGFR* or T790M mutations. The incidence of peripheral lung cancers, such as adenocarcinoma, which is usually confirmed by PCNB, is increasing. Moreover, the location of lung cancer development is clearly moving from central airways, in the past, to small airways or alveoli at present. GGNs detected by low-dose computed tomography are typically not accessible without surgical resection. Lung biopsy is an indispensable procedure for the diagnosis and treatment of lung cancer patients, but it is difficult to obtain adequate tissue for precision oncology in lung cancer. All of these are essential reasons for adopting liquid biopsy rapidly into the diagnosis and treatment of lung cancer, especially for NSCLC. As mentioned above, although cfDNA has been popularly used, it has intrinsic defects as a biosource for liquid biopsy due to its low stability. Although the use of improved technology with superior sensitivities, like digital PCR, BEAMing, and ultra-deep sequencing, can improve its utility to some degree, blood liquid biopsy using cfDNA cannot ultimately replace tissue biopsy due to its shortcomings. Specifically, that cfDNA is passively released from dead or dying tumor cells is a critical limitation, while EV DNA is actively released by living tumor cells, thereby reflecting their characteristics in real time.

Liquid biopsy will likely face challenges to becoming a reliable biosource despite technological advances. In this regard, EV-based BALF liquid biopsy is a highly-anticipated liquid biopsy platform for lung cancers. In the light of recent increases in the occurrence of peripheral lung adenocarcinomas, which carry a high risk of complications, the use of BALF is advantageous as it provides a unique, direct access route to the TME and a way to collect tumor-derived EVs in vivo. Studies on *EGFR* genotyping using BALF EV DNAs demonstrated that the use of EV DNAs, which are representative of genomic DNA, could yield results equivalent to those obtained using tissue DNA.

EV-based liquid biopsies are not widely available in hospitals and medical labs at present, as they require specific technology and equipment. For example, multiple different methods are being used to isolate EVs, such as differential centrifugation or density gradients used to remove larger cellular debris and isolate EVs, which means the biological properties and contents of the EVs are largely influenced by the method of isolation. Therefore, the optimization and validation of EV isolation methods remains crucial to establish EVs as a biomarker for diagnostic use. Nevertheless, with its high sensitivity and specificity, the application of

 https://doi.org/10.4132/jptm.2020.08.13

liquid biopsy using EV DNAs is expected to become more widely used clinically in the near future when an established method becomes available.

Ethics Statement

Not applicable.

ORCID

In Ae Kim https://orcid.org/0000-0002-8994-2891
Jae Young Hur https://orcid.org/0000-0001-6105-9899
Hee Joung Kim https://orcid.org/0000-0002-2516-5085
Seung Eun Lee https://orcid.org/0000-0002-7459-0061
Wan Seop Kim https://orcid.org/0000-0001-7704-5942
Kye Young Lee https://orcid.org/0000-0003-4687-5593

Author Contributions

Conceptualization: KYL, IAK, JYH. Investigation: IAK, JYH, SEL, WSK. Supervision: KYL. Writing—original draft: KYL, IAK, JYH, HJK. Writing—review & editing: KYL, IAK, JYH. Approval of final manuscript: all authors.

Conflicts of Interest

The authors declare that they have no potential conflicts of interest.

Funding Statement

No funding to declare.

Acknowledgments

We thank Dr. Min Kyo Jung for the electron microscopy image of BALF EVs.

References

1. Barta JA, Powell CA, Wisnivesky JP. Global epidemiology of lung cancer. Ann Glob Health 2019; 85: 8.
2. de Groot PM, Wu CC, Carter BW, Munden RF. The epidemiology of lung cancer. Transl Lung Cancer Res 2018; 7: 220-33.
3. Dela Cruz CS, Tanoue LT, Matthay RA. Lung cancer: epidemiology, etiology, and prevention. Clin Chest Med 2011; 32: 605-44.
4. Wu SG, Shih JY. Management of acquired resistance to EGFR TKI-targeted therapy in advanced non-small cell lung cancer. Mol Cancer 2018; 17: 38.
5. Imakita T, Matsumoto H, Hirano K, Morisawa T, Sakurai A, Kataoka Y. Impact on prognosis of rebiopsy in advanced non-small cell lung cancer patients after epidermal growth factor receptor-tyrosine kinase inhibitor treatment: a systematic review. BMC Cancer 2019; 19: 105.
6. Bollinger MK, Agnew AS, Mascara GP. Osimertinib: A third-generation tyrosine kinase inhibitor for treatment of epidermal growth factor receptor-mutated non-small cell lung cancer with the acquired Thr790Met mutation. J Oncol Pharm Pract 2018; 24: 379-88.
7. Akamatsu H, Katakami N, Okamoto I, et al. Osimertinib in Japanese patients with EGFR T790M mutation-positive advanced non-small-cell lung cancer: AURA3 trial. Cancer Sci 2018; 109: 1930-8.
8. Odogwu L, Mathieu L, Goldberg KB, et al. FDA benefit-risk assessment of osimertinib for the treatment of metastatic non-small cell lung cancer harboring epidermal growth factor receptor T790M mutation. Oncologist 2018; 23: 353-9.
9. Cheng F, Su L, Qian C. Circulating tumor DNA: a promising biomarker in the liquid biopsy of cancer. Oncotarget 2016; 7: 48832-41.
10. Mouliere F, Chandrananda D, Piskorz AM, et al. Enhanced detection of circulating tumor DNA by fragment size analysis. Sci Transl Med 2018; 10: eaat4921.
11. Gorgannezhad L, Umer M, Islam MN, Nguyen NT, Shiddiky MJ. Circulating tumor DNA and liquid biopsy: opportunities, challenges, and recent advances in detection technologies. Lab Chip 2018; 18: 1174-96.
12. Colombo M, Raposo G, Thery C. Biogenesis, secretion, and intercellular interactions of exosomes and other extracellular vesicles. Annu Rev Cell Dev Biol 2014; 30: 255-89.
13. Thery C, Zitvogel L, Amigorena S. Exosomes: composition, biogenesis and function. Nat Rev Immunol 2002; 2: 569-79.
14. Kahlert C, Melo SA, Protopopov A, et al. Identification of double-stranded genomic DNA spanning all chromosomes with mutated KRAS and p53 DNA in the serum exosomes of patients with pancreatic cancer. J Biol Chem 2014; 289: 3869-75.
15. Armstrong D, Wildman DE. Extracellular vesicles and the promise of continuous liquid biopsies. J Pathol Transl Med 2018; 52: 1-8.
16. Hur JY, Kim HJ, Lee JS, et al. Extracellular vesicle-derived DNA for performing EGFR genotyping of NSCLC patients. Mol Cancer 2018; 17: 15.
17. Cui S, Cheng Z, Qin W, Jiang L. Exosomes as a liquid biopsy for lung cancer. Lung Cancer 2018; 116: 46-54.
18. Crowley E, Di Nicolantonio F, Loupakis F, Bardelli A. Liquid biopsy: monitoring cancer-genetics in the blood. Nat Rev Clin Oncol 2013; 10: 472-84.
19. Pantel K, Alix-Panabieres C. Liquid biopsy and minimal residual disease: latest advances and implications for cure. Nat Rev Clin Oncol 2019; 16: 409-24.
20. Bracht JW, Mayo-de-Las-Casas C, Berenguer J, Karachaliou N, Rosell R. The present and future of liquid biopsies in non-small cell lung cancer: combining four biosources for diagnosis, prognosis, prediction, and disease monitoring. Curr Oncol Rep 2018; 20: 70.
21. Rolfo C, Castiglia M, Hong D, et al. Liquid biopsies in lung cancer: the new ambrosia of researchers. Biochim Biophys Acta 2014; 1846: 539-46.
22. Calabuig-Farinas S, Jantus-Lewintre E, Herreros-Pomares A, Camps C. Circulating tumor cells versus circulating tumor DNA in lung cancer-which one will win? Transl Lung Cancer Res 2016; 5: 466-82.
23. Haber DA, Velculescu VE. Blood-based analyses of cancer: circulating tumor cells and circulating tumor DNA. Cancer Discov 2014; 4: 650-61.
24. Cristofanilli M, Budd GT, Ellis MJ, et al. Circulating tumor cells, disease progression, and survival in metastatic breast cancer. N Engl J Med 2004; 351: 781-91.
25. Krebs MG, Hou JM, Sloane R, et al. Analysis of circulating tumor cells in patients with non-small cell lung cancer using epithelial marker-dependent and -independent approaches. J Thorac Oncol 2012; 7: 306-15.
26. Poudineh M, Sargent EH, Pantel K, Kelley SO. Profiling circulating tumour cells and other biomarkers of invasive cancers. Nat Biomed Eng 2018; 2: 72-84.
27. Nagrath S, Sequist LV, Maheswaran S, et al. Isolation of rare circulating tumour cells in cancer patients by microchip technology. Nature 2007; 450: 1235-9.
28. Qian W, Zhang Y, Chen W. Capturing cancer: emerging microflu-

idic technologies for the capture and characterization of circulating tumor cells. Small 2015; 11: 3850-72.
29. Diaz LA Jr, Bardelli A. Liquid biopsies: genotyping circulating tumor DNA. J Clin Oncol 2014; 32: 579-86.
30. Leon SA, Shapiro B, Sklaroff DM, Yaros MJ. Free DNA in the serum of cancer patients and the effect of therapy. Cancer Res 1977; 37: 646-50.
31. Karachaliou N, Sosa AE, Molina MA, Centelles Ruiz M, Rosell R. Possible application of circulating free tumor DNA in non-small cell lung cancer patients. J Thorac Dis 2017; 9(Suppl 13): S1364-72.
32. Chen M, Zhao H. Next-generation sequencing in liquid biopsy: cancer screening and early detection. Hum Genomics 2019; 13: 34.
33. Goldman JW, Noor ZS, Remon J, Besse B, Rosenfeld N. Are liquid biopsies a surrogate for tissue EGFR testing? Ann Oncol 2018; 29: i38-46.
34. Hochmair MJ, Buder A, Schwab S, et al. Liquid-biopsy-based identification of *EGFR* T790M mutation-mediated resistance to afatinib treatment in patients with advanced *EGFR* mutation-positive NSCLC, and subsequent response to osimertinib. Target Oncol 2019; 14: 75-83.
35. Rolfo C, Mack PC, Scagliotti GV, et al. Liquid biopsy for advanced non-small cell lung cancer (NSCLC): a statement paper from the IASLC. J Thorac Oncol 2018; 13: 1248-68.
36. Wan JC, Massie C, Garcia-Corbacho J, et al. Liquid biopsies come of age: towards implementation of circulating tumour DNA. Nat Rev Cancer 2017; 17: 223-38.
37. Best MG, Wesseling P, Wurdinger T. Tumor-educated platelets as a noninvasive biomarker source for cancer detection and progression monitoring. Cancer Res 2018; 78: 3407-12.
38. Nilsson RJ, Karachaliou N, Berenguer J, et al. Rearranged EML4-ALK fusion transcripts sequester in circulating blood platelets and enable blood-based crizotinib response monitoring in non-small-cell lung cancer. Oncotarget 2016; 7: 1066-75.
39. Liu L, Lin F, Ma X, Chen Z, Yu J. Tumor-educated platelet as liquid biopsy in lung cancer patients. Crit Rev Oncol Hematol 2020; 146: 102863.
40. McAllister SS, Weinberg RA. The tumour-induced systemic environment as a critical regulator of cancer progression and metastasis. Nat Cell Biol 2014; 16: 717-27.
41. Best MG, Sol N, Kooi I, et al. RNA-Seq of tumor-educated platelets enables blood-based pan-cancer, multiclass, and molecular pathway cancer diagnostics. Cancer Cell 2015; 28: 666-76.
42. Choi DS, Kim DK, Kim YK, Gho YS. Proteomics of extracellular vesicles: exosomes and ectosomes. Mass Spectrom Rev 2015; 34: 474-90.
43. Keller S, Ridinger J, Rupp AK, Janssen JW, Altevogt P. Body fluid derived exosomes as a novel template for clinical diagnostics. J Transl Med 2011; 9: 86.
44. Carnino JM, Lee H, Jin Y. Isolation and characterization of extracellular vesicles from broncho-alveolar lavage fluid: a review and comparison of different methods. Respir Res 2019; 20: 240.
45. Aldick T, Bielaszewska M, Uhlin BE, Humpf HU, Wai SN, Karch H. Vesicular stabilization and activity augmentation of enterohaemorrhagic *Escherichia coli* haemolysin. Mol Microbiol 2009; 71: 1496-508.
46. Dutta S, Iida K, Takade A, Meno Y, Nair GB, Yoshida S. Release of Shiga toxin by membrane vesicles in Shigella dysenteriae serotype 1 strains and in vitro effects of antimicrobials on toxin production and release. Microbiol Immunol 2004; 48: 965-9.
47. Choi D, Lee TH, Spinelli C, Chennakrishnaiah S, D'Asti E, Rak J. Extracellular vesicle communication pathways as regulatory targets of oncogenic transformation. Semin Cell Dev Biol 2017; 67: 11-22.
48. Soldevilla B, Rodriguez M, San Millan C, et al. Tumor-derived exosomes are enriched in DeltaNp73, which promotes oncogenic potential in acceptor cells and correlates with patient survival. Hum Mol Genet 2014; 23: 467-78.
49. Peinado H, Aleckovic M, Lavotshkin S, et al. Melanoma exosomes educate bone marrow progenitor cells toward a pro-metastatic phenotype through MET. Nat Med 2012; 18: 883-91.
50. Umezu T, Ohyashiki K, Kuroda M, Ohyashiki JH. Leukemia cell to endothelial cell communication via exosomal miRNAs. Oncogene 2013; 32: 2747-55.
51. Abd Elmageed ZY, Yang Y, Thomas R, et al. Neoplastic reprogramming of patient-derived adipose stem cells by prostate cancer cell-associated exosomes. Stem Cells 2014; 32: 983-97.
52. Melo SA, Sugimoto H, O'Connell JT, et al. Cancer exosomes perform cell-independent microRNA biogenesis and promote tumorigenesis. Cancer Cell 2014; 26: 707-21.
53. Greening DW, Gopal SK, Xu R, Simpson RJ, Chen W. Exosomes and their roles in immune regulation and cancer. Semin Cell Dev Biol 2015; 40: 72-81.
54. Hsu YL, Hung JY, Chang WA, et al. Hypoxic lung cancer-secreted exosomal miR-23a increased angiogenesis and vascular permeability by targeting prolyl hydroxylase and tight junction protein ZO-1. Oncogene 2017; 36: 4929-42.
55. Li X, Wang S, Zhu R, Li H, Han Q, Zhao RC. Lung tumor exosomes induce a pro-inflammatory phenotype in mesenchymal stem cells via NFkappaB-TLR signaling pathway. J Hematol Oncol 2016; 9: 42.
56. Fujita Y, Kosaka N, Araya J, Kuwano K, Ochiya T. Extracellular vesicles in lung microenvironment and pathogenesis. Trends Mol Med 2015; 21: 533-42.
57. Jung JH, Lee MY, Choi DY, et al. Phospholipids of tumor extracellular vesicles stratify gefitinib-resistant nonsmall cell lung cancer cells from gefitinib-sensitive cells. Proteomics 2015; 15: 824-35.
58. Logozzi M, De Milito A, Lugini L, et al. High levels of exosomes expressing CD63 and caveolin-1 in plasma of melanoma patients. PLoS One 2009; 4: e5219.
59. Hoshino A, Costa-Silva B, Shen TL, et al. Tumour exosome integrins determine organotropic metastasis. Nature 2015; 527: 329-35.
60. Lu Q, Zhang J, Allison R, et al. Identification of extracellular delta-catenin accumulation for prostate cancer detection. Prostate 2009; 69: 411-8.
61. Moon PG, Lee JE, Cho YE, et al. Identification of developmental endothelial locus-1 on circulating extracellular vesicles as a novel biomarker for early breast cancer detection. Clin Cancer Res 2016; 22: 1757-66.
62. Rontogianni S, Synadaki E, Li B, et al. Proteomic profiling of extracellular vesicles allows for human breast cancer subtyping. Commun Biol 2019; 2: 325.
63. Liu Q, Yu Z, Yuan S, et al. Circulating exosomal microRNAs as prognostic biomarkers for non-small-cell lung cancer. Oncotarget 2017; 8: 13048-58.
64. Yuwen DL, Sheng BB, Liu J, Wenyu W, Shu YQ. MiR-146a-5p level in serum exosomes predicts therapeutic effect of cisplatin in non-small cell lung cancer. Eur Rev Med Pharmacol Sci 2017; 21: 2650-8.
65. Thakur BK, Zhang H, Becker A, et al. Double-stranded DNA in

exosomes: a novel biomarker in cancer detection. Cell Res 2014; 24: 766-9.
66. Vagner T, Spinelli C, Minciacchi VR, et al. Large extracellular vesicles carry most of the tumour DNA circulating in prostate cancer patient plasma. J Extracell Vesicles 2018; 7: 1505403.
67. Kahlert C. Liquid biopsy: is there an advantage to analyzing circulating exosomal DNA compared to cfDNA or are they the same? Cancer Res 2019; 79: 2462-5.
68. Lazaro-Ibanez E, Lasser C, Shelke GV, et al. DNA analysis of low- and high-density fractions defines heterogeneous subpopulations of small extracellular vesicles based on their DNA cargo and topology. J Extracell Vesicles 2019; 8: 1656993.
69. Sharma A, Johnson A. Exosome DNA: critical regulator of tumor immunity and a diagnostic biomarker. J Cell Physiol 2020; 235: 1921-32.
70. Mouliere F, Robert B, Arnau Peyrotte E, et al. High fragmentation characterizes tumour-derived circulating DNA. PLoS One 2011; 6: e23418.
71. Zill OA, Greene C, Sebisanovic D, et al. Cell-free DNA next-generation sequencing in pancreatobiliary carcinomas. Cancer Discov 2015; 5: 1040-8.
72. San Lucas FA, Allenson K, Bernard V, et al. Minimally invasive genomic and transcriptomic profiling of visceral cancers by next-generation sequencing of circulating exosomes. Ann Oncol 2016; 27: 635-41.
73. Song Z, Cai Z, Yan J, Shao YW, Zhang Y. Liquid biopsies using pleural effusion-derived exosomal DNA in advanced lung adenocarcinoma. Transl Lung Cancer Res 2019; 8: 392-400.
74. Lee DH, Yoon H, Park S, et al. Urinary Exosomal and cell-free DNA detects somatic mutation and copy number alteration in urothelial carcinoma of bladder. Sci Rep 2018; 8: 14707.
75. Schwarzenbach H, Hoon DS, Pantel K. Cell-free nucleic acids as biomarkers in cancer patients. Nat Rev Cancer 2011; 11: 426-37.
76. Hur JY, Lee JS, Kim IA, Kim HJ, Kim WS, Lee KY. Extracellular vesicle-based *EGFR* genotyping in bronchoalveolar lavage fluid from treatment-naive non-small cell lung cancer patients. Transl Lung Cancer Res 2019; 8: 1051-60.
77. Bernard V, Kim DU, San Lucas FA, et al. Circulating nucleic acids are associated with outcomes of patients with pancreatic cancer. Gastroenterology 2019; 156: 108-18.
78. Allenson K, Castillo J, San Lucas FA, et al. High prevalence of mutant *KRAS* in circulating exosome-derived DNA from early-stage pancreatic cancer patients. Ann Oncol 2017; 28: 741-7.
79. Karlovich C, Goldman JW, Sun JM, et al. Assessment of *EGFR* mutation status in matched plasma and tumor tissue of NSCLC patients from a phase I study of rociletinib (CO-1686). Clin Cancer Res 2016; 22: 2386-95.
80. Oxnard GR, Thress KS, Alden RS, et al. Association between plasma genotyping and outcomes of treatment with osimertinib (AZD9291) in advanced non-small-cell lung cancer. J Clin Oncol 2016; 34: 3375-82.
81. Sacher AG, Paweletz C, Dahlberg SE, et al. Prospective validation of rapid plasma genotyping for the detection of *EGFR* and *KRAS* mutations in advanced lung cancer. JAMA Oncol 2016; 2: 1014-22.
82. Helman E, Nguyen M, Karlovich CA, et al. Cell-free DNA next-generation sequencing prediction of response and resistance to third-generation EGFR inhibitor. Clin Lung Cancer 2018; 19: 518-30.
83. Brinkman K, Meyer L, Bickel A, et al. Extracellular vesicles from plasma have higher tumour RNA fraction than platelets. J Extracell Vesicles 2020; 9: 1741176.
84. Qi Y, Zha W, Zhang W. Exosomal miR-660-5p promotes tumor growth and metastasis in non-small cell lung cancer. J BUON 2019; 24: 599-607.
85. Zhang Y, Zhang Y, Yin Y, Li S. Detection of circulating exosomal miR-17-5p serves as a novel non-invasive diagnostic marker for non-small cell lung cancer patients. Pathol Res Pract 2019; 215: 152466.
86. Grimolizzi F, Monaco F, Leoni F, et al. Exosomal miR-126 as a circulating biomarker in non-small-cell lung cancer regulating cancer progression. Sci Rep 2017; 7: 15277.
87. Jin X, Chen Y, Chen H, et al. Evaluation of tumor-derived exosomal miRNA as potential diagnostic biomarkers for early-stage non-small cell lung cancer using next-generation sequencing. Clin Cancer Res 2017; 23: 5311-9.
88. Hu Z, Chen X, Zhao Y, et al. Serum microRNA signatures identified in a genome-wide serum microRNA expression profiling predict survival of non-small-cell lung cancer. J Clin Oncol 2010; 28: 1721-6.
89. Krug AK, Enderle D, Karlovich C, et al. Improved *EGFR* mutation detection using combined exosomal RNA and circulating tumor DNA in NSCLC patient plasma. Ann Oncol 2018; 29: 700-6.
90. Morgensztern D, Waqar S, Subramanian J, Trinkaus K, Govindan R. Prognostic impact of malignant pleural effusion at presentation in patients with metastatic non-small-cell lung cancer. J Thorac Oncol 2012; 7: 1485-9.
91. William WN Jr, Lin HY, Lee JJ, Lippman SM, Roth JA, Kim ES. Revisiting stage IIIB and IV non-small cell lung cancer: analysis of the surveillance, epidemiology, and end results data. Chest 2009; 136: 701-9.
92. Hooper C, Lee YC, Maskell N, Group BTSPG. Investigation of a unilateral pleural effusion in adults: British Thoracic Society Pleural Disease Guideline 2010. Thorax 2010; 65 Suppl 2: ii4-17.
93. Lin J, Gu Y, Du R, Deng M, Lu Y, Ding Y. Detection of *EGFR* mutation in supernatant, cell pellets of pleural effusion and tumor tissues from non-small cell lung cancer patients by high resolution melting analysis and sequencing. Int J Clin Exp Pathol 2014; 7: 8813-22.
94. Shin S, Kim J, Kim Y, Cho SM, Lee KA. Assessment of real-time PCR method for detection of *EGFR* mutation using both supernatant and cell pellet of malignant pleural effusion samples from non-small-cell lung cancer patients. Clin Chem Lab Med 2017; 55: 1962-9.
95. Qu X, Li Q, Yang J, et al. Double-stranded DNA in exosomes of malignant pleural effusions as a novel DNA source for *EGFR* mutation detection in lung adenocarcinoma. Front Oncol 2019; 9: 931.
96. Lee JS, Hur JY, Kim IA, et al. Liquid biopsy using the supernatant of a pleural effusion for EGFR genotyping in pulmonary adenocarcinoma patients: a comparison between cell-free DNA and extracellular vesicle-derived DNA. BMC Cancer 2018; 18: 1236.
97. Domagala-Kulawik J. The relevance of bronchoalveolar lavage fluid analysis for lung cancer patients. Expert Rev Respir Med 2020; 14: 329-37.
98. Miller RJ, Casal RF, Lazarus DR, Ost DE, Eapen GA. Flexible bronchoscopy. Clin Chest Med 2018; 39: 1-16.

JPTM
Journal of Pathology and Translational Medicine 2020; 54: 462-470
https://doi.org/10.4132/jptm.2020.07.11

ORIGINAL ARTICLE

A machine-learning expert-supporting system for diagnosis prediction of lymphoid neoplasms using a probabilistic decision-tree algorithm and immunohistochemistry profile database

Yosep Chong[1,2], Ji Young Lee[1], Yejin Kim[3,4], Jingyun Choi[5], Hwanjo Yu[5], Gyeongsin Park[1], Mee Yon Cho[6], Nishant Thakur[1]

[1]Department of Hospital Pathology, College of Medicine, The Catholic University of Korea, Seoul;
[2]Postech-Catholic Biomedical Engineering Institute, College of Medicine, The Catholic University of Korea, Seoul;
[3]Department of Creative Information Technology, POSTECH, Pohang, Korea;
[4]University of Texas Health Science Center, Houston, TX, USA;
[5]Computer Science and Engineering, POSTECH, Pohang;
[6]Department of Pathology, Yonsei University Wonju College of Medicine, Wonju, Korea

Background: Immunohistochemistry (IHC) has played an essential role in the diagnosis of hematolymphoid neoplasms. However, IHC interpretations can be challenging in daily practice, and exponentially expanding volumes of IHC data are making the task increasingly difficult. We therefore developed a machine-learning expert-supporting system for diagnosing lymphoid neoplasms. **Methods:** A probabilistic decision-tree algorithm based on the Bayesian theorem was used to develop mobile application software for iOS and Android platforms. We tested the software with real data from 602 training and 392 validation cases of lymphoid neoplasms and compared the precision hit rates between the training and validation datasets. **Results:** IHC expression data for 150 lymphoid neoplasms and 584 antibodies was gathered. The precision hit rates of 94.7% in the training data and 95.7% in the validation data for lymphomas were not statistically significant. Results in most B-cell lymphomas were excellent, and generally equivalent performance was seen in T-cell lymphomas. The primary reasons for lack of precision were atypical IHC profiles for certain cases (e.g., CD15-negative Hodgkin lymphoma), a lack of disease-specific markers, and overlapping IHC profiles of similar diseases. **Conclusions:** Application of the machine-learning algorithm to diagnosis precision produced acceptable hit rates in training and validation datasets. Because of the lack of origin- or disease-specific markers in differential diagnosis, contextual information such as clinical and histological features should be taken into account to make proper use of this system in the pathologic decision-making process.

Key Words: Database; Expert-supporting system; Machine learning; Immunohistochemistry; Probabilistic decision tree

Received: October 10, 2019 **Revised:** July 3, 2020 **Accepted:** July 11, 2020
Corresponding Author: Yosep Chong, MD, PhD, Department of Hospital Pathology, Yeouido St. Mary's Hospital, College of Medicine, The Catholic University of Korea, 10 63-ro, Yeongdeungpo-gu, Seoul 07345, Korea
Tel: +82-2-3779-1295, Fax: +82-2-783-6648, E-mail: ychong@catholic.ac.kr

Immunohistochemical (IHC) staining is a valuable and unique tissue-staining method for pathologic diagnosis of hematolymphoid neoplasms using an antigen-antibody reaction [1-6]. It was developed as an indirect immunofluorescence technique in 1941 by Albert Coons at Harvard University [1,7]. As the IHC technique evolved to use paraffin-embedded tissues and enzymatic markers, it has become an essential and routine tool in pathologic diagnoses, notably in hematopathology [2-6]. Hematolymphoid neoplasms are categorized as B-cell, T-cell, NK/T-cell, and histiocytic neoplasms according to the IHC profiles of CD3 (T-cell marker), CD20 (B-cell marker), CD56 (NK-cell marker), CD68 (histiocytic marker), and other markers related to the development of hematolymphoid cells. Once the morphologic features that distinguish among the possible groups are recognized in differential diagnosis, relevant IHC panels can be chosen for subtype determination (Supplementary Fig. S1). This process requires the pathologists' intuition and comprehensive integration of both the clinicopathologic findings and IHC results because hematolymphoid neoplasms share many cytomorphologic and clinicopathologic features across different diseases. The accurate subtyping of lymphomas is therefore highly dependent on the appropriate choice of IHC panels and the inter-

pISSN 2383-7837
eISSN 2383-7845

pretation of IHC results [1-3,8].

However, increasing knowledge of IHC positivity in each tumor can produce conflicting interpretations in daily practice, especially in some more complex cases [9]. The pathologic analysis of IHC results depends largely on the expertise of pathologists, who can be easily biased by their experiences [2,4,6]. New antibodies and IHC data from various tumors are introduced annually, and more than 100,000 studies using IHC have been published since 2000, making it difficult to memorize the newly developed antibodies and recognize the expression characteristics of tumors just in the human brain [10-14]. In addition, recent advances in digital pathology require an appropriate reference database of ancillary tests to integrate medical knowledge and individual medical problems [15].

Attempts have been made to address this problem by adopting an algorithmic approach or using standardized IHC panels for specific differential diagnosis [9,14,16]. However, the clinical situation of each case is unique, and generalized application of a particular IHC panel or specific algorithm can be time- and labor-consuming.

We therefore developed an expert-supporting system using software based on a machine-learning algorithm and an IHC database that supports pathological decision-making and differential diagnosis. We developed the software as a mobile application for iOS and Android devices for practical utility.

MATERIALS AND METHODS

Development of a machine-learning algorithm using a probabilistic decision tree

According to Bayes' theorem, post-event probability can be calculated when pre-event probability is given. Bayes' theorem is stated mathematically as

$$P(A|B) = \frac{P(B|A)P(A)}{P(B)},$$

where A and B are events and P(B)≠016 and P(A|B), and P(B|A) are the respective conditional probability that the likelihood of event A occurring given that B is true and vice versa. P(A) and P(B) are the probabilities of observing A and B independently of each other [16,17].

A probabilistic decision tree is a predictive modeling approach in statistics and data mining. It is often used for machine-learning algorithms, especially when test node results are binary (Fig. 1). We adopted such a tree for our machine-learning algorithm because IHC results are binary, and the probability can be expressed as a database.

To apply the probabilistic decision-tree algorithm, we required a database of a 2×2 table with tests, diseases, and the probability of positivity of each test for each disease (Fig. 2). Test results were binary, and the probability of positivity was the number of positive cases among all cases of the disease. Once test results were available, we calculated the probability of each disease by multiplying prior probability by the probability that each test was positive or negative to determine the most probably illness by comparing post-probabilities.

IHC database build

We assembled a database of IHC expression profiles of the lymphoid neoplasms using five primary textbooks and other publications, including the World Health Organization (WHO) classification of tumors of hematopoietic and lymphoid tissues (IARC, Lyon, France) and major IHC textbooks (Supplementary Table S1) [4,5,18-21]. More than 200 lymphoid neoplasms and tumor names were documented according to the WHO classification. Tumors without IHC profile data or no diagnostic use were excluded. Subtypes of certain tumors were documented separately from the primary type if there was a difference in IHC

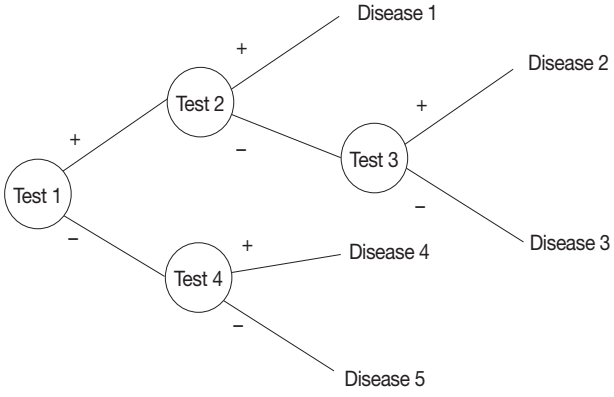

Fig. 1. A probabilistic decision tree for a machine-learning algorithm in diagnostic tests and disease.

	Test A	Text B	Text C	Prior probability		Post probability
Disease 1 (30%)	60%	30%	0%	0.3×	0.6×0.7×0.0	= 0.000
Disease 2 (50%)	20%	80%	10%	0.5×	0.2×0.2×0.1	= 0.002
Disease 3 (20%)	50%	50%	70%	0.2×	0.5×0.5×0.7	= 0.035
Test results	+	–	+	The probability of disease 3 is the highest with the test results		

Fig. 2. Prior and post probability based on Bayes' theorem.

profiles.

The IHC positivity for each tumor was drawn from textbook descriptions; if there was exact numerical value was replaced by arbitrary expressions such as "always positive," "often positive," or "rarely/occasionally positive," positivity was documented as follows: always, 95%; often, 75%; in about a half of cases, 50%; seldom, 30%; rarely/occasionally, 10%; never, 0%. If the positivity differed between textbooks, the average value was used. An example of the IHC database appears in Supplementary Fig. S2.

Approximately 600 IHC antibody names were documented using the textbooks, and their synonyms were recorded and revised with online references (Supplementary Table S2).

Development of a mobile application

The reactive native (network-free) mobile application "ImmunoGenius" was developed using NoSQL for iOS and Android (Fig. 3), which can be used on iOS and Android devices. It was designed to search and select diseases and generate a 2×2 table with the disease name in the left column and IHC antibody names on the first row. Representative IHC profiles appear in the corresponding cells as ++ for 75%–100% positivity (positive cases per all tumors), + for 50%–74%, +/– for 30%–49%, –/+ for 10%–29%, and – for 0%–9% with graded shades (Fig. 3, Supplementary Fig. S3, Supplementary Video 1). Users can compare IHC profiles between the selected diseases and add or remove rows (diseases) or columns (IHC antibodies) to customize the table. Additional IHCs can be added using the buttons on the right side. Once the user inputs the IHC results for their case, the 10 most probable diagnoses as calculated by the diagnosis precision algorithm appear below, along with estimated probability in percentage (red numbers) (Supplementary Fig. S3, Supplementary Video 1, 2). For predictive diagnosis of lymphomas, prior probability was set according to epidemiologic data for Korea in 2010 (but can be changed to other epidemiologic groups later).

Diagnosis precision algorithm validation using patient data

To validate the hit rate of the diagnosis precision algorithm, the IHC profile data and diagnoses originally made by pathologists were compared with the top 10 predictive diagnoses produced by the algorithm. Approximately 1,000 cases of the lymphoma-patient IHC profile data were obtained from the archives of two independent university hospitals: Yeouido, and Seoul St. Mary's Hospital, College of Medicine, The Catholic University of Korea, from 2010 to 2017. Approximately 80 percent of the lymphoma cases at Seoul St. Mary's Hospital were referred from various institutes in Korea. Any patient data related to identification except the original diagnosis and the IHC results were blinded before data processing. The retrieved data were divided 6:4 for training and validation. Cases with an inconclusive diagnosis or inadequate IHC profile (fewer than three antibodies, inconclusive results, absence of markers for tumor origins, but only prognostic or therapeutic markers such as epidermal growth factor receptor or p53) were excluded. An example of a retrieved patient IHC profile dataset appeared in Supplementary Fig. S4. The diagnosis precision hit rate was determined by the inclusion of the original diagnosis in the top 10 predictive diagnoses drawn by the algorithm. It was considered inclusive if there was no sig-

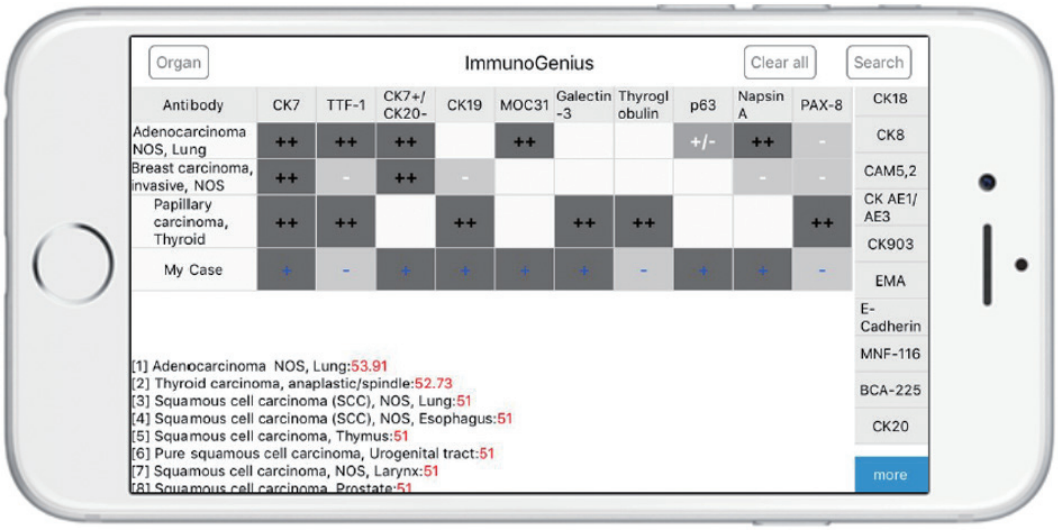

Fig. 3. A screenshot of the mobile application "ImmunoGenius."

https://doi.org/10.4132/jptm.2020.07.11

nificant difference in the IHC profile between the original and predictive diagnosis, and the only difference was in location if two diagnoses shared the same origin of cells (e.g., nodal marginal zone lymphoma vs. extranodal marginal zone lymphoma). Validation of the algorithm was carried out by comparing the hit rate of the training and validation data in lymphomas. If no statistically significant difference was found between the training and validation dataset, the algorithm was considered validated.

Statistical analysis

Time and computational complexity were evaluated by testing the mobile application. The hit rate between original and predictive diagnoses was compared by chi-square tests. Statistical analysis was performed using Web-R ("http://web-r.org"), a web-based statistical analysis program.

RESULTS

IHC database build and recruitment of training and validation datasets

A total of 150 hematolymphoid neoplasms and 584 IHC antibodies and their IHC profiles were documented. The obtained training and validation data of lymphoma amounted to 639 and 392 cases, respectively. In the lymphoma cases, an average of 8.5 IHC antibodies (range, 1 to 18) were used for diagnosis, and 40 types of lymphomas were included. Two cases were excluded because of inconclusive diagnosis, and 35 cases with fewer than 3 IHC tested antibodies were omitted. As a result, 602 cases of lymphomas were used for training. The original diagnoses of the training data cases are provided in Table 1. Diffuse large B-cell lymphoma, not otherwise specified (DLBCL, NOS) was the most common, with 216 cases (34.3%), and the second most common was extranodal marginal zone lymphoma of mucosa-associated lymphoid tissue (MALT), with 78 cases (13.0%). The original diagnoses of the validation cases are also provided in Table 1. The most and the second most common type were the same as DLBCL, NOS, and MALT lymphoma, with similar percentages (145, 37.0% and 74, 18.9%, respectively).

Training data

The hit rate for training data of the predictive diagnosis (top 10) was 94.7% (Table 2). Detailed results of discordant cases between the original and predictive diagnoses are supplied in Table 2. In B-cell lymphomas, the hit rate of the predictive diagnosis was relatively high, particularly in DLBCL, follicular lymphoma, chronic lymphocytic leukemia/small lymphocytic lymphoma (CLL/SLL) and MALT lymphoma with zero error rates. The diagnoses showed generally good performance in most B-cell lymphomas, with the exception of plasmablastic lymphoma (three errors out of three cases, 100%) and one mantle cell lymphoma (MCL). In T-cell lymphomas, the algorithm achieved a performance that is generally equivalent to that in B-cell lymphomas except for T lymphoblastic leukemia/lymphoma (no error in 17 cases) and extranodal NK/T-cell lymphoma, nasal type (no error in 25 cases). In enteropathy-associated T-cell lymphoma, peripheral T-cell lymphoma, NOS, anaplastic large cell lymphoma (ALCL), anaplastic lymphoma kinase (ALK)–negative, and angioimmunoblastic T-cell lymphoma, the error rates were 50.0%, 34.7%, 43.8%, and 33.3%, respectively. In Hodgkin lymphomas, the error rates were 12.5% in classical Hodgkin lymphoma, NOS, and 14.3% in nodular sclerosis subtype.

Validation data

In the validation data, the hit rate of the predictive diagnosis (top 10) was 95.7% (Table 2). Detailed results of the discordant cases for the original and predictive diagnoses are provided in Table 2. In B-cell lymphomas, the hit rate of predictive diagnosis was relatively high for DLBCL, follicular lymphoma, CLL/SLL, MALT lymphoma, and MCL with zero error rates. Generally good performance was seen in most B-cell lymphomas, with the exception of primary cutaneous follicle center lymphoma (1 error out of 2 cases, 50.0%). In T-cell lymphomas, performance was generally equivalent to that in B-cell lymphomas with the exception of T lymphoblastic leukemia/lymphoma (no errors in 7 cases), extranodal NK/T-cell lymphoma, and nasal type (no errors in 15 cases). In enteropathy-associated T-cell lymphoma, primary cutaneous CD8-positive, aggressive epidermotropic cytotoxic T-cell lymphoma, peripheral T-cell lymphoma, NOS, ALCL, ALK-negative, and angioimmunoblastic T-cell lymphoma, the error rates were 50.0%, 50.0%, 33.3%, 42.8%, and 33.3%, respectively. In Hodgkin lymphomas, the error rates were 50.0% in nodular lymphocyte-predominant Hodgkin lymphoma, 18.2% in classical Hodgkin lymphoma, NOS, 20.0% in nodular sclerosis subtype, and 33.3% in lymphocyte-depleted subtype.

Precision error rates between training and validation dataset

The error rates of the predictive diagnosis were 5.3% in training data and 4.3% in validation data. The error rates of both groups were not significantly different ($p = 0.543$) (Table 3). The overall hit rate was 95.0% in lymphomas (Table 3).

DISCUSSION

We verified that it is possible to calculate the probability of a specific disease for a particular case, especially lymphomas, using IHC results, a probabilistic decision tree, and a mobile application. The diagnosis precision drawn by the probabilistic decision-tree algorithm achieved a hit rate of 95.0% for lymphomas. The hit rates between training and validation dataset did not differ significantly in lymphomas (94.7% vs. 95.7%, p = 0.543).

The hit rate of the diagnosis precision algorithm was relatively

Table 1. The original diagnosis of the training and validation dataset of lymphomas

Original diagnosis	Training data	Validation data
B lymphoblastic leukemia/lymphoma	8 (1.3)	5 (1.3)
Chronic lymphocytic leukemia/small lymphocytic lymphoma	20 (3.3)	11 (2.8)
Extranodal marginal zone lymphoma of MALT (lymphoma)	78 (13.0)	74 (18.9)
Nodal marginal zone lymphoma	4 (0.7)	5 (1.3)
Plasma cell myeloma	3 (0.5)	0
Follicular lymphoma		
Grade 1, 2, 3A	59 (9.8)	16 (4.1)
Grade 3B	3 (0.5)	6 (1.5)
Mantle cell lymphoma	24 (4.0)	19 (4.8)
DLBCL		
NOS	216 (34.3)	145 (37.0)
T-cell/histiocyte-rich	2 (0.3)	0
Primary DLBCL of the CNS	9 (1.4)	0
CD5+ DLBCL	1 (0.2)	2 (0.5)
EBV positive DLBCL of elderly	1 (0.2)	0
Anaplastic variant	0	4 (1.0)
Primary cutaneous DLBCL, leg type	0	1 (0.3)
Primary mediastinal (thymic) large B-cell lymphoma	9 (1.5)	3 (0.8)
Plasmablastic lymphoma	3 (0.5)	0
Primary effusion lymphoma	1 (0.2)	0
Burkitt lymphoma	17 (2.8)	11 (2.8)
B-cell lymphoma, unclassifiable, with features intermediate between DLBCL and Burkitt lymphoma	3 (0.5)	0
Primary cutaneous follicle centre lymphoma	0	2 (0.5)
T lymphoblastic leukemia/lymphoma	17 (2.8)	7 (1.8)
Extranodal NK/T-cell lymphoma. nasal type	25 (4.2)	15 (3.8)
Adult T-cell leukemia/ lymphoma	1 (0.2)	0
Enteropathy-associated T-cell lymphoma	6 (1.0)	4 (1.0)
Aggressive NK-cell leukemia	1 (0.2)	0
Lymphomatoid papulosis type B	1 (0.2)	0
Mycosis fungoides	0	3 (0.8)
Primary cutaneous (CD30-positive T-cell) ALCL	1 (0.2)	0
Primary cutaneous CD8 positive aggressive epidermotropic cytotoxic T-cell lymphoma	0	2 (0.5)
Subcutaneous panniculitis-like T-cell lymphoma	0	1 (0.3)
Peripheral T-cell lymphoma, NOS	23 (3.8)	12 (3.1)
Angioimmunoblastic T-cell lymphoma	16 (2.7)	7 (1.8)
ALCL, ALK-positive	5 (0.8)	2 (0.5)
ALCL, ALK-negative	9 (1.5)	6 (1.5)
Nodular lymphocyte-predominant Hodgkin lymphoma	0	2 (0.5)
Classical Hodgkin lymphoma, NOS	8 (1.3)	11 (2.8)
Nodular sclerosis classical Hodgkin lymphoma	21 (3.5)	5 (1.3)
Mixed cellularity classical Hodgkin lymphoma	7 (1.2)	8 (2.0)
Lymphocyte-depleted classical Hodgkin lymphoma	0	3 (0.8)
Total	602 (100)	392 (100)

Values are presented as number (%).
MALT, mucosa-associated lymphoid tissue; DLBCL, diffuse large B-cell lymphoma; NOS, not otherwise specified; CNS, central nervous system; EBV, Epstein-Barr virus; NK, natural killer; ALCL, anaplastic large cell lymphoma; ALK, anaplastic lymphoma kinase.

https://doi.org/10.4132/jptm.2020.07.11

Table 2. Cases with discordant results between the original and predictive diagnosis in training and validation data when searched among lymphomas

Original diagnosis	Error/No. (%)	
	Training data	Validation data
B lymphoblastic leukemia/lymphoma	0/8	0/5
Chronic lymphocytic leukemia/small lymphocytic lymphoma	0/20	0/11
Extranodal marginal zone lymphoma of MALT (lymphoma)	0/78	0/74
Nodal marginal zone lymphoma	0/4	0/5
Plasma cell myeloma	0/3	0/0
Follicular lymphoma		
Grade 1, 2, 3A	0/59	0/16
Grade 3B	0/3	0/6
Mantle cell lymphoma	1/24 (4.2)	0/19
DLBCL		
NOS	0/216	0/145
T-cell/histiocyte-rich	0/2	0/0
Primary DLBCL of the CNS	0/9	0/0
CD5+ DLBCL	0/1	0/2
EBV positive DLBCL of elderly	0/1	0/0
Anaplastic variant	0/0	0/4
Primary cutaneous DLBCL, leg type	0/0	0/1
Primary mediastinal (thymic) large B-cell lymphoma	0/9	0/3
Plasmablastic lymphoma	3/3 (100)	0/0
Primary effusion lymphoma	0/1	0/0
Burkitt lymphoma	0/17	0/11
B-cell lymphoma, unclassifiable, with features intermediate between DLBCL and Burkitt lymphoma	0/3	0/0
Primary cutaneous follicle centre lymphoma	0/0	1/2 (50.0)
T lymphoblastic leukemia/lymphoma	0/17	0/7
Extranodal NK/T-cell lymphoma, nasal type	0/25	0/15
Adult T-cell leukemia/ lymphoma	1/1 (100)	0/0
Enteropathy-associated T-cell lymphoma	3/6 (50.0)	2/4 (50.0)
Aggressive NK-cell leukemia	0/1	0/0
Lymphomatoid papulosis type B	0/1	0/0
Mycosis fungoides	0/0	0/3
Primary cutaneous (CD30-positive T-cell) ALCL	0/1	0/0
Primary cutaneous CD8-positive aggressive epidermotropic cytotoxic T-cell lymphoma	0/0	1/2 (50.0)
Subcutaneous panniculitis-like T-cell lymphoma	0/0	0/1
Peripheral T-cell lymphoma, NOS	9/23 (34.7)	4/12 (33.3)
Angioimmunoblastic T-cell lymphoma	8/16 (43.8)	3/7 (42.8)
ALCL, ALK-positive	0/5	0/2
ALCL, ALK-negative	3/9 (33.3)	2/6 (33.3)
Nodular lymphocyte-predominant Hodgkin lymphoma	0/0	1/2 (50.0)
Classical Hodgkin lymphoma, NOS	1/8 (12.5)	2/11 (18.2)
Nodular sclerosis classical Hodgkin lymphoma	3/21 (14.3)	1/5 (20.0)
Mixed cellularity classical Hodgkin lymphoma	0/7	0/8
Lymphocyte-depleted classical Hodgkin lymphoma	0/0	1/3 (33.3)
Total	32/602 (5.3)	17/392 (4.3)

MALT, mucosa-associated lymphoid tissue; DLBCL, diffuse large B-cell lymphoma; NOS, not otherwise specified; CNS, central nervous system; EBV, Epstein-Barr virus; NK, natural killer; ALCL, anaplastic large cell lymphoma; ALK, anaplastic lymphoma kinase.

Table 3. A comparison of precision error rates between the training and validation dataset of lymphomas

Precision diagnosis	Training data	Validation data	Total	p-value
Accurate results	570 (94.7)	365 (95.7)	935 (95.0)	0.543
Error results	32 (5.3)	17 (4.3)	49 (5.0)	
Total	602 (100)	382 (100)	984 (100)	

Values are presented as number (%).

high in most B-cell lymphomas, including DLBCL, follicular lymphoma, CLL/SLL, MALT lymphoma, and Burkitt lymphoma with zero errors, which represents the majority of all lymphoma cases (approximately two-thirds). One case of MCL showed an incorrect predictive diagnosis that was an atypical case of a cyclinD1-negative MCL with a CCND1/IGH translocation proven by fluorescence in situ hybridization (IHC results; CD20+, Bcl-2+, CD3–, CD10–, Bcl-6–, CD23–, MUM1–, p53–). The IHC for CD5 was not available, and this atypical IHC profile appeared to explain the incorrect precision. Another case of cyclinD1-negative MCL occurred in the validation data set. Although the cyclinD1 was negative, CD5 was positive, and the predictive diagnosis included MCL. In plasmablastic lymphomas, the predictive diagnosis was incorrect in all three cases. Plasmablastic lymphoma shares an IHC profile with plasma cell neoplasms, large B-cell lymphomas, and MALT lymphoma, in that CD38, CD138, CD79a, are positive and CD30 is positive but CD20 is often negative [5,18,19,20]. All three recruited cases of plasmablastic lymphoma showed CD20 positivity and were presumed to be plasma cell neoplasms such as multiple myeloma and solitary plasmacytoma, diffuse large B-cell lymphoma, anaplastic variant (CD30 positive), and extranodal MALT lymphoma with plasmacytoid differentiation. The main reason for the error in diagnosis precision is thought to be a lack of disease-specific markers and overlapping IHC profiles similar to those of other diseases. Likewise, in primary cutaneous follicle center lymphoma of the validation dataset, the similarity of IHC profiles to follicular lymphomas appeared to explain the lack of precision. Because the algorithm does not take into account clinicopathologic information such as tumor location, skin versus lymph node, in this case, this incoherence can be explained.

In T-cell lymphomas, by comparison, the algorithm achieved a generally equivalent performance compared with B-cell lymphomas, with the exception of T lymphoblastic leukemia/lymphoma and extranodal NK/T-cell lymphoma, and nasal type. The accurate precision in T lymphoblastic leukemia/lymphoma and extranodal NK/T-cell lymphoma in the nasal type is due to the presence of disease-specific markers such as TdT, and CD56, and Epstein-Barr virus–encoded small RNA. However, in adult T-cell leukemia/lymphoma, enteropathy-associated T-cell lymphoma, primary cutaneous CD8-positive, aggressive epidermotropic cytotoxic T-cell lymphoma, peripheral T-cell lymphoma, NOS, ALCL, ALK-negative, and angioimmunoblastic T-cell lymphoma, error rates were high as 33.3% to 100.0%. Adult T-cell leukemia/lymphoma shares an IHC profile with peripheral T-cell lymphoma, NOS, with no disease-specific markers, but distinctive clinicopathologic features [18-20]. Enteropathy-associated T-cell lymphomas also do not have pathognomic IHC markers but distinctive clinicopathologic findings and often share an IHC profile with peripheral T-cell lymphomas [18-20]. Primary cutaneous CD8-positive, aggressive epidermotropic cytotoxic T-cell lymphoma is a rare subtype of peripheral T-cell lymphoma that involves primarily skin, and the IHC profile is not specific enough to rule out other diseases by IHC alone [4,5,20]. ALCL, ALK-negative is a lymphoma of anaplastic morphology with negative ALK, which can often share IHC profiles with ALCL, ALK-positive, Hodgkin lymphomas, and peripheral T-cell lymphoma, NOS [18-20]. In angioimmunoblastic T-cell lymphoma, programmed death-1 (PD-1) has been considered a specific marker [22]. However, many other lymphomas often express PD-1 at varying rates, and its positivity is often interpreted based on characteristic histologic features [4,5,20]. Peripheral T-cell lymphoma, NOS, is a different category of nodal and extranodal mature T-cell lymphomas that do not correspond to any explicitly defined entities by definition [18,19]. Therefore, its IHC profiles cover a wide variety of expressions and are often shared by other entities in T-cell lymphomas. In summary, many T-cell lymphomas often share IHC profiles and have no disease-specific IHC markers but can be differentially diagnosed based on clinicopathologic findings with or without IHC profiles.

In Hodgkin lymphomas, the error rates were 50.0% in nodular lymphocyte-predominant Hodgkin lymphoma (1 out of 2), 15.8% in classical Hodgkin lymphoma, NOS (3 out of 19), 15.4% in nodular sclerosis subtype (4 out of 26), 0% in mixed cellularity subtype (0 out of 15), and 33.3% in lymphocyte-depleted subtype (1 out of 3). Nodular lymphocyte-predominant Hodgkin lymphoma shares the IHC profile with T-cell/histiocyte-rich DLBCL and ALCL, ALK-negative, as well as clinicopathologic features. Classical Hodgkin lymphoma, including subtypes, also showed overlapping IHC profiles to peripheral T-cell lymphoma, NOS, but a differential diagnosis based only on IHC profiles is not feasible, particularly if CD15, a specific Hodgkin's marker, is negative. Integrated and comprehensive diagnosis, including the clinicopathologic findings in addition to the possible diagnosis by IHC profiles is therefore essential.

In terms of time and user experience, it is difficult to mathematically compare the amount of time that is consumed during the process of diagnosis with or without using this application. In general, however, most pathologists gave us positive feedback about time-saving and easy-to-use user experiences.

This study demonstrates the feasibility and clinical utility of the diagnosis precision algorithm and corresponding mobile ap-

 https://doi.org/10.4132/jptm.2020.07.11

plication in differential diagnosis of lymphomas using IHC profiles. The overall hit rate of this machine-learning algorithm was 95.0% in lymphomas, and the hit rates were not significantly different between training and validation data in lymphoma, which showed a relatively good generalization. Significant errors were associated with atypical IHC profiles, a lack of site- and disease-specific markers, overlapping IHC profiles between disease entities, mixed/combined tumors, etc. Although this system will help pathologists make better decisions during pathologic diagnosis by supplying comprehensive IHC information relevant to efficient and accurate differential diagnosis, integrated interpretation with contextual information such as clinical and pathological findings are recommended, and the supportive use of this application is desirable. Further studies of possible recommendations for IHC panels for specific situations involving differential diagnosis and application of artificial neural network algorithms are required to optimize the algorithm's sensitivity to disease, organ incidence, and antibody weight.

Supplementary Information

The Data Supplement is available with this article at https://doi.org/10.4132/jptm.2020.07.11.

Ethics Statement

This study was approved by the Institutional Review Board of The Catholic University of Korea, College of Medicine (SC17RCDI0074), and the Institutional Review Board of Yonsei University, Wonju College of Medicine (CR316306). The need for informed consent was waived under the permission of the review boards.

ORCID

Yosep Chong	https://orcid.org/0000-0001-8615-3064
Ji Young Lee	https://orcid.org/0000-0002-4578-6735
Yejin Kim	https://orcid.org/0000-0001-7815-6310
Jingyun Choi	https://orcid.org/0000-0001-7696-4154
Hwanjo Yu	https://orcid.org/0000-0002-7510-0255
Gyeongsin Park	https://orcid.org/0000-0002-9727-5566
Mee Yon Cho	https://orcid.org/0000-0002-7955-4211
Nishant Thakur	https://orcid.org/0000-0001-8761-0837

Author Contributions

Conceptualization: YC, HY. Data curation: YC, JYL. Funding acquisition: YC, JC, YK. Investigation: YC, JC, YK. Methodology: YC, MYC, HY. Project administration: JYL. Resources: YC, GP. Supervision: MYC, GP, HY. Validation: YC, JYL. Visualization: YC, NT. Writing—original draft: YC. Writing—review & editing: YC, MYC, NT. Approval of final manuscript: all authors.

Conflicts of Interest

Y.C., a contributing editor of the *Journal of Pathology and Translational Medicine*, was not involved in the editorial evaluation or decision to publish this article. All remaining authors have declared no conflicts of interest.

Funding Statement

This research was partly supported by the Basic Science Research Program through the National Research Foundation of Korea (NRF) funded by the Ministry of Education (2016R1D1A1A02937427), partially supported by the Research Fund of the Korean Society for Pathologist, and supported by the Po-Ca Networking Groups funded by The Postech-Catholic Biomedical Engineering Institute(PCBMI) (No.5-2015-B0001-00112).

Acknowledgments

I appreciate Myungjin Choi, Dasom X Inc. for technical support in the development of mobile application and Young Dong Seo for reviewing the manuscript style.

References

1. Elias JM. Immunohistochemistry: a brief historical perspective: commentary. In: Shi SR, Gu J, Taylor CR, eds. Antigen retrieval techniques: immunohistochemistry and molecular morphology. Natick: Eaton Pub, 2000; 7-13.
2. Buchwalow IB, Bocker W. Immunohistochemistry: basics and methods. Heidelberg: Springer, 2010.
3. Matos LL, Trufelli DC, de Matos MG, da Silva Pinhal MA. Immunohistochemistry as an important tool in biomarkers detection and clinical practice. Biomark Insights 2010; 5: 9-20.
4. Chu P, Weiss L. Modern immunohistochemistry. 2nd ed. Cambridge: Cambridge University Press, 2014.
5. Dabbs DJ. Diagnostic immunohistochemistry: theranostic and genomic applications. 4th ed. Philadelphia: Elsevier/Saunders, 2014.
6. Kalyuzhny AE. Immunohistochemistry: essential elements and beyond. Cham: Springer, 2016.
7. Coons AH. Labeling Techniques in the diagnosis of viral diseases. Bacteriol Rev 1964; 28: 397-9.
8. Werner B, Campos AC, Nadji M, Torres LF. Practical use of immunohistochemistry in surgical pathology. J Bras Patol Med Lab 2005; 41: 353-64.
9. DeYoung BR, Wick MR. Immunohistologic evaluation of metastatic carcinomas of unknown origin: an algorithmic approach. Semin Diagn Pathol 2000; 17: 184-93.
10. Bishop JA, Sharma R, Illei PB. Napsin A and thyroid transcription factor-1 expression in carcinomas of the lung, breast, pancreas, colon, kidney, thyroid, and malignant mesothelioma. Hum Pathol 2010; 41: 20-5.
11. Yu H, Li L, Liu D, Li WM. Expression of TTF-1, napsinA, P63, CK5/6 in lung cancer and its diagnostic values for histological classification. Sichuan Da Xue Xue Bao Yi Xue Ban 2017; 48: 336-41.
12. El-Maqsoud NM, Tawfiek ER, Abdelmeged A, Rahman MF, Moustafa AA. The diagnostic utility of the triple markers Napsin A, TTF-1, and PAX8 in differentiating between primary and metastatic lung carcinomas. Tumour Biol 2016; 37: 3123-34.
13. Gweon HM, Kim JA, Youk JH, et al. Can galectin-3 be a useful marker for conventional papillary thyroid microcarcinoma? Diagn Cytopathol 2016; 44: 103-7.
14. Kandalaft PL, Gown AM. Practical applications in immunohistochemistry: carcinomas of unknown primary site. Arch Pathol Lab Med 2016; 140: 508-23.
15. Nam S, Chong Y, Jung CK, et al. Introduction to digital pathology and computer-aided pathology. J Pathol Transl Med 2020; 54: 125-34.
16. Lin F, Prichard J. Handbook of practical immunohistochemistry:

frequently asked questions. 2nd ed. New York: Springer, 2015.
17. Lesaffre E, Lawson AB. Bayesian biostatistics. Chichester: John Wiley & Sons, 2012.
18. Swerdlow SH, Campo E, Harris NL, et al. WHO classification of tumours of haematopoietic and lymphoid tissues. 4th ed. Lyon: International Agency for Research on Cancer, 2008.
19. Swerdlow SH, Campo E, Harris NL, et al. WHO classification of tumours of haematopoietic and lymphoid tissues. Revised 4th ed. Lyon: International Agency for Research on Cancer, 2017.
20. Rekhtman N, Bishop JA. Quick reference handbook for surgical pathologists. Heidelberg: Springer, 2011.
21. ImmunoQuery [Internet]. Philadelphia: Elsevier, 2020 [cited 2020 Mar 1]. Available from: http://www.immunoquery.com.
22. Dorfman DM, Brown JA, Shahsafaei A, Freeman GJ. Programmed death-1 (PD-1) is a marker of germinal center-associated T cells and angioimmunoblastic T-cell lymphoma. Am J Surg Pathol 2006; 30: 802-10.

https://doi.org/10.4132/jptm.2020.07.11

JPTM
Journal of Pathology and Translational Medicine 2020; 54: 471-479
https://doi.org/10.4132/jptm.2020.07.23

ORIGINAL ARTICLE

The frequency of *POLE*-mutation in endometrial carcinoma and prognostic implications: a systemic review and meta-analysis

Alaa Salah Jumaah[1], Mais Muhammed Salim[1], Hawraa Sahib Al-Haddad[2], Katherine Ann McAllister[3], Akeel Abed Yasseen[1]

[1]Department of Pathology and Forensic Medicine, Faculty of Medicine, University of Kufa, Kufa;
[2]Al-Furat Al-Awsat Hospital, Kufa, Iraq;
[3]School of Biomedical Science, University of Ulster, Northern Ireland, UK

Background: Endometrial carcinoma (EC) is classified into four distinct molecular subgroups including ultramutated DNA polymerase epsilon (POLE). *POLE*-mutated tumors have the best prognosis and are a promising target for immunotherapy. This meta-analysis consolidated the reported variation of *POLE*-mutant frequency and assessed prognostic value in EC. **Methods:** Internet searches explored scientific data bases: EMBASE, PubMed, and the Cochrane Central Register of Controlled Trials databases. Data was extracted from eligible studies including: sample size, number of positive *POLE*-mutant cases, sequencing information, clinicopathologic data, and survival data. Meta-analysis and a random-effects model produced pooled estimates of POLE frequency and prognostic parameters using 95% confidence intervals (CI), hazard ratios (HR), and odd ratios (OR). **Results:** Six thousand three hundred and forty-six EC patient cases were pooled from 25 studies. The pooled proportion of *POLE* gene mutation in EC was 8.59% (95% CI, 7.01 to 10.32), of which 8.22% (95% CI, 6.27 to 10.42) were type I and 0.93% (95% CI, 0.34 to 1.81) type 2. Clinicopathologic data showed that *POLE*-mutated tumors are mostly endometrioid. They present at higher levels in earlier stages (I–II) of EC (89.51%; 95% CI, 81.11 to 95.66) at the highest grade III (51.53%; 95% CI, 36.08 to 66.84) with reduced myometrial invasion (OR, 1.48, 95% CI, 0.99 to 2.20). Survival analysis indicated favorable overall survival (HR, 0.90), disease-specific survival (HR, 0.41), and progression-free survival (HR, 0.23) for *POLE* mutant EC. **Conclusions:** Almost one-tenth of EC patients have *POLE*-mutated tumors. Given their improved prognostic potential, identifying the *POLE* mutation status is key for the management of EC patients.

Key Words: Endometrial carcinoma; *POLE* gene

Received: February 27, 2020 **Revised:** July 18, 2020 **Accepted:** July 23, 2020
Corresponding Author: Akeel Abed Yasseen, PhD, Department of Pathology and Forensic Medicine, Faculty of Medicine, University of Kufa, Kufa, P.O. Box 21, Najaf Governorate, Iraq
Tel: +96-47811131586, E-mail: akeelyasseen@uokufa.edu.iq

Endometrial carcinoma (EC) is the most common cancer of the female reproductive system. In the United States, EC was the sixth-cause of cancer-related death in 2018, accounting for 11,350 deaths. The disease affects an estimated 1 out of every 37 and 49 women respectively during their lifetime in the United States and Australia [1,2]. The outlook for 5-year survival after treatment ranges from 74% to 91% [3,4]. EC has been historically classified into estrogen dependent (type I) and estrogen-independent (type II) cancers [4]. Type II tumors are less common, more clinically aggressive, and may have serous, clear cell or undifferentiated histology. In contrast, type I tumors present in 70%–80% of cases, with endometrioid histology and a more favorable outcome. The updated classification of EC identifies four molecular subtypes according to The Cancer Genomic Atlas (TCGA): "*POLE*-mutated (ultramutated), microsatellite unstable (hypermutated), copy number low (endometrioid), and copy number high (serous-like)" [1]. The *POLE*-ultramutated subgroup holds great promise for the outlook of EC patients. The tumors have a more favorable outcome, and are usually noted to be of endometrioid type and associated with lymphoid infiltrates [5].

The *POLE* gene encodes the catalytic subunit of DNA polymerase epsilon, which synthesizes the leading strand of replicating DNA. The epsilon polymerase recognizes and removes mispaired nucleotides using exonuclease activity. This proofreading capacity of epsilon enables high fidelity DNA replication [6]. Mutations can occur in the exonuclease domain of the polymerase,

pISSN 2383-7837
eISSN 2383-7845

within hotspot regions [7]. These genetic alterations inactivate or suppress the proofreading abilities of the polymerase, causing increased replicative error rates and the ultra-mutated phenotype. Studies show that ultra-mutated POLE EC harbors up to 10-fold more mutations than the microsatellite instability subgroup [6,7]. In the TCGA study [8], whole genome and exon sequencing of EC tumors uncovered the *POLE* hotspot mutations of v411L and P286R. Follow-up studies mainly used the Sanger method [9-23], next generation sequencing [13,24] and unspecified sequencing approaches [10,11,25-29] to target the exonuclease domain (exons 9–14) of *POLE*. The reported proportion of mutated *POLE* is highly variable [8-31]: ranging from absent in studies of clear cell carcinoma [15,18] to levels as high as 43% in one study of rare undifferentiated/dedifferentiated EC histotypes [28]. In order to consolidate the studies, we conducted a meta-analysis of reported *POLE* gene mutation in EC to confirm its overall frequency. We also extracted clinicopathologic and survival data, to evaluate how mutated *POLE* can affect prognosis of EC patients.

MATERIALS AND METHODS

This study was conducted according to the guidelines of Preferred Reporting for Systemic Review and Meta-analysis (PRISMA) statement [32].

Literature search strategy

Searches were conducted according to the guidelines of PRISMA statement 2009 [32]. Two authors (A.S.J. and H.S.A.) searched independently the following data bases from inceptions to October 2019: Embase, PubMed, Cochrane central Register of Controlled trials, and Ovid. The reference lists were also scanned within the articles. There were no language limits and international papers were translated. All pathology and oncology journals indexed in the Scimago directory were reviewed and relevant papers scanned (A.S.J. and M.M.S.). The following search terms were used:

1) 'Endometrial cancer' or 'uterine cancer.'

2) '*POLE* gene' or 'ultramutated endometrial carcinoma.'

Inclusion criteria

The following patient inclusion criteria were used:

1) EC or one of its histological variants was present in patients.

2) The expression of *POLE* gene was reported using genetic testing (e.g. sequencing, Sanger sequencing, next generation sequencing, polymerase chain reaction).

3) A full paper was published and studies published in abstract format only were excluded.

4) When similar studies were generated from the same patient, only the most recent investigation was included.

Study selection

Studies were identified using different data bases. The title of the paper and abstract were assessed by two independent authors (A.S.J. and H.S.A.). The full texts were also reviewed independently by two authors (M.M.S. and K.A.M.). Any disagreement was resolved under guidance of the senior author (A.A.Y.).

Data collection

The following data was extracted from eligible studies by two authors (A.S.J. and H.S.A.): study information (first author and year of publication), patient characteristics (sample size and gender), site of the study, and test method for *POLE* gene and proportion detected. Clinicopathologic data extracted included tumor stage and grade, presence of lymphovascular and myometrial invasion, and patient survival. If the relevant data was not available, it was recorded as NR (not reported). All datasets were checked independently (M.M.S.). Any disagreements were resolved by discussion and consultation with the senior author (A.A.Y.).

Meta-analysis and statistical methods

The proportion of endometrial cancers that harbor *POLE* gene mutations was calculated using medcalc software [33]. The pooled proportion of *POLE* was calculated using the random effect model [32] for meta-analysis. For clinicopathologic meta-analysis, proportions of tumour stage, grade, lymphovascular invasion, myometrial invasion (MI), and survival analysis (overall survival, disease-free survival, and progression-free survival) were pooled from each study. The variation between datasets was assessed using the heterogeneity test with inconsistency index (I^2) and Q statistic. The level of study heterogeneity was considered low at 25% (I^2 = 25%), medium at 50% (I^2 = 50%) or high at 75% (I^2 = 75%). In regard to the Q statistic, a p-value of less than 0.1 was considered to represent significant heterogeneity. The possibility of publication bias was assessed by visual method using a funnel plot. This determined funnel plot asymmetry resulting from factors such as non-publication of studies with negative results.

Sensitivity and subgroup analysis

Lastly, sensitivity analysis was conducted by omitting each study one-by-one to discover its contribution on the pooled meta-analysis results. Subgroup analysis was performed according to

https://doi.org/10.4132/jptm.2020.07.23

geographical area (Asia, West-Europe, and America) and to different histological types to discover sources of heterogeneity. The subgroup analysis was further extended by using a meta regression model.

RESULTS

Study selection for meta-analysis

The inclusion criteria were met by 1,252 studies, of which 345 studies were excluded for duplication, and 605 studies were excluded as irrelevant by reviewing the title and abstract. The full texts of the remaining 302 studies were considered for review. Approximately 25 studies were left for the final meta-analysis as illustrated in the flowchart diagram (Fig. 1). All of the studies were published from 2013–2019, and there were no unpublished studies of relevance. The study characteristics and *POLE* gene sequencing methods are listed in (Table 1). The majority used Sanger sequencing to detect tumor mutations in exons 9–14 of the *POLE* exonuclease domain (Table 1) [8-29].

Meta-analysis of EC

There were 6,346 EC patient cases pooled from the 25 studies and investigated for *POLE* gene tumor alterations. All studies (except one) were performed in western countries. The studies were published in English and full texts obtained. There was significant heterogeneity between the studies ($Q = 109.57$, $I^2 = 78.10\%$; 95% confidence interval [CI] for I^2, 68.15 to 84.94; $p < .001$). The random effect model was used for final meta-analysis because

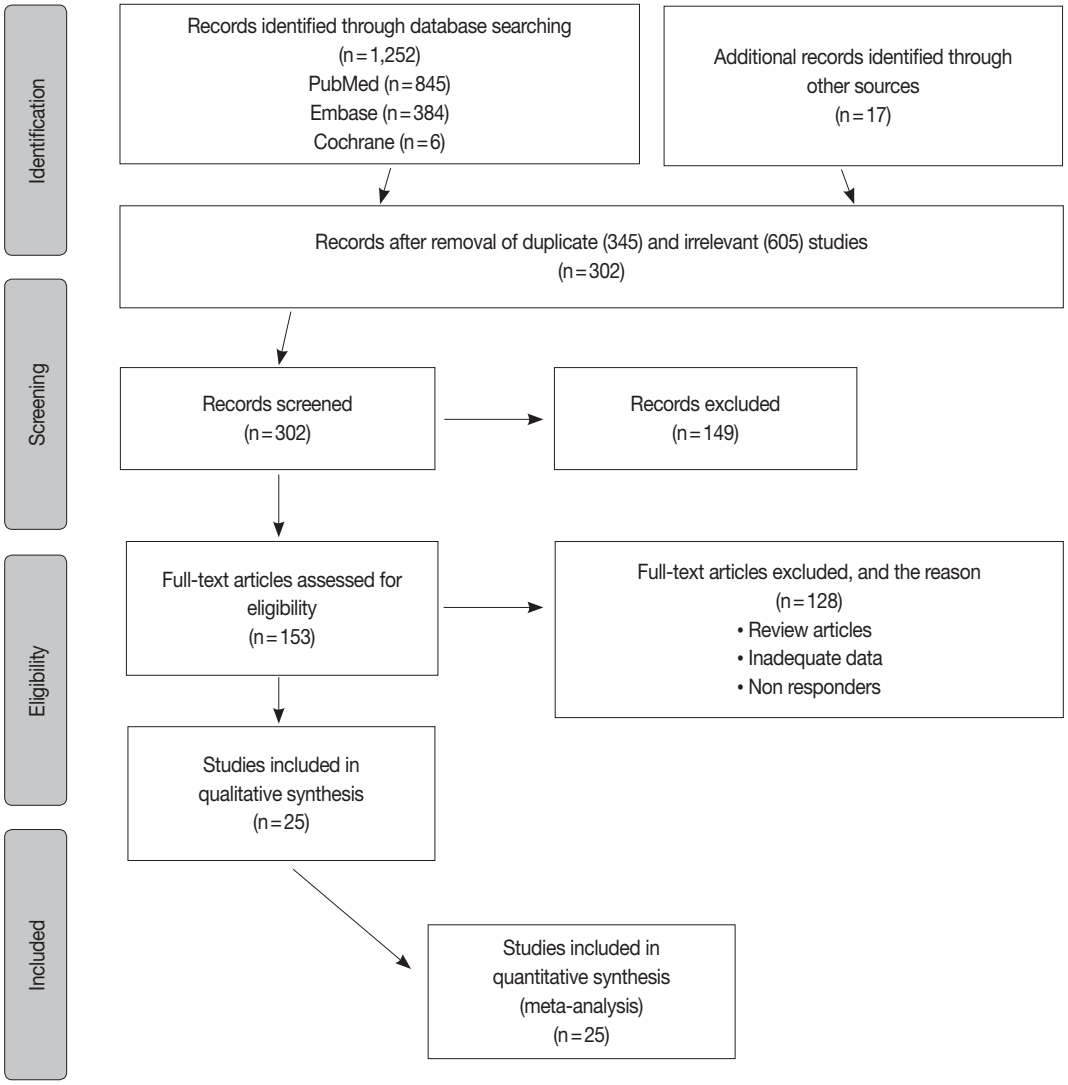

Fig. 1. Flow chart of the studies identified, screened and included for final meta-analysis. A total of 1,252 studies met the eligibility criteria for inclusion, of which 26 were selected for final meta-analysis.

Table 1. Study characteristics and *POLE* sequencing methodology

Study	EC cohort size	Proportion *POLE*-mutant	Country	Sequencing method	Location of exonuclease mutations
The Cancer Genome Atlas Research Network (2013) [8]	248	17	USA	Exome sequencing	Hotspots: Pro286Arg and Val411Leu
Auguste et al. (2018) [9]	102	9	Canada and Europe	Sanger sequencing	Exons 9 and 13
Talhouk et al. (2015) [10]	143	12	Canada	Fluidigm-MiSeq and sanger sequencing	Exons 9–14
Stelloo et al. (2015) [11]	116	14	Europe and Australia	Sanger sequencing	Exons 9 and 13
Eggink et al. (2017) [12]	116	15	Europe and Australia	Sanger sequencing	Exons 9, 13 and 14
Wortman et al. (2018) [25]	344	16	Netherlands	Sequencing	Not reported
Kommoss et al. (2018) [26]	452	42	Germany	Sequencing	Exons 9–14
Bosse et al. (2018) [13]	376	48	USA, Canada, and Europe	Sanger or next-generation approaches	Hotspots in the exonuclease domain (exons 9–14)
Billingsley et al. (2015) [14]	535	30	USA	Sanger sequencing	Residues 268–471
Le Gallo et al. (2017) [15]	63	0	USA and Europe	Sanger sequencing	Not reported
Karnezis et al. (2017) [27]	460	42	Canada	Sequencing	Not reported
Talhouk et al. (2017) [16]	319	30	Canada	Sanger sequencing	Exons 9–14
Rosa-Rosa et al. (2016) [17]	18	2	USA and Europe	Sanger sequencing	Exons 9 and 13
Wortman et al. (2018) [25]	416	16	Netherlands	Sequencing	Not reported
Espinosa et al. (2017) [28]	21	9	Spain	Sequencing	Exons 9 to 14
Stelloo et al. (2015) [11]	116	14	Europe	Sanger sequencing	Exons 9 and 13
Hoang et al. (2015) [18]	14	0	Canada	Sanger sequencing	Exons 9–14
DeLair et al. (2017) [29]	30	2	USA	Sequencing	Exons 9–14
Abdulfatah et al. (2019) [19]	60	2	USA	Sanger sequencing	Exons 9 and 13
Wong et al. (2016) [24]	47	14	Singapore	Next generation sequencing	Exons 9–14
Stelloo et al. (2016) [20]	834	49	Netherlands	Sanger sequencing	Exons 9 and 13
Imboden et al. (2019) [21]	599	38	Sweden	Sanger sequencing	Exons 9–14
Church et al. (2015) [7]	788	48	Europe	Sanger sequencing	Exons 9 and 13
Billingsley et al. (2016) [22]	72	7	USA	Sanger sequencing	Residues 268–471
Talhouk et al. (2016) [23]	57	10	USA and Canada	Ultra-deep MiSeq or sanger sequencing	Exons 9–14

POLE, DNA polymerase epsilon; EC, endometrial carcinoma.

Table 2. The association between *POLE* mutated EC and clinicopathology characteristics

Clinicopathological characteristics in EC	Pooled % portion (95% CI, %)	No. of studies	I^2 (95% CI)	p-value	Model
Overall *POLE* mutation	8.59 (7.01–10.32)	25	78.10 (68.15–84.94)	<.001	Random effect
POLE mutation in type I	8.22 (6.27–10.42)	9	74.88 (51.43–87.00)	<.001	Random effect
POLE mutation in type II	0.93 (0.34–1.81)	10	75.32 (54.08–86.74)	<.001	Random effect
Stage I–II	89.51 (81.11–95.66)	10	69.09 (40.43–83.96)	<.001	Random effect
Stage III–IV	14.77 (5.99–26.59)	7	65.96 (23.79–84.79)	<.001	Random effect
Grade I–II	46.36 (30.66–62.43)	7	82.15 (64.34–91.06)	<.001	Random effect
Grade III	51.53 (36.08–66.84)	8	81.79 (65.23–90.46)	<.001	Random effect
Lymphovascular invasion	31.11 (10.44–56.86)	8	93.34 (89.15–95.91)	<.001	Random effect
Myometrial invasion less than 50%	49.90 (43.71–56.21)	7	22.10 (0.00–65.16)	.260	Fixed effect

POLE, DNA polymerase epsilon; EC, endometrial carcinoma; CI, confidence interval.

of the significant heterogeneity. The pooled proportion of *POLE* gene mutated in EC was determined at 8.59% (95% CI, 7.01 to 10.32) as shown in Table 2. A forest plot representation of the EC patient cases comprising each study included for meta-analysis is shown in Fig. 2. Publication bias was assessed by funnel plot (Fig. 3) and the visual assessment was symmetrical.

Analysis of EC histologic variants type I and type II

There were 3,363 patients included for the type 1 meta-analysis using a total of 9 studies (Supplementary Fig. S1). The mutated *POLE* gene proportion in type I EC was 8.22% (95% CI, 7.01 to 10.32). There was significant heterogeneity between studies (I^2 inconsistency = 74.88%; 95% CI, 51.43 to 87.00; p < .001) as shown in Table 2. A total of 3,423 patients with EC type II

https://doi.org/10.4132/jptm.2020.07.23

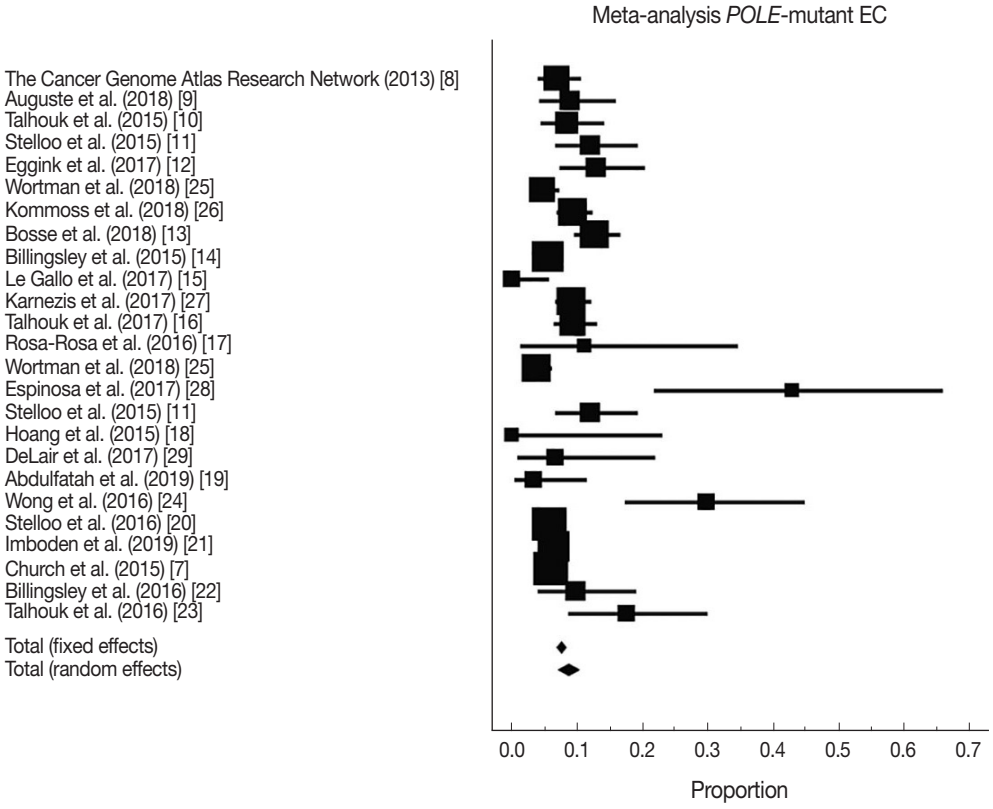

Fig. 2. Forest plot representation of the endometrial carcinoma (EC) patient cases for each study included for meta-analysis. *POLE*, DNA polymerase epsilon.

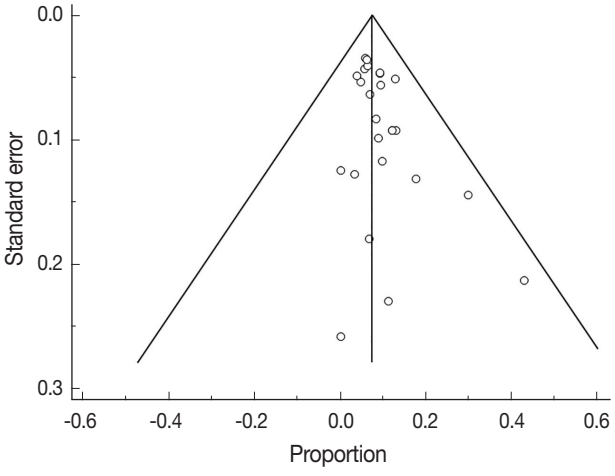

Fig. 3. Funnel plot for cases included for analysis. The visual assessment was symmetrical indicating no publication bias.

were obtained from 10 studies for the final meta-analysis (Supplementary Fig. S2). The histological types in EC type II are show in (Supplementary Table S1). The pooled proportion of mutated *POLE* gene in type II was 0.93% (95% CI, 0.34 to 1.81) with a high I^2 value (75.32%; 95% CI, 54.08 to 86.74; p < .001).

Subgroup analysis (country of origin)

In order to explore the role of heterogeneity, a subgroup analysis was performed according to the study site (Supplementary Fig. S3, S4). The studies were separated into two groups according to geographical area (USA and Canada vs. European countries). The heterogeneity was higher (I^2, inconsistency) for *POLE* genetic analysis in the European countries (78.41%; 95% CI, 59.27 to 88.55) compared to the USA and Canada (37.41%; 95% CI, 0.00 to 69.22).

Sensitivity analysis

There were 2 identified study outliers [24,28]. Meta-analysis was performed after outlier exclusion. There was still significant heterogeneity (I^2 = 70.39% [95% CI for I^2, 54.78 to 80.61; p < .001]) and exclusion did not significantly affect the final pooled proportion (pooled proportion = 7.76 [95% CI, 6.45 to 9.18]) (Supplementary Fig. S5). There were also two studies without *POLE* gene mutated EC [15,18]. Here, the pooled proportion was re-calculated using the random effect model (Supplementary Fig. S6). Significant heterogeneity was still present (I^2 = 76.31%; 95% CI for I^2, 64.98 to 83.97; p < .001). There were

10 studies [9,13,15,17,19-21,23,24,30] identified with a low sample size (< 100). These cases were excluded and the pooled proportions re-estimated (Supplementary Fig. S7). There was still significant heterogeneity (I^2 = 74.41%; 95% CI for I^2, 53.56 to 85.90; p < .001).

Meta-regression

Meta-regression was performed to identify the source of heterogeneity using the study country of origin and the *POLE* gene detection method (Supplementary Table S2). There was increased heterogeneity when considering the site of study performance in the European countries (I^2 = 78.41%) compared to United States and Canadian studies (I^2 = 37.41%).

Clinicopathological characteristics

Clinicopathologic data was extracted from eligible studies of *POLE* mutant EC for meta-analysis (Supplementary Fig. S8-S14). The pooled proportions for stage, grade, lymphovascular invasion (LVI) and MI parameter are reported in Table 2. High heterogeneity was noted for pooled stage, grade, and LVI data. The pooled odd ratios were also calculated for *POLE*-mutant versus wild type *POLE* according to each clinicopathologic variable (Table 3).

Tumor stage and grade in POLE mutant EC

The pooled proportion of mutant *POLE* presented at high levels of 89.51% (95% CI, 81.11 to 95.66) at the earliest EC stages of I–II (Table 2). This reduced to 14.77% by stages III–IV (95% CI, 5.99 to 26.59). The pooled odd ratio of stage I–II *POLE* mutant EC versus wild type was 3.72 (2.06 to 6.73), while stage III–IV was 0.26 (95% CI, 0.14 to 0.49) (Table 2, Supplementary Fig. S15, S16). The pooled collective proportions of grade I–II *POLE* mutant tumors was lower at 46.36% (95% CI, 30.66 to 62.43) compared to 51.53 of grade III (95% CI, 36.08 to 66.844) as shown in Table 2. The pooled odd ratio of grade I–II *POLE* mutant EC versus wild type tumors was 0.40 (95% CI, 0.29 to 0.54) (Supplementary Fig. S17) with low heterogeneity (I^2 = 3.95%, 95% CI, 0.00 to 69.18). Therefore, *POLE* mutated tumors present with a higher grade but at lower stage than wild type *POLE* mutant EC.

LVI and MI in *POLE*-mutant EC

The pooled proportion of LVI was 31.11% (95% CI, 10.44 to 56.86). The pooled odd ratio of LVI positive in *POLE* mutant EC vs. wild type EC was 0.92 (0.643 to 1.34) (Table 3). The pooled proportion of MI either less or greater than 50% of myometrium in *POLE*-mutant tumor was equal at 49.90% (95% CI, 43.71 to 56.21) and 49.05% (95% CI, 39.17 to 58.98), respectively. Heterogeneity was low for pooled MI data (< 50% myometrium) at 22.10%; 95% CI, 0.00 to 65.16 (Table 2, Supplementary Figs. S13, S14). The pooled odd ratio of MI <50% in *POLE* mutant EC versus MI < 50% in wild type *POLE* EC was 1.481 (95% CI, 0.99 to 2.20) with 47.63% heterogeneity (95% CI, 0.00 to 79.24) (Table 3). Overall, these findings imply that *POLE* mutant EC tumors have reduced ability to progress to myometrial invasion, which is an important prognostic finding.

Endometrioid and non-endometrioid histologic types in *POLE* mutant EC

POLE mutant tumors were found to mainly present with endometrioid histologic type. The pooled proportions of type I and type II EC are shown in Table 2. The pooled odd ratio of endometrioid (type I) *POLE* mutant EC vs. endometrioid (type I) in wild type POLE EC was 1.72 (95% CI: 1.11 to 2.66), with very low heterogeneity (I^2 = 0.00%; 95% CI: 0.00 to 68.45) (Table 3, Supplementary Fig. S18).

Survival analysis

The studies used for survival meta-analysis are listed in Table 4. Survival analysis was expressed using overall survival (OS),

Table 3. Pooled odd ratio of clinicopathology variables in *POLE*-mutant EC vs. wild type

Clinicopathology: *POLE*-mutant vs. wild type	Pooled odd ratio (95% CI)	No. of studies	I^2 (95% CI, %)	p-value for I^2	Model
Stage I–II EC	3.727 (2.063–6.732)	8	0.00 (0.00–25.07)	.890	Fixed effect
Stage III–IV EC	0.269 (0.147–0.494)	7	0.00 (0.00–53.51)	.716	Fixed effect
Grade I–II EC	0.400 (0.295–0.542)	8	3.95 (0.00–69.18)	.399	Fixed effect
Grade III EC	2.246 (1.655–3.048)	8	0.00 (0.00–29.91)	.865	Fixed effect
LVI	0.929 (0.643–1.341)	8	6.95 (0.00–70.15)	.376	Fixed effect
MI less than 50%	1.481 (0.996–2.202)	6	47.63 (0.00–79.24)	.089	Random effect
Type I endometrioid histology	1.721 (1.113–2.662)	9	0.00 (0.00–68.45)	.486	Fixed effect

POLE, DNA polymerase epsilon; EC, endometrial carcinoma; CI, confidence interval; LVI, lymphovascular invasion; MI, myometrial invasion.

https://doi.org/10.4132/jptm.2020.07.23

Table 4. Survival analysis in *POLE* mutated EC

Study	OS estimated HR (95% CI)	DSS estimated HR (95% CI)	PFS estimated HR (95% CI)	Survival analysis test	Method
Talhouk et al. (2017) [16]	1.01 (0.29–3.42)	0.42 (0.30–0.57)	-	Multivariable analysis	Kaplan-Meier survival analysis
Talhouk et al. (2015) [10]	0.17 (0.01–1.98)	0.170 (0.01–1.99)	-	Multivariable analysis	Kaplan-Meier with log-rank significance testing and Cox proportional hazard regression models
Church et al. (2015) [7]	1.06 (0.58–1.91)	0.19 (0.02–1.31)	-	Multivariable analysis	Kaplan-Meier method and compared by the log-rank test
Karnezis et al. (2017) [27]	0.59 (0.21–1.60)	0.49 (0.12–1.90)	0.26 (0.04–1.49)	Univariable survival analysis	Kaplan-Meier survival curve
Stelloo et al. (2016) [20]	1.10 (0.39–3.10)			Multivariable analysis	Kaplan-Meier survival analysis
Bosse et al. (2018) [13]			0.23 (0.06–0.76)	Multivariable analysis	Kaplan-Meier survival curve
Pooled HR (95% CI)	0.90 (0.59–1.38)	0.41 (0.30–0.55)	0.23 (0.08–0.64)		
I^2 (95% CI, %)	0.00 (0.00–73.28)	0.00 (0.00–67.34)	0.00 (0.00–0.00)		

POLE, DNA polymerase epsilon; EC, endometrial carcinoma; OS, overall survival; DSS, disease-specific survival; PFS, progression-free survival; HR, hazard ratio; CI, confidence interval.

disease-specific survival (DSS), and progression-free survival (Supplementary Fig. S19–S21). All the survival parameters had a hazard ratio (HR) of less than 1. The estimated HR for OS was 0.90 (95% CI, 0.59 to 1.38) with low heterogeneity 0.00% (95% CI, 0.00 to 73.28). On the other hand, estimated HR for DSS was 0.41 (95% CI, 0.30 to 0.55), also with low heterogeneity (0.00%; 95% CI, 0.00 to 67.34). Likewise, the estimated HR of progression-free survival in *POLE*-mutant EC was 0.23 (95% CI, 0.08 to 0.64) with a low level of heterogeneity (I^2 = 0.00%, 95% CI, 0.00 to 0.00). These findings indicate better survival and favorable prognosis in *POLE* mutant EC patients.

DISCUSSION

EC is the most common gynecologic malignancy in the western world [2,3,34], and survival rates are not improving. There is urgent need for strategies to improve outlook for patients with aggressive subtypes and advanced disease. TCGA first identified the very interesting molecular subset of *POLE*-ultramutated EC [1] that features a favorable prognostic potential, despite high tumor grading. Many follow-up studies investigated *POLE* mutant EC tumors, however the frequency reported is variable [8-31]. Some studies show ultra-high levels of mutation at 42.9% [28] compared to zero in others [15,18]. This meta-analysis aimed to resolve these datasets to estimate *POLE* gene mutational frequency in EC and the overall effect on patient prognosis.

Our meta-analysis determined that 8.595% of endometrial tumors harbor *POLE* gene mutations. The majority have endometrioid histology and present at the earlier stage of disease progression. Paradoxically the *POLE* mutant tumors present at the highest grade (grade III, 51.5%) and yet have a better outcome with survival analysis. They also have reduced ability to progress to myometrial invasion which is an important prognostic marker. Many studies confirm that *POLE* mutant tumors have a better prognosis [6-8,13,22,28]. *POLE* mutations in high grade (grade III) endometrioid EC are shown to be associated with a lower risk of recurrence and death [22]. The presence of *POLE* mutations even offers a favorable prognosis for rare and aggressive undifferentiated EC [28]. *POLE* mutation could potentially act as a prognostic biomarker to guide treatment of women with grade III, early-stage disease, with either the common endometrioid or more rare histological types. The lower risk of occurrence means that administration of adjuvant therapy for these patient subsets could be inappropriate. *POLE* proofreading mutations have also been shown to elicit an anti-tumor response [35]. There is now an emerging link between high mutation burden in tumors, the immune response and improved prognosis in cancer patients. Indeed, ultramutated *POLE* tumors have been shown to feature higher immune infiltrations and programmed death-1 and programmed death-ligand 1 expression [36]. These immune cells may offset the survival risk caused by higher tumor grades in ultramutated *POLE*. Overall, mutant *POLE* is a key proportion of EC patients to target therapeutically for maximizing clinical impact, and a future target for immunotherapy [9].

However, it is important to note that significant heterogeneity was present in this meta-analysis. Indeed, heterogeneity is a key problem for meta-analysis studies. We tried to resolve the heterogeneity sources. Initially, all studies were re-checked with respect to data extraction and entry. The sensitivity analysis was conducted by re-estimating the pooled proportion of *POLE* gene after exclu-

sion of outlier studies and studies with low sample size. We also adopted a random effect model for final pooled estimation as this model assumed that effects estimated in different studies are not identical. We also tried to perform subgroup analysis with respect to patient age but unfortunately this parameter was not recorded in the majority of studies. Publication bias was investigated; in our study the plot was relatively symmetrical, indicating that publication bias is unlikely [37]. The presence of high heterogeneity was reduced by subgroup and meta-regression according to geographical distribution. European studies were found to be the main contributor to the heterogeneity. Therefore, data obtained from different countries can cause confounding effects and is a potential study limitation. The issue of heterogeneity in genetic studies is also further compounded with recent advances in sequencing technology. The improved yield of genetic testing can increase detection of variants of unknown significance. However in our *POLE* gene study the lack of standardized clarification of variants of unknown significance may have contributed to heterogeneity. This will be a key area to investigate during future studies.

Conclusion

Our meta-analysis consolidates previous study estimates of *POLE*-mutated EC frequency and confirms its prognostic benefit for patients. The status and frequencies of the *POLE* gene mutation in EC has implications for medical management and future administration of immunotherapy. The *POLE* mutational status serves as an important prognostic marker, and grade III, early-stage disease patients with endometrioid histology could favor a change in medical management.

Supplementary Information

The Data Supplement is available with this article at https://doi.org/10.4132/jptm.2020.07.23.

Ethics Statement

The present study was approved by the Institutional Review Board of the University of Kufa (IRB approval No. UK-2018-0456) in accordance with the 1964 Helsinki declaration and its later amendments. Formal written informed consent was not required with a waiver issued by the Institutional Review Board of the University of Kufa. All the authors will be held responsible for any false statements or failure to follow the ethical guidelines.

ORCID

Alaa Salah Jumaah https://orcid.org/0000-0001-9709-1460
Mais Muhammed Salim http://orcid.org/0000-0001-8014-1863
Hawraa Sahib Al-Haddad http://orcid.org/0000-0002-8564-3202
Katherine Ann McAllister https://orcid.org/0000-0002-2893-7706
Akeel Abed Yasseen https://orcid.org/0000-0001-5050-4408

Author Contributions

Conceptualization: ASJ, MMS. Data curation: ASJ. Formal analysis: ASJ, MMS. Methodology: ASJ, HSA, MMS. Project administration: HSA, MMS. Resources: HSA. Software: ASJ, MMS. Supervision: ASJ, AAY. Validation: MMS, HSA. Visualization: HSA, MMS. Writing—original draft: ASJ, AAY, KAM. Writing—review & editing: AAY, ASJ, KAM. Approval of final manuscript: all authors.

Conflicts of Interest

The authors declare that they have no potential conflicts of interest.

Funding Statement

No funding to declare.

References

1. Bell DW, Ellenson LH. Molecular genetics of endometrial carcinoma. Annu Rev Pathol 2019; 14: 339-67.
2. Howlader N, Noone AM, Krapcho M, et al. SEER cancer statistics review, 1975-2011. Bethesda: National Cancer Institute, 2014.
3. Siegel RL, Miller KD, Jemal A. Cancer statistics, 2015. CA Cancer J Clin 2015; 65: 5-29.
4. Spurdle AB, Bowman MA, Shamsani J, Kirk J. Endometrial cancer gene panels: clinical diagnostic vs research germline DNA testing. Mod Pathol 2017; 30: 1048-68.
5. Stelloo E, Nout RA, Naves LC, et al. High concordance of molecular tumor alterations between pre-operative curettage and hysterectomy specimens in patients with endometrial carcinoma. Gynecol Oncol 2014; 133: 197-204.
6. Hussein YR, Weigelt B, Levine DA, et al. Clinicopathological analysis of endometrial carcinomas harboring somatic POLE exonuclease domain mutations. Mod Pathol 2015; 28: 505-14.
7. Church DN, Stelloo E, Nout RA, et al. Prognostic significance of POLE proofreading mutations in endometrial cancer. J Natl Cancer Inst 2015; 107: 402.
8. Cancer Genome Atlas Research Network, Kandoth C, Schultz N, et al. Integrated genomic characterization of endometrial carcinoma. Nature 2013; 497: 67-73.
9. Auguste A, Genestie C, De Bruyn M, et al. Refinement of high-risk endometrial cancer classification using DNA damage response biomarkers: a TransPORTEC initiative. Mod Pathol 2018; 31: 1851-61.
10. Talhouk A, McConechy MK, Leung S, et al. A clinically applicable molecular-based classification for endometrial cancers. Br J Cancer 2015; 113: 299-310.
11. Stelloo E, Bosse T, Nout RA, et al. Refining prognosis and identifying targetable pathways for high-risk endometrial cancer: a TransPORTEC initiative. Mod Pathol 2015; 28: 836-44.
12. Eggink FA, Van Gool IC, Leary A, et al. Immunological profiling of molecularly classified high-risk endometrial cancers identifies POLE-mutant and microsatellite unstable carcinomas as candidates for checkpoint inhibition. Oncoimmunology 2017; 6: e1264565.
13. Bosse T, Nout RA, McAlpine JN, et al. Molecular classification of grade 3 endometrioid endometrial cancers identifies distinct prognostic subgroups. Am J Surg Pathol 2018; 42: 561-8.
14. Billingsley CC, Cohn DE, Mutch DG, Stephens JA, Suarez AA, Goodfellow PJ. Polymerase varepsilon (POLE) mutations in endometrial cancer: clinical outcomes and implications for Lynch syndrome testing. Cancer 2015; 121: 386-94.
15. Le Gallo M, Rudd ML, Urick ME, et al. Somatic mutation profiles of clear cell endometrial tumors revealed by whole exome and targeted gene sequencing. Cancer 2017; 123: 3261-8.

16. Talhouk A, McConechy MK, Leung S, et al. Confirmation of ProMisE: a simple, genomics-based clinical classifier for endometrial cancer. Cancer 2017; 123: 802-13.
17. Rosa-Rosa JM, Leskela S, Cristobal-Lana E, et al. Molecular genetic heterogeneity in undifferentiated endometrial carcinomas. Mod Pathol 2016; 29: 1390-8.
18. Hoang LN, McConechy MK, Meng B, et al. Targeted mutation analysis of endometrial clear cell carcinoma. Histopathology 2015; 66: 664-74.
19. Abdulfatah E, Wakeling E, Sakr S, et al. Molecular classification of endometrial carcinoma applied to endometrial biopsy specimens: towards early personalized patient management. Gynecol Oncol 2019; 154: 467-74.
20. Stelloo E, Nout RA, Osse EM, et al. Improved risk assessment by integrating molecular and clinicopathological factors in early-stage endometrial cancer-combined analysis of the PORTEC cohorts. Clin Cancer Res 2016; 22: 4215-24.
21. Imboden S, Nastic D, Ghaderi M, et al. Phenotype of *POLE*-mutated endometrial cancer. PLoS One 2019; 14: e0214318.
22. Billingsley CC, Cohn DE, Mutch DG, Hade EM, Goodfellow PJ. Prognostic significance of POLE exonuclease domain mutations in high-grade endometrioid endometrial cancer on survival and recurrence: a subanalysis. Int J Gynecol Cancer 2016; 26: 933-8.
23. Talhouk A, Hoang LN, McConechy MK, et al. Molecular classification of endometrial carcinoma on diagnostic specimens is highly concordant with final hysterectomy: earlier prognostic information to guide treatment. Gynecol Oncol 2016; 143: 46-53.
24. Wong A, Kuick CH, Wong WL, et al. Mutation spectrum of *POLE* and *POLD1* mutations in South East Asian women presenting with grade 3 endometrioid endometrial carcinomas. Gynecol Oncol 2016; 141: 113-20.
25. Wortman BG, Creutzberg CL, Putter H, et al. Ten-year results of the PORTEC-2 trial for high-intermediate risk endometrial carcinoma: improving patient selection for adjuvant therapy. Br J Cancer 2018; 119: 1067-74.
26. Kommoss FK, Karnezis AN, Kommoss F, et al. L1CAM further stratifies endometrial carcinoma patients with no specific molecular risk profile. Br J Cancer 2018; 119: 480-6.
27. Karnezis AN, Leung S, Magrill J, et al. Evaluation of endometrial carcinoma prognostic immunohistochemistry markers in the context of molecular classification. J Pathol Clin Res 2017; 3: 279-93.
28. Espinosa I, Lee CH, D'Angelo E, Palacios J, Prat J. Undifferentiated and dedifferentiated endometrial carcinomas with POLE exonuclease domain mutations have a favorable prognosis. Am J Surg Pathol 2017; 41: 1121-8.
29. DeLair DF, Burke KA, Selenica P, et al. The genetic landscape of endometrial clear cell carcinomas. J Pathol 2017; 243: 230-41.
30. Meng B, Hoang LN, McIntyre JB, et al. POLE exonuclease domain mutation predicts long progression-free survival in grade 3 endometrioid carcinoma of the endometrium. Gynecol Oncol 2014; 134: 15-9.
31. Bellone S, Bignotti E, Lonardi S, et al. Polymerase epsilon (*POLE*) ultra-mutation in uterine tumors correlates with T lymphocyte infiltration and increased resistance to platinum-based chemotherapy in vitro. Gynecol Oncol 2017; 144: 146-52.
32. Moher D, Shamseer L, Clarke M, et al. Preferred reporting items for systematic review and meta-analysis protocols (PRISMA-P) 2015 statement. Syst Rev 2015; 4: 1.
33. MedCalc statistical software version 13.0.6 [Internet]. Ostend: MedCalc Software, 2014 [cited 2020 Feb 27]. Available from: http://www.medcalc.org.
34. Jumaah AS, Al-Haddad HS, Mahdi LH, et al. Increased *PTEN* gene expression in patients with endometrial carcinoma from areas of high risk depleted uranium exposure. BMC Res Notes 2019; 12: 708.
35. van Gool IC, Eggink FA, Freeman-Mills L, et al. *POLE* proofreading mutations elicit an antitumor immune response in endometrial cancer. Clin Cancer Res 2015; 21: 3347-55.
36. Bakhsh S, Kinloch M, Hoang LN, et al. Histopathological features of endometrial carcinomas associated with *POLE* mutations: implications for decisions about adjuvant therapy. Histopathology 2016; 68: 916-24.
37. Sterne JA, Sutton AJ, Ioannidis JP, et al. Recommendations for examining and interpreting funnel plot asymmetry in meta-analyses of randomised controlled trials. BMJ 2011; 343: d4002.

JPTM
Journal of Pathology and Translational Medicine 2020; 54: 480-488
https://doi.org/10.4132/jptm.2020.07.18

ORIGINAL ARTICLE

Evaluation of human papillomavirus (HPV) prediction using the International Endocervical Adenocarcinoma Criteria and Classification system, compared to p16 immunohistochemistry and HPV RNA in-situ hybridization

Hezhen Ren[1], Jennifer Pors[1], Christine Chow[2], Monica Ta[2], Simona Stolnicu[3], Robert Soslow[4], David Huntsman[1,5], Lynn Hoang[1,2,6]

[1]Department of Pathology and Laboratory Medicine, University of British Columbia, Vancouver, BC;
[2]Genetic Pathology Evaluation Center (GPEC), Vancouver, BC, Canada;
[3]Department of Pathology, University of Medicine, Pharmacy, Sciences and Technology of Targu Mures, Targu Mures, Romania;
[4]Department of Pathology, Memorial Sloan Kettering Cancer Center, New York, NY, USA;
[5]Molecular Oncology, British Columbia Cancer Research Centre, Vancouver, BC;
[6]Department of Anatomical Pathology, Vancouver General Hospital, Vancouver, BC, Canada

Background: The International Endocervical Adenocarcinoma Criteria and Classification (IECC) separated endocervical adenocarcinomas into human papillomavirus (HPV) associated (HPVA) and non–HPV-associated (NHPVA) categories by morphology alone. Our primary objective was to assess the accuracy of HPV prediction by the IECC system compared to p16 immunohistochemistry and HPV RNA in-situ hybridization (RISH). Our secondary goal was to directly compare p16 and HPV RISH concordance. **Methods:** Cases were classified by IECC and stained for p16 and HPV RISH on tissue microarray, with discordant p16/HPV RISH cases re-stained on whole tissue sections. Remaining discordant cases (p16/HPV, IECC/p16, IECC/HPV discordances) were re-reviewed by the original pathologists (n=3) and external expert pathologists (n=2) blinded to the p16 and HPV RISH results. Final IECC diagnosis was assigned upon independent agreement between all reviewers. **Results:** One hundred and eleven endocervical adenocarcinomas were classified originally into 94 HPVA and 17 NHPVA cases. p16 and HPV RISH was concordant in 108/111 cases (97%) independent of the IECC. HPV RISH and p16 was concordant with IECC in 103/111 (93%) and 106/111 (95%), respectively. After expert review, concordance improved to 107/111 (96%) for HPV RISH. After review of the eight discordant cases, one remained as HPVA, four were reclassified to NHPVA from HPVA, two were unclassifiable, and one possibly represented a mixed usual and gastric-type adenocarcinoma. **Conclusions:** p16 and HPV RISH have excellent concordance in endocervical adenocarcinomas, and IECC can predict HPV status in most cases. Focal apical mitoses and apoptotic debris on original review led to the misclassification of several NHPVA as HPVA.

Key Words: p16; Human papillomavirus; Immunohistochemistry; In-situ hybridization; Cervix; Adenocarcinoma; International Endocervical Adenocarcinoma Criteria and Classification; IECC

Received: April 9, 2020 **Revised:** July 15, 2020 **Accepted:** July 17, 2020
Corresponding Author: Lynn Hoang, MD, Department of Pathology and Laboratory Medicine, University of British Columbia, Vancouver General Hospital, 1215-910 West 10th Avenue, Vancouver, BC V5Z 1M9, Canada
Tel: +1-604-875-4731, Fax: +1-604-875-4497, E-mail: Lien.Hoang@vch.ca

Cervical cancer is the fourth most frequent cancer in woman worldwide, and up to 10%–20% of all cases are adenocarcinomas [1-3]. The classification of endocervical adenocarcinomas (ECA) as per the 2014 World Health Organization (WHO), stratifies ECA into different subtypes based predominantly on morphologic features. However, these categories do not reflect our modern understanding of ECA pathogenesis. Carcinomas of the uterine cervix and multiple other organ sites prone to high-risk human papillomavirus (HPV) infections, such as the vulva and oropharynx, have demonstrated worse overall survival for tumors that are HPV-independent [4-9]. Therefore, a similar framework was set out by the International Endocervical Adenocarcinoma Criteria and Classification (IECC) that divides tumors into HPV-associated (HPVA) and non–HPV-associated

pISSN 2383-7837
eISSN 2383-7845

(NHPVA) adenocarcinomas. The IECC assigns HPV status based on morphologic features alone, without the need for HPV testing. The IECC has shown superior interobserver reproducibility in comparison to the WHO system and it also confers clinical and prognostic significance [10,11].

Several techniques have been used to test for the presence of HPV. Traditional methods have included HPV DNA polymerase chain reaction (PCR) and DNA in-situ hybridization (ISH). Although positive HPV DNA PCR results demonstrate HPV presence, the result does not differentiate viral-induced tumorigenesis from a transient infection [12,13]. PCR for HPV E6/E7 mRNA served as the historical gold standard for pathogenic HPV but the test is not readily available and does not allow for direct visualization on tissue slides to assess for nuclear localization. HPV RNA ISH (RISH) is a relatively newer technology that circumvents the barriers of PCR and tests for the presence of HPV E6 and E7 mRNA by direct visualization on tissue slides. HPV RISH has shown higher sensitivity and specificity when compared to HPV DNA ISH and PCR, and has been officially endorsed by the College of American Pathologists (CAP) as the preferred methodology in 2020 [14-16].

In most laboratories, p16 immunohistochemistry (IHC) is the most frequently used surrogate marker for high-risk HPV infection. However, while the use of p16 IHC as a surrogate marker for HPV RISH has been examined in multiple squamous neoplasms of the uterine cervix, head and neck, penis and anus, few studies have actually assessed its performance in glandular neoplasms, particularly of the uterine cervix [17-27]. Moreover, in some recent studies, cervical gastric-type adenocarcinomas, a NHPVA tumor, actually showed diffuse p16 IHC staining, which is a potential pitfall for pathologists [28-30].

The primary goal of this study was to evaluate the accuracy of the IECC system to predict HPV status (morphology alone) by comparing it to HPV RISH and p16 IHC. Given the recent reports of p16 positivity in NHPVA adenocarcinomas, our secondary goal was to evaluate the usefulness of p16 IHC in predicting HPV status in ECAs using HPV RISH as the reference standard.

MATERIALS AND METHODS

Selection criteria and tumor classification

All ECAs diagnosed on resection (hysterectomy or trachelectomy) were identified from the archives of Vancouver General Hospital. Biopsies were excluded. Cases with prior neoadjuvant chemoradiation rendering histologic assessment difficult were excluded. Additional specimens from the same patient were excluded. Slides of all ECAs were originally reviewed and reclassified under the IECC criteria (L.H., J.P., and H.R.). The observers had variable expertise (junior attending, senior resident, junior resident), and the IECC assignment was made with all observers in agreement. As per the IECC, ECAs were assigned as HPVA based on the presence of apical mitotic features and apoptotic bodies present at scanning magnification. The HPVA ECAs were further substratified into usual-type, villoglandular-type, mucinous intestinal-type, mucinous signet ring-type, invasive stratified mucin-producing intraepithelial lesion (iSMILE), and mucinous not otherwise specified (NOS), as defined previously [11,31]. When these features were absent, the slides were reexamined at ×200. Cases were classified as NHPVA if HPVA features were absent. The NHPVA ECAs were further substratified into gastric-type, clear cell, mesonephric, endometrioid, and serous carcinoma based on their morphological features.

Tissue microarray construction

A tissue microarray (TMA) was constructed using formalin fixed paraffin embedded blocks. At least two 0.6 mm cores were taken from each case using the Pathology Devices TMArrayer (Pathology Devices, San Diego, CA, USA).

IHC and RNA in-situ hybridization

p16 (clone E6H4, mouse monoclonal, 1:5 dilution, Roche Diagnostics, Laval, Canada) IHC was performed on 4-μm sections using the Dako Omnis (Agilent, Santa Clara, CA, USA) and Dako EnVision FLEX+ detection system as per manufacturer recommendations. Sections were mounted onto Dako FLEX microscope slides, air-dried for 20 minutes and baked at 60°C for 20 minutes. The heat-induced antigen retrieval method was performed using Envision FLEX Target Retrieval Solution (Dako) in Dako PT Link.

HPV RISH was performed using the Advanced Cell Diagnostics (ACD) RNAScope 2.5 assay (Cat# 322300 ACD, Advanced Cell Diagnostics, Newark, NJ, USA) with RNAscope Probe HPV-HR18 (Cat#312591 ACD) which targets E6 and E7 mRNA for 18 high-risk HPV subtypes (HPV 16, 18, 26, 31, 33, 35, 39, 45, 51, 52, 53, 56, 58, 59, 66, 68, 73, and 82), as per manufacturer instructions [11]. In brief, 4-μm sections were baked at 60°C and air-dried. The slides were briefly treated with hydrogen peroxide for 10 minutes and then underwent target retrieval for 15 minutes and protease treatment for 30 minutes. Hybridization with probe was done at 40°C for 2 hours followed by series of signal amplification. Signal detection was achieved

through DAB staining before counterstaining with hematoxylin. Both RNAscope Positive Control Probe (Hs-PPIB, Cat# 313901 ACD) and RNAscope Negative Control Probe (DapB, Cat#310043 ACD) were used on separate sections for quality control purposes.

p16 IHC and HPV RISH were repeated on whole 4-μm sections when there was equivocal staining or when there was a discrepancy between p16 and HPV RISH scores on TMA. Cases not within the TMA were stained using whole sections directly.

p16 IHC and HPV RISH scoring

p16 IHC was scored positive only when there was strong and continuous diffuse staining in neoplastic glands (nuclear or nuclear and cytoplasmic) as previously established [32]. Absent, weak, or patchy staining was scored as negative. HPV RISH was scored positive only when there was dot-like nuclear staining as detailed previously [20].

Review of discordant cases

All cases which had discordance (either p16 IHC-HPV RISH, IECC-HPV RISH, IECC-p16 IHC) underwent re-review by the original institutional pathologists as well as by two external expert pathologists (R.S. and S.S.) who were blinded to the p16 IHC and HPV RISH findings. The final IECC diagnostic designation was determined when all observers (original pathologists and two expert pathologists) completely agreed on the diagnosis. Any cases without complete agreement were considered unclassifiable.

RESULTS

Case selection

A total of 129 ECAs were initially acquired. After exclusion of cases with biopsy specimen only, neoadjuvant therapy, insufficient tissue, or repeats, 111 cases were included in the study. The 111 cases grouped by the IECC included: 94 HPVA cases (63 usual-type, 4 intestinal, 4 villoglandular, 1 iSMILE, and 22 mucinous NOS) and 17 NHPVA cases (12 gastric, 4 mesonephric, and 1 NOS).

Eighteen cases in the tissue microarray had both p16 IHC and HPV RISH repeated on whole tissue sections. Twelve of 18 cases (66%) had a change in their p16 IHC and/or HPV RISH status after repeat staining on whole tissue sections. Of these 12 cases, six (50%) were positive for p16 IHC and negative for HPV RISH on TMA but showed positive staining for both p16 IHC and HPV RISH on whole sections. Four cases (33%) had absent or necrotic tumor cells on both p16 IHC and HPV RISH TMAs and showed positive staining for both p16 IHC and HPV RISH on whole sections. Two cases (17%) had positive p16 IHC on TMA but no tumor cells on HPV RISH TMA, and whole sections confirmed HPV RISH positivity. Three cases were not included in the construction of the TMA initially, and were stained using only whole sections.

Assessment of p16 IHC, HPV RISH, and IECC accuracy on original review

On initial assessment, p16 IHC and HPV RISH were concordant in 108/111 cases (97%) independent of the IECC assignment Eighty-eight cases were positive for both p16 IHC and HPV RISH, and 20 cases were negative for both p16 IHC and HPV RISH. The three cases that were discordant were all p16 positive and HPV RISH negative. These three cases are discussed in detail below.

On original review, the IECC assignment was concordant with HPV RISH in 103/111 cases (93%) and with p16 IHC in 106/111 cases (95%) (Table 1). Altogether, there were a total of eight cases with p16 IHC/HPV RISH and/or IECC/HPV RISH and/or IECC/p16 discordance. These eight discordant cases included seven HPVA cases (one usual-type, one mucinous intestinal-type, and five mucinous NOS [3 are mentioned

Table 1. Concordance of HPV RISH and p16 IHC with IECC histotype in 111 endocervical adenocarcinomas before and after external reviews

	Concordant		Discordant[a]		Unclassifiable	Overall concordance, n (%)
	HPVA/HPV+	NHPVA/HPV–	HPVA/HPV–	NHPVA/HPV+		
Original review	87	16	7	1	0	103/111 (92.8)
Expert review	87	20	1	1	2	107/111 (96.4)
	HPVA/p16+	NHPVA/p16–	HPVA/p16–	NHPVA/p16+		
Original review	90	16	4	1	0	106/111 (95.4)
Expert review	87	19	1	2	2	106/111 (95.4)

HPV, human papillomavirus; RISH, RNA in-situ hybridization; IHC, immunohistochemistry; IECC, International Endocervical Adenocarcinoma Criteria and Classification; HPVA, HPV associated.
[a]Discordant cases are detailed in Table 2.

https://doi.org/10.4132/jptm.2020.07.18

above in the preceding paragraph]) that were all found to be HPV RISH negative. There was one NHPVA case (gastric-type) that was found to be HPV RISH positive, which is described in detail below.

Histology re-examination with by original reviewers and by external expert reviewers

The histology of each of the eight discordant cases was reviewed again by the original internal reviewers as well as independently by two expert external reviewers (Table 2). Histology review of the one discordant usual-type ECA demonstrated classic HPVA features with apoptotic bodies and floating mitosis. The two external reviewers also independently thought it was HPVA. Its classification remained unchanged as HPVA usual-type ECA, despite the negativity for both p16 IHC and HPV RISH (Fig. 1).

One case initially called HPVA-mucinous intestinal-type, showed an ECA with ample eosinophilic cytoplasm with well-defined cell borders, with histologic features in keeping with NHPVA-gastric type ECA. Focally, the presence of goblet cells was identified, which was the initial rationale for classifying it as a HPVA-mucinous intestinal-type. Upon review, the intestinal-type ECA was reclassified as gastric-type ECA. The two external reviewers also called this NHPVA.

Of the five HPVA-mucinous NOS cases, two were negative for both p16 IHC and HPV RISH. On reassessment of both cases, there was only very focal apoptotic bodies and apical mitoses present. There were also other areas in the same tumor which showed ample intracytoplasmic mucin. Both cases were reclassified as a NHPVA-gastric type. The two external reviewers also agreed independently on the diagnosis.

Of the five HPVA-mucinous NOS cases, three were positive for p16 IHC and negative for HPV RISH. These cases were difficult to reclassify even after external reviews. One case exhibited villoglandular and glandular architecture. There were admixed columnar cells with vague mucinous cytoplasm and cuboidal cells forming small papillae (Fig. 2A, B). While all reviewers agreed that this case belonged in the NHPVA category, the precise histotype could not be agreed upon by morphology alone, yielding a final designation of NHPVA-NOS. The second case showed mostly solid nested growth and the cells exhibited severe cytologic atypia and admixed neutrophils. The nuclei were enlarged with conspicuous nucleoli. There was no agreement in histotype and this case was deemed unclassifiable (Fig. 2C). IHC performed in the clinical pathology workup showed positivity for estrogen receptor and negativity for monoclonal carcinoembryonic antigen and vimentin. The third case was similar. It comprised of nests

Table 2. p16 IHC/HPV RISH and histotype discordant cases with histology review and reclassification

Original histotype	p16	HPV RISH	Histology review	Reclassified
HPVA-usual	Neg	Neg	Internal review: Demonstrated HPVA features, with morphology in keeping with usual-type External reviewer 2: HPVA-usual External reviewer 3: HPVA-usual	HPVA-usual
HPVA-mucinous (intestinal)	Neg	Neg	Internal review: Goblet cells present; Lack of significant HPVA features, with morphology in keeping with gastric-type External reviewer 2: NHPVA-gastric External reviewer 3: NHPVA-gastric	NHPVA-gastric
HPVA-mucinous NOS	Neg	Neg	Internal review: Lack of significant HPVA features, with morphology in keeping with gastric-type External reviewer 2: NHPVA-gastric or endometrioid External reviewer 3: NHPVA-gastric or endometrioid	NHPVA-gastric
HPVA-mucinous NOS	Neg	Neg	Internal review: Lack of significant HPVA features, with morphology in keeping with gastric-type External reviewer 2: NHPVA-gastric External reviewer 3: NHPVA-gastric	NHPVA-gastric
HPVA-mucinous NOS	Pos	Neg	Internal review: Lack of significant HPVA features; Mixture of cuboidal and columnar cells with vague intracytoplasmic mucin; Likely NHPVA-gastric External reviewer 2: NHPVA-gastric or endometrioid External reviewer 3: NHPVA-clear cell	NHPVA-NOS
HPVA-mucinous NOS	Pos	Neg	Internal review: Usual or adenocarcinoma NOS unclassified, need HPV status External reviewer 2: HPVA-usual or NOS External reviewer 3: Unclassifiable	Unclassifiable
HPVA-mucinous NOS	Pos	Neg	Internal review: Nested cells with amphophilic cytoplasm and dense lymphoplasmacytic infiltrate–Unclassifiable External reviewer 2: HPVA-usual External reviewer 3: Unclassifiable	Unclassifiable
NHPVA-gastric	Pos	Mixed	Internal review: HPVA features focally present, hybrid morphology in keeping with mixed usual and gastric-type Not available for external review	Mixed (usual and gastric)

IHC, immunohistochemistry; HPV, human papillomavirus; RISH, RNA in-situ hybridization; HPVA, HPV associated; Neg, negative; NHPVA, non–HPV-associated; Pos, positive; NOS, not otherwise indicated.

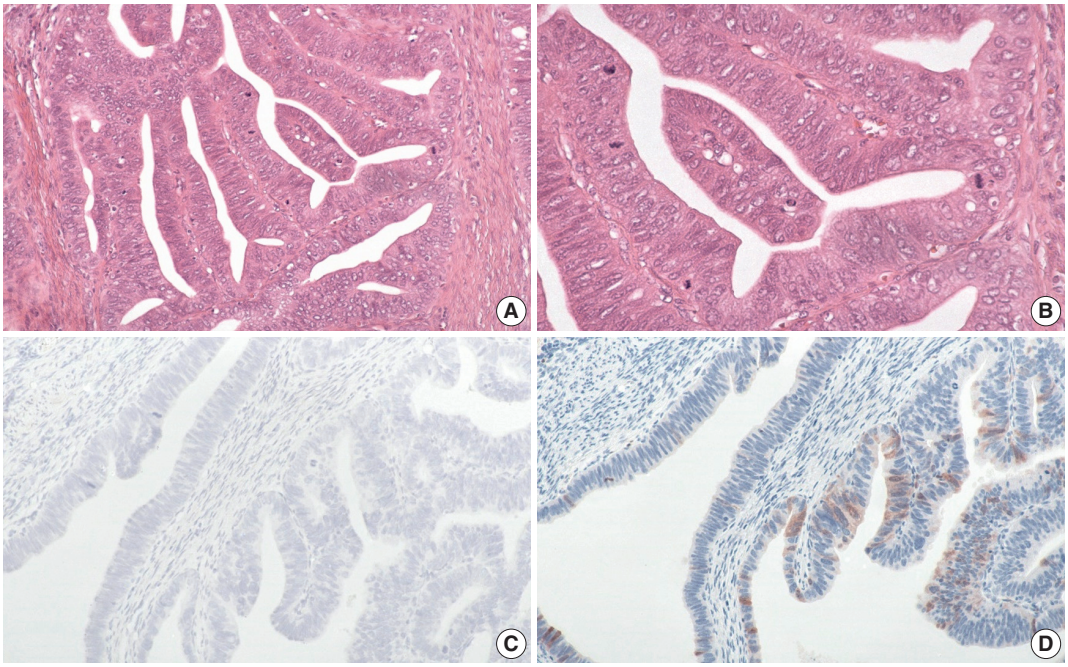

Fig. 1. The discordant human papillomavirus (HPV) associated (HPVA) usual-type case demonstrates classic HPVA features with floating mitosis and apoptotic bodies (A, B). Both HPV RNA in-situ hybridization (C) and p16 immunohistochemistry (D) are negative on whole slide staining. The classification remains unchanged as HPVA usual-type.

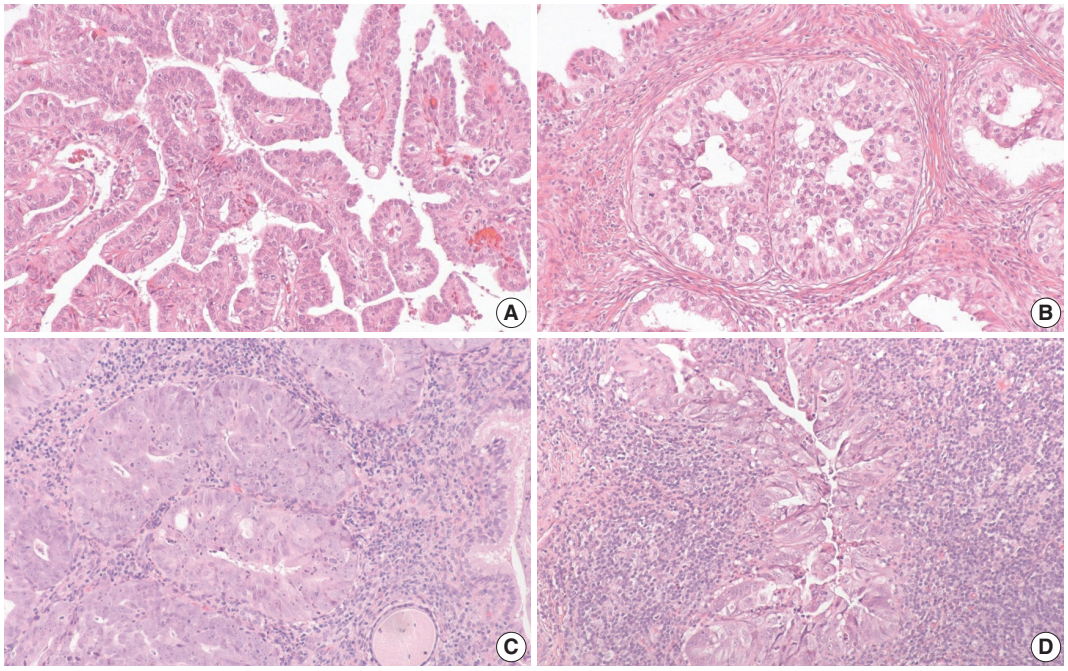

Fig. 2. Three discordant human papillomavirus (HPV) associated (HPVA)-mucinous not otherwise indicated (NOS) cases with positive p16 immunohistochemistry (IHC) and negative HPV RNA in-situ hybridization are difficult to classify. First HPVA-mucinous NOS case is reclassified as non–HPV-associated NOS, which demonstrates a component with papillary architecture with cuboidal cells (A), and a second component with columnar cells and mucin (B). Second HPVA-mucinous NOS case is deemed unclassifiable, which demonstrates solid nested growth with severe cytological atypia (C). The last HPVA-mucinous NOS case is also deemed unclassifiable, which demonstrates nested cells with amphophilic cytoplasm and dense lymphoplasmacytic infiltrate (D).

https://doi.org/10.4132/jptm.2020.07.18

of mucinous cells with severe cytologic atypia. There was a background of dense lymphoplasmacytic inflammation. This case was also deemed unclassifiable (Fig. 2D). No additional IHC was performed in the clinical pathology workup; however, this patient did have a history of cervical intraepithelial neoplasia 2 and adenocarcinoma-in-situ on a prior loop electrosurgical exci-

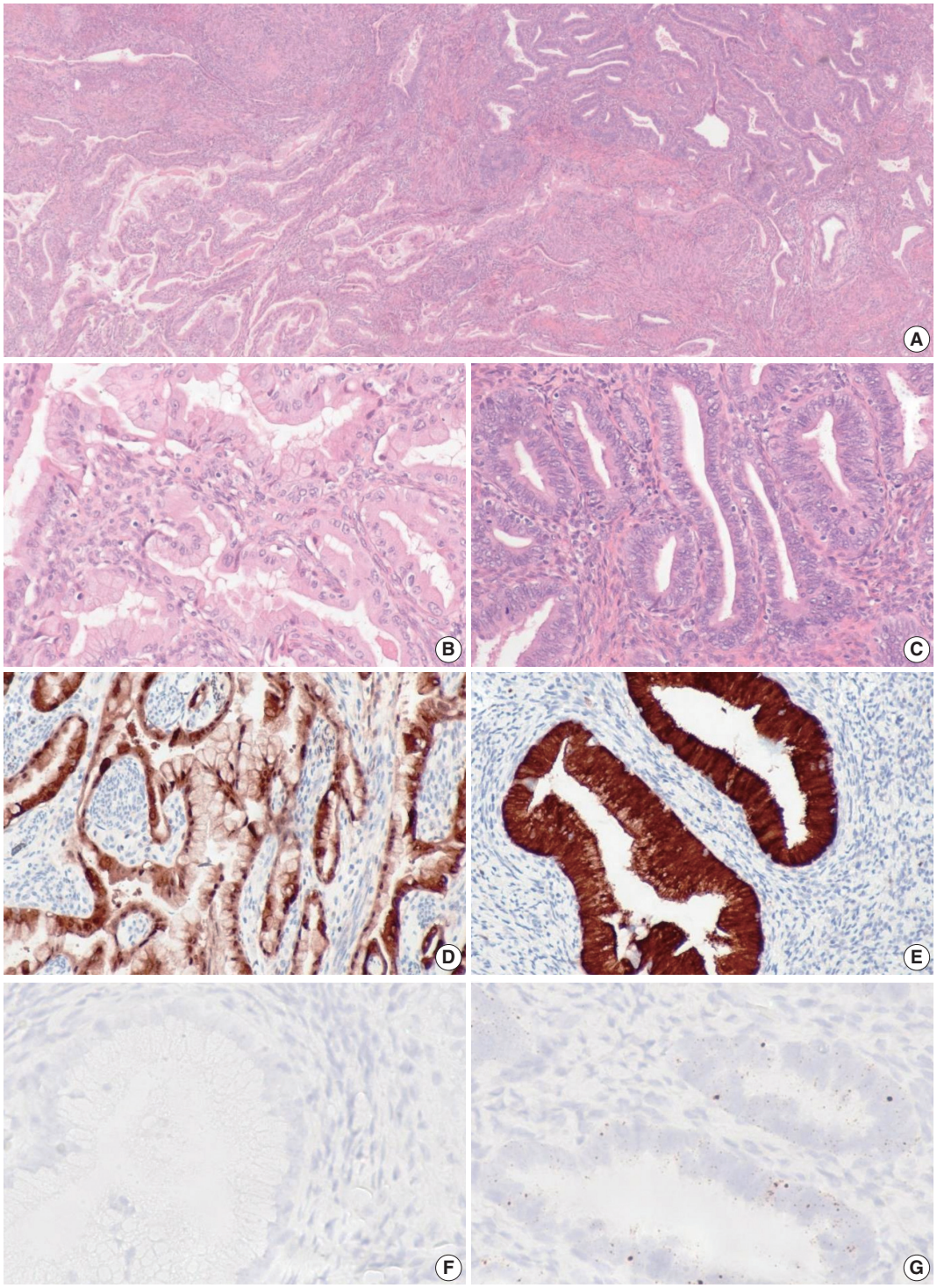

Fig. 3. One case of endocervical adenocarcinomas originally classified as gastric-type demonstrates mixed features showing both gastric-type and usual-type morphology on hematoxylin and eosin staining (A). The gastric-type component (B) does not have typical human papillomavirus (HPV) associated (HPVA) features and is positive for p16 immunohistochemistry (IHC) (D) and negative for HPV RNA in-situ hybridization (RISH) (F). The usual-type component does demonstrate HPVA features (C) and is positive for p16 IHC (E) and positive for HPV RISH (G).

sion procedure specimen.

When the one discordant NHPVA-gastric type ECA was re-reviewed, the histology demonstrated intermixed gastric-type and usual-type morphology, which were spatially distinct (Fig. 3). The two histotypes showed positive p16 IHC but a distinct HPV RISH profile. The usual-type component was positive for HPV RISH and more superficial, while the gastric-type component was negative for HPV RISH and more deep and infiltrative. Therefore, this case was reclassified as an ECA of mixed type. This patient presented with International Federation of Gynecology and Obstetrics stage IIB disease and was treated with adjuvant chemotherapy and radiation. Follow up after 5 years revealed no evidence of disease recurrence.

DISCUSSION

In our large series of cervical adenocarcinomas, we found that p16 IHC is concordant with HPV RISH in 97% of cases and is an excellent surrogate biomarker for high-risk HPV. On original review, p16 IHC and HPV RISH was concordant with IECC in 106/111 (95%) and 103/111 (93%) of cases, which remained unchanged for p16 IHC and improved to 107/111 (96%) for HPV RISH after expert review. Our study reiterates that the morphological guidelines denoted by the IECC are robust and can be relied on as the first step in reaching the correct ECA classification in the vast majority of cases.

Our results are in keeping with recent findings by Chen et al. [27], who demonstrated 100% sensitivity of p16 IHC for HPV RISH in HPVA ECAs, but demonstrated a lower specificity (88.89%). We also found 100% sensitivity of p16 IHC for HPV RISH, and a lower specificity (86.9%). Our p16 IHC and IECC concordance is also similar to that presented previously by Hodgson et al. [10] (92% in HPVA, 100% in NHPVA). However, their study demonstrated a higher false negative rate for p16 IHC in HPVA (5 of 63, 8% of cases). We only saw false-negative p16 IHC in one case (1%). The difference between our concordance rate is likely because any discordance in our study prompted staining of p16 on whole tissue sections.

It has been shown that p16 IHC can be positive in up to one-third of NHPVA-gastric type, which is a pitfall for pathologists [31]. In our series, our one hybrid ECA showed diffuse p16 IHC staining in the gastric-type component, two cases of gastric-type ECA showed patchy staining and the remainder of the gastric-type ECA showed negligible staining. We did not actually encounter a high rate of true p16 IHC positivity in our NHPVA-gastric cases. However, we did have three p16 IHC+/HPV RISH– cases which were reclassified after expert review as one NHPVA-NOS and two unclassifiable adenocarcinomas.

The HPVA-mucinous group posed the greatest challenge on our initial histologic assessment. Five HPVA-mucinous were reclassified after review (2 into NHPVA-gastric, 1 into NHPVA-NOS, and 2 were unclassifiable). In some of the cases, the low-power architecture (villoglandular), mucin-deplete columnar cells and goblet cells, prompted an initial diagnosis of HPVA. More often, it was the finding of very focal areas of luminal mitotic figures or apoptotic bodies that prompted a diagnosis of HPVA. The original reviews were performed by pathologists with varying levels of training and we believe this was a reflection of experience. Novice pathologists appear to take a more prescriptive approach, following the IECC rules very literally, such that any evidence of luminal mitoses or apoptotic debris renders a diagnosis of HPVA. The more seasoned pathologists appear to take a broader approach, incorporating the entire constellation of morphologic features and only considering luminal mitoses and apoptotic bodies when they are more conspicuous. This is an important finding to emphasize as many pathologists new to the IECC system may encounter this same problem. In practice, more time would be spent on each case assessing for these features as well as any adjacent in-situ lesions (adenocarcinoma in situ, lobular endocervical glandular hyperplasia) that would be informative for real-life practice. Even after careful review, some mucinous NOS cases were not classifiable, albeit a very small number (2/111, 2% of cases). In practice, additional immunohistochemical markers available in the clinical pathology laboratory (such as estrogen receptor, Napsin, p53) would likely allow for a refined diagnosis in these cases. For example, one of the unclassified cases had limited IHC workup which was positive for estrogen receptor and negative for vimentin and monoclonal carcinoembryonic antigen. It was subsequently signed out as invasive poorly differentiated adenocarcinoma, consistent with cervical primary, favor endometrioid.

Using morphology alone, we have identified one hybrid case with both NHPVA and HPVA features. Like the 13 cases reported by Wada et al. [33], the hybrid case contained features of both gastric and usual-type ECA. However, the cases presented in their study demonstrated either positive HPV or negative HPV in both gastric and usual-type components using HPV DNA ISH. Using HPV RISH, we showed a different staining pattern in the two components. Although a collision tumor is a possibility, we hypothesize that this tumor started as an HPV driven neoplasm which then gained additional mutations allowing for oncogenesis independent of HPV, with a subclone of the tumor

 https://doi.org/10.4132/jptm.2020.07.18

presenting as loss of HPVA and gain of NHPVA morphologic features. The favorable prognosis after 5 years also supports an HPVA origin.

There are a couple of minor limitations of this study to highlight. First, the HPV RISH kit detects 18 high-risk HPV subtypes, but more than 200 types of HPV have been recognized [34]. This could explain why the one usual-type ECA was negative for HPV RISH. Second, although p16 IHC is a robust surrogate marker for HPV infection, p16 IHC can be falsely negative in HPVA tumors in the setting of methylation induced-inactivation and allelic loss [35,36]. We did not assess for these advanced molecular features.

In summary, p16 IHC and HPV RISH have excellent concordance in endocervical adenocarcinomas. IECC classification demonstrated strong concordance with HPV testing using p16 IHC and HPV RISH, with HPV RISH being slightly superior to p16. Classification by IECC was excellent in novice pathologists, with only a slight improvement with the addition of expert pathologists. Of the IECC/HPV RISH or IECC/p16 IHC discordant cases, the majority were mucinous (i.e., mucinous intestinal-type, mucinous NOS and gastric-types). Therefore, in any cases with mucinous cytoplasm, pathologists should be extra careful to examine for conspicuous HPV-related histologic features, along with any associated in-situ lesions. The presence of goblet cells or very focal apoptotic bodies or luminal mitoses are not enough to designate a case as HPVA. Ambiguous cases may warrant referral for HPV RISH or PCR.

Ethics Statement

All procedures performed in the current study were approved by the Institutional Review Board (IRB) (H18-01652, October 1, 2018) in accordance with the 1964 Helsinki declaration and its later amendments. Formal written informed consent was not required with a waiver by the appropriate IRB.

ORCID

Hezhen Ren https://orcid.org/0000-0002-2779-7297
Jennifer Pors https://orcid.org/0000-0002-8675-916X
Christine Chow https://orcid.org/0000-0001-5098-5731
Monica Ta https://orcid.org/0000-0003-0281-393X
Simona Stolnicu https://orcid.org/0000-0002-4459-7019
Robert Soslow https://orcid.org/0000-0002-7269-5898
David Huntsman https://orcid.org/0000-0003-4934-3322
Lynn Hoang https://orcid.org/0000-0003-3692-8057

Author Contributions

Conceptualization: LH, DH. Data curation: HR, JP. Formal analysis: HR, LH. Investigation: CC, MT. Methodology: CC, MT. Supervision: LH, DH. Validation: LH. Visualization: HR, LH. Writing—original draft: HR, LH. Writing—review & editing: SS, RS, LH. Approval of final manuscript: all authors.

Conflicts of Interest

The authors declare that they have no potential conflicts of interest.

Funding Statement

This study has supported by the Carraressi Foundation, Sumiko Kobayashi Marks Memorial Fund, OVCare and the UBC & VGH Hospital Foundations.

References

1. Adegoke O, Kulasingam S, Virnig B. Cervical cancer trends in the United States: a 35-year population-based analysis. J Womens Health (Larchmt) 2012; 21: 1031-7.
2. Smith HO, Tiffany MF, Qualls CR, Key CR. The rising incidence of adenocarcinoma relative to squamous cell carcinoma of the uterine cervix in the United States: a 24-year population-based study. Gynecol Oncol 2000; 78: 97-105.
3. Stolnicu S, Hoang L, Soslow RA. Recent advances in invasive adenocarcinoma of the cervix. Virchows Arch 2019; 475: 537-49.
4. McAlpine JN, Leung SC, Cheng A, et al. Human papillomavirus (HPV)-independent vulvar squamous cell carcinoma has a worse prognosis than HPV-associated disease: a retrospective cohort study. Histopathology 2017; 71: 238-46.
5. Nooij LS, Ter Haar NT, Ruano D, et al. Genomic characterization of vulvar (pre)cancers identifies distinct molecular subtypes with prognostic significance. Clin Cancer Res 2017; 23: 6781-9.
6. Ang KK, Harris J, Wheeler R, et al. Human papillomavirus and survival of patients with oropharyngeal cancer. N Engl J Med 2010; 363: 24-35.
7. Fakhry C, Westra WH, Li S, et al. Improved survival of patients with human papillomavirus-positive head and neck squamous cell carcinoma in a prospective clinical trial. J Natl Cancer Inst 2008; 100: 261-9.
8. Rischin D, Young RJ, Fisher R, et al. Prognostic significance of p16INK4A and human papillomavirus in patients with oropharyngeal cancer treated on TROG 02.02 phase III trial. J Clin Oncol 2010; 28: 4142-8.
9. Posner MR, Lorch JH, Goloubeva O, et al. Survival and human papillomavirus in oropharynx cancer in TAX 324: a subset analysis from an international phase III trial. Ann Oncol 2011; 22: 1071-7.
10. Hodgson A, Park KJ, Djordjevic B, et al. International endocervical adenocarcinoma criteria and classification: validation and interobserver reproducibility. Am J Surg Pathol 2019; 43: 75-83.
11. Stolnicu S, Barsan I, Hoang L, et al. International Endocervical Adenocarcinoma Criteria and Classification (IECC): a new pathogenetic classification for invasive adenocarcinomas of the endocervix. Am J Surg Pathol 2018; 42: 214-26.
12. Prigge ES, Arbyn M, von Knebel Doeberitz M, Reuschenbach M. Diagnostic accuracy of p16(INK4a) immunohistochemistry in oropharyngeal squamous cell carcinomas: a systematic review and meta-analysis. Int J Cancer 2017; 140: 1186-98.
13. Jordan RC, Lingen MW, Perez-Ordonez B, et al. Validation of methods for oropharyngeal cancer HPV status determination in US cooperative group trials. Am J Surg Pathol 2012; 36: 945-54.
14. Wang F, Flanagan J, Su N, et al. RNAscope: a novel in situ RNA analysis platform for formalin-fixed, paraffin-embedded tissues. J Mol Diagn 2012; 14: 22-9.
15. Schache AG, Liloglou T, Risk JM, et al. Validation of a novel diagnostic standard in HPV-positive oropharyngeal squamous cell car-

cinoma. Br J Cancer 2013; 108: 1332-9.
16. Keung ES, Souers RJ, Bridge JA, et al. Comparative performance of high-risk human papillomavirus RNA and DNA in situ hybridization on college of American pathologists proficiency tests. Arch Pathol Lab Med 2020; 144: 344-9.
17. Satgunaseelan L, Chia N, Suh H, et al. p16 expression in cutaneous squamous cell carcinoma of the head and neck is not associated with integration of high risk HPV DNA or prognosis. Pathology 2017; 49: 494-8.
18. Augustin J, Outh-Gauer S, Mandavit M, et al. Evaluation of the efficacy of the 4 tests (p16 immunochemistry, polymerase chain reaction, DNA, and RNA in situ hybridization) to evaluate a human papillomavirus infection in head and neck cancers: a cohort of 348 French squamous cell carcinomas. Hum Pathol 2018; 78: 63-71.
19. Bishop JA, Ma XJ, Wang H, et al. Detection of transcriptionally active high-risk HPV in patients with head and neck squamous cell carcinoma as visualized by a novel E6/E7 mRNA in situ hybridization method. Am J Surg Pathol 2012; 36: 1874-82.
20. Evans MF, Peng Z, Clark KM, et al. HPV E6/E7 RNA in situ hybridization signal patterns as biomarkers of three-tier cervical intraepithelial neoplasia grade. PLoS One 2014; 9: e91142.
21. Roldan Urgoiti GB, Gustafson K, Klimowicz AC, Petrillo SK, Magliocco AM, Doll CM. The prognostic value of HPV status and p16 expression in patients with carcinoma of the anal canal. PLoS One 2014; 9: e108790.
22. Zappacosta R, Colasante A, Viola P, et al. Chromogenic in situ hybridization and p16/Ki67 dual staining on formalin-fixed paraffin-embedded cervical specimens: correlation with HPV-DNA test, E6/E7 mRNA test, and potential clinical applications. Biomed Res Int 2013; 2013: 453606.
23. Aumayr K, Susani M, Horvat R, et al. P16INK4A immunohistochemistry for detection of human papilloma virus-associated penile squamous cell carcinoma is superior to in-situ hybridization. Int J Immunopathol Pharmacol 2013; 26: 611-20.
24. Winters R, Trotman W, Adamson CS, et al. Screening for human papillomavirus in basaloid squamous carcinoma: utility of p16(INK4a), CISH, and PCR. Int J Surg Pathol 2011; 19: 309-14.
25. Evans MF, Matthews A, Kandil D, Adamson CS, Trotman WE, Cooper K. Discrimination of 'driver' and 'passenger' HPV in tonsillar carcinomas by the polymerase chain reaction, chromogenic in situ hybridization, and p16(INK4a) immunohistochemistry. Head Neck Pathol 2011; 5: 344-8.
26. Sheng Z, Minato H, Sasagawa T, et al. Detection of high-risk human papillomavirus subtypes in cervical glandular neoplasia by in situ hybridization. Int J Clin Exp Pathol 2013; 6: 2168-77.
27. Chen T, Li J, Wang S, Ning Y, Zhou X, Wang Y. High-risk HPV E6/E7 mRNA in situ hybridization in endocervical glandular neoplasia: performance compared with p16(INK4a) and Ki67 immunochemistry. Am J Transl Res 2019; 11: 6498-506.
28. Peng WX, Kure S, Ishino K, et al. P16-positive continuous minimal deviation adenocarcinoma and gastric type adenocarcinoma in a patient with Peutz-Jeghers syndrome. Int J Clin Exp Pathol 2015; 8: 5877-82.
29. Houghton O, Jamison J, Wilson R, Carson J, McCluggage WG. p16 Immunoreactivity in unusual types of cervical adenocarcinoma does not reflect human papillomavirus infection. Histopathology 2010; 57: 342-50.
30. Lu S, Shen D, Zhao Y, Kang N, Wang X. Primary endocervical gastric-type adenocarcinoma: a clinicopathologic and immunohistochemical analysis of 23 cases. Diagn Pathol 2019; 14: 72.
31. Stolnicu S, Barsan I, Hoang L, et al. Diagnostic algorithmic proposal based on comprehensive immunohistochemical evaluation of 297 invasive endocervical adenocarcinomas. Am J Surg Pathol 2018; 42: 989-1000.
32. Singh N, Gilks CB, Wong RW, McCluggage WG, Herrington CS. Interpretation of p16 immunohistochemistry in lower anogenital tract neoplasia [Internet]. Derby: British Association of Gynaecological Pathologists; 2018 [cited 2019 Dec 11]. Available from: https://www.bgcs.org.uk/wp-content/uploads/2019/05/BAGP-UKNEQAS-cIQC-project-p16-interpretation-guide-2018.pdf.
33. Wada T, Ohishi Y, Kaku T, et al. Endocervical adenocarcinoma with morphologic features of both usual and gastric types: clinicopathologic and immunohistochemical analyses and high-risk HPV detection by in situ hybridization. Am J Surg Pathol 2017; 41: 696-705.
34. Burd EM. Human papillomavirus and cervical cancer. Clin Microbiol Rev 2003; 16: 1-17.
35. Poetsch M, Hemmerich M, Kakies C, et al. Alterations in the tumor suppressor gene p16(INK4A) are associated with aggressive behavior of penile carcinomas. Virchows Arch 2011; 458: 221-9.
36. Nuovo GJ, Plaia TW, Belinsky SA, Baylin SB, Herman JG. In situ detection of the hypermethylation-induced inactivation of the p16 gene as an early event in oncogenesis. Proc Natl Acad Sci U S A 1999; 96: 12754-9.

 https://doi.org/10.4132/jptm.2020.07.18

JPTM
Journal of Pathology and Translational Medicine 2020; 54: 489-496
https://doi.org/10.4132/jptm.2020.07.19

ORIGINAL ARTICLE

Primary squamous cell carcinoma of the salivary gland: immunohistochemical analysis and comparison with metastatic squamous cell carcinoma

Uiree Jo[1], Joon Seon Song[1], Seung-Ho Choi[2], Soon Yuhl Nam[2], Sang Yoon Kim[2], Kyung-Ja Cho[1]

Departments of [1]Pathology and [2]Otorhinolaryngology-Head and Neck Surgery, Asan Medical Center, University of Ulsan College Medicine, Seoul, Korea

Background: Primary squamous cell carcinoma (SCC) of the salivary gland is a rare disease, and distinguishing primary SCC from metastatic SCC is difficult. This study investigated the histological and immunohistochemical differences between primary and metastatic salivary gland SCC to improve the accuracy of diagnosis and to explore the pathogenesis of this disease. **Methods:** Data of 16 patients who underwent surgery for SCC of salivary glands between 2000 and 2018 at Asan Medical Center were retrieved. Eight patients had a history of SCC at other sites, and eight patients had only salivary gland SCC. Immunostaining for p16, p53, androgen receptor (AR), gross cystic disease fluid protein 15 (GCDFP-15), and c-erbB2, as well as mucicarmine staining, were compared between the two groups. **Results:** Most tumors were located in the center of the salivary glands with extraparenchymal extension. The histology of primary SCC of the salivary gland was consistent with moderately differentiated SCC with extensive desmoplastic reaction and peritumoral inflammation. Involvement of the salivary gland ducts and transition into the ductal epithelium were observed in two cases. Metastatic SCC resembled the primary tumor histologically and was associated with central necrosis. Both groups exhibited negative mucin staining. Two, one, and one primary SCC case exhibited AR, GCDFP-15, and c-erbB2 positivity, respectively. **Conclusions:** A subset of primary SCCs originated in salivary ducts or was related to salivary duct carcinoma. Distinguishing primary from metastatic SCC of the salivary gland is difficult using histologic features and immunoprofiles. A comprehensive review of the medical history is essential.

Key Words: Primary squamous cell carcinoma; Metastatic squamous cell carcinoma; Salivary gland

Received: May 19, 2020 **Revised:** July 16, 2020 **Accepted:** July 17, 2020
Corresponding Author: Kyung-Ja Cho, MD, PhD, Departments of Pathology, Asan Medical Center, University of Ulsan College of Medicine, 88 Olympic-ro 43-gil, Songpa-gu, Seoul 05505, Korea
Tel: +82-2-3010-4545, Fax: +82-2-472-7898, E-mail: kjc@amc.seoul.kr

Primary squamous cell carcinoma (SCC) of the salivary gland is a rare disease, accounting for 1.6% (0.3%–6.9%) of salivary gland neoplasms [1-5]. The salivary gland is histologically composed of secretory, ductal, and myoepithelial cells. Various neoplasms exhibit secretory, ductal, or myoepithelial differentiation. Therefore, in patients with SCC in the salivary gland, the possibility of metastasis or direct invasion from the adjacent skin or the external auditory canal must be considered [3,4,6,7]. In addition, primary SCC must be differentiated from mucoepidermoid carcinoma (MEC) and salivary duct carcinoma using mucicarmine staining and androgen receptor (AR) and gross cystic disease fluid protein 15 (GCDFP-15) immunostainings. Most common events of carcinogenesis are associated with TP53 genetic mutation, and p16 is involving with multiple processes of carcinogenesis in cases of head and neck SCC [8,9]. This study was performed to discover expressional differences of p53 and p16 immunohistochemical (IHC) stainings between primary SCC and metastatic SCC. Wolff et al. [10] studied c-erbB2 expression in salivary gland carcinoma according to histologic subtype and aggressive behavior. Considering previous results, this study intended to determine the expressional characteristics in primary SCC and metastatic SCC [10-12]. Although the pathogenesis of primary SCC of the salivary gland is unknown, it can be associated with squamous metaplasia of the salivary duct or previous radiation treatment [4,5]. The aim of this study was to improve our understanding of the pathology and pathogenesis of primary

pISSN 2383-7837
eISSN 2383-7845

SCC of the salivary gland by comparing its features with those of metastatic SCC.

MATERIALS AND METHODS

Materials

Sixteen patients with surgically resected SCC of the salivary gland were identified after searching an anonymized research database at Asan Medical Center between 2000 and 2018. Patient characteristics are listed in Tables 1 and 2. Eight patients (50%) had primary SCC in the salivary gland. The cases of primary SCC in the salivary gland had no past history of cancer and revealed no other concurrent lesions through imaging studies such as computed tomography (CT) and positron emission tomography. SCC that had been diagnosed at other sites and metastasized to the salivary gland were designated as metastatic SCC in this study. The remaining eight cases (50%) in this study had a history of SCC at other sites and were classified as metastatic SCC. The clinical parameters collected from the electronic medical records were age at onset, sex, smoking history, survival, and treatment history.

Histologic analysis

All cases were histologically reviewed by two pathologists (K.J.C. and U.J.) with standard immunohistochemistry tests for diagnosis. Pathologic review included the following features: degree of differentiation of SCC, comprehensive (general) histologic features of SCC, pattern of infiltration, lymphovascular invasion, presence of peritumoral lymphocytes, and desmoplastic reactions. The histologic features were compared between the primary tumor and metastatic SCC. Regarding the previous studies, the possible presence of squamous ductal metaplasia, ductal dysplasia, or a ductal carcinoma component was investigated to help elucidate the pathogenesis of primary SCC of the salivary gland [6,13].

Immunohistochemical analysis and special staining

Formalin-fixed paraffin-embedded tissue specimens from primary and metastatic SCCs of the salivary gland were subjected to mucicarmine staining and IHC staining for p16, p53, AR, GCDFP-15, and c-erbB2. IHC staining was performed using the autoimmunostainer BENCHMARK XT (Ventana Medical Systems, Tucson, AZ, USA) with the OptiView DAB IHC Detection Kit (Ventana Medical Systems) according to the manufacturer's instructions using the reagents supplied with the kit. The antibodies used were as follows: mouse anti–GCDFP-15 (1:50, cat. MS1170A, clone 23A3, Neomarkers, Fremont, CA, USA), mouse anti-AR (1:100, cat. 200R-16, clone SP107, Cell

Table 1. Clinical characteristics of patients with primary SCC of the salivary gland

Case No.	Sex/Age (yr)	Location of tumor	Therapy	Survival (mo)	Smoking Hx (PY)	Previous radiation Hx
1	M/71	Parotid gland	Parotidectomy and adjuvant RT	Expired (32.2)	45	None
2	M/62	Parotid gland	Parotidectomy and adjuvant CCRT	Alive (97)	40	None
3	M/58	Parotid gland	Parotidectomy and adjuvant RT	Expired (21.7)	30	None
4	F/62	Submandibular gland	Excision	Alive (67)	None	None
5	M/62	Parotid gland	Parotidectomy and adjuvant CCRT	Alive (58.7)	40	None
6	M/65	Parotid gland	Parotidectomy	Alive (48.7)	30	None
7	M/62	Submandibular gland	Excision and adjuvant CCRT	Expired (11)	20	None
8	F/77	Submandibular gland	Excision and adjuvant RT	Expired (16.3)	None	None

SCC, squamous cell carcinoma; Hx, history; PY, pack years; M, male; RT, radiotherapy; CCRT, combined chemoradiotherapy; F, female.

Table 2. Clinical characteristics of patients with metastatic SCC of the salivary gland

Case No.	Sex/Age (yr)	Origin site of SCC	Location of metastatic tumor	Therapy for metastatic SCC	Survival after metastasis (mo)	Smoking Hx (PY)	Radiation Hx for original SCC
9	M/70	Cheek skin	Parotid gland	Parotidectomy	Expired (9.8)	50	None
10	F/76	Preauricular skin	Parotid gland	Parotidectomy and adjuvant RT	Expired (142)	None	None
11	M/69	EAC	Parotid gland	Parotidectomy and adjuvant RT	Expired (16.1)	None	None
12	F/75	Eyelid	Parotid gland	Parotidectomy and adjuvant RT	Expired (98.9)	None	None
13	F/57	Tongue	Parotid gland	Parotidectomy and adjuvant RT	Expired (8.7)	5	Present
14	M/85	EAC	Parotid gland	Wide excision	Alive (26.7)	30	None
15	M/76	Cheek skin	Parotid gland	Excision and adjuvant RT	Alive (24.2)	60	None
16	F/45	Scalp	Parotid gland	Parotidectomy and adjuvant CTx	Alive (24.2)	None	None

SCC, squamous cell carcinoma; Hx, history; PY, pack years; M, male; F, female; RT, radiotherapy; EAC, external auditory canal; CTx, chemotherapy.

https://doi.org/10.4132/jptm.2020.07.19

Marque, Rocklin, CA, USA), mouse anti-p53 (1:1,000, cat. M7001, clone DO-7, Dako, Glostrup, Denmark), mouse anti-p16 INK4 (1:6, cat. 805-7413, clone E6H4, Ventana Medical Systems), and rabbit anti-c-erbB2 (1:8, cat. 790-4493, clone 4B5, Ventana Medical Systems). Tumor sections at a thickness of 4 μm were deparaffinized, and antigen retrieval was performed by incubation in EDTA buffer (cell conditioner #1) for 32 minutes. After inactivation of the endogenous peroxidases and rinsing with Tris buffer, the sections were incubated in diluted primary antibodies for 16 minutes at 37°C. Staining for mucicarmine was performed using the Mucicarmine Staining Kit (Ventana Medical Systems).

Immunostaining for p53 and AR was identified by a dark brown stain confined to the nucleus and was scored as positive regardless of proportion. For GCDFP-15 and p16, cytoplasmic staining was interpreted as an immunopositive response. C-erbB2 staining was evaluated using the American Society of Clinical Oncology (ASCO) 2018 system [10]. For mucicarmine staining, intracytoplasmic rose-red coloring was interpreted as a positive result.

RESULTS

Clinical features

Overall, 16 patients were diagnosed with SCC of the salivary gland after surgery. Eight cases were classified as primary SCC, and the remaining eight cases were metastatic SCC of the salivary gland. Primary SCC of the salivary gland was located in the parotid gland in five cases (63%) and the submandibular gland in three cases (38%). Metastasis to the salivary glands occurred in the parotid glands and originated from facial skin in three cases, external auditory canal in two cases, tongue in one case, eyelid in one case, and scalp in one case. Patients ranged in age from 45 to 85 years, with an average age of 64.8 years for patients with primary SCC and 69.1 years for those diagnosed with metastatic SCC. Ten men and six women were involved in the study.

The clinical characteristics of each patient diagnosed with primary SCC are summarized in Table 1. Six men and two women aged 58–77 years presented with a gradual increase in swelling of the parotid (5/8, 63%) or submandibular region (3/8, 38%). None of the participants had received radiation to the head and neck, and six patients had a history of smoking. Most salivary gland tumors were identified as a heterogeneous enhancing mass with a spiculated border and invasion of adjacent tissues on CT imaging except one case that presented as a benign tumor with a well-defined border. Resected tumors measured 2.8–6.3 cm in the greatest dimension. The pathological stage for the TNM Classification of Malignant Tumors (TNM) of primary SCC in the salivary gland was adjusted in each case according to the American Joint Committee on Cancer (AJCC) Staging Manual 8th edition (Supplementary Table S1). Four cases of primary SCC were assessed as pT3, while the other four cases of primary SCC were evaluated as pT2. Five cases of primary SCC had lymph node metastasis. Among them, three were classified as pN3b, while the remaining two were classified as pN2b and pN1. Of the eight patients, seven received adjuvant treatment in the form of radiotherapy or combined chemoradiotherapy after surgery. Four patients died after treatment, one experienced metastasis of the primary SCC to the lungs at one year, and one developed local recurrence upon follow-up.

Table 3. Histologic analysis of primary and metastatic SCC

	Primary SCC	Metastatic SCC
Keratinization and keratin pearls	Present (6 of 8 cases)	Present (7 of 8 cases)
Intercellular bridges with large nuclei and eosinophil cytoplasm	Present	Present
Tumor border	Serrated and pointed	Bosselated and expansile
Peritumoral inflammation	Abundant	Variable
Necrosis	Variable	Central tumor necrosis
Desmoplasia	Abundant	Variable
Extraparenchymal extension	Present (8 of 8 cases)	Present (7 of 8 cases)
Ductal involvement	Present (2 of 8 cases)	Absent
Ductal differentiation	Present (1 of 8 cases)	Absent
Lymphatic invasion	Abundant (7 of 8 cases)	Variable (4 of 8 cases)
Vascular invasion[a]	Present (1 of 8 cases)	Present (1 of 8 cases)
Lymph node metastasis	Present (5 of 8 cases)	Present (3 of 8 cases)
Ipsilateral	4 of 8 cases	3 of 8 cases
Bilateral	1 of 8 cases	None

[a]The case of vascular invasion was concurrently observed with lymphatic invasion in both primary and metastatic squamous cell carcinomas (SCCs).

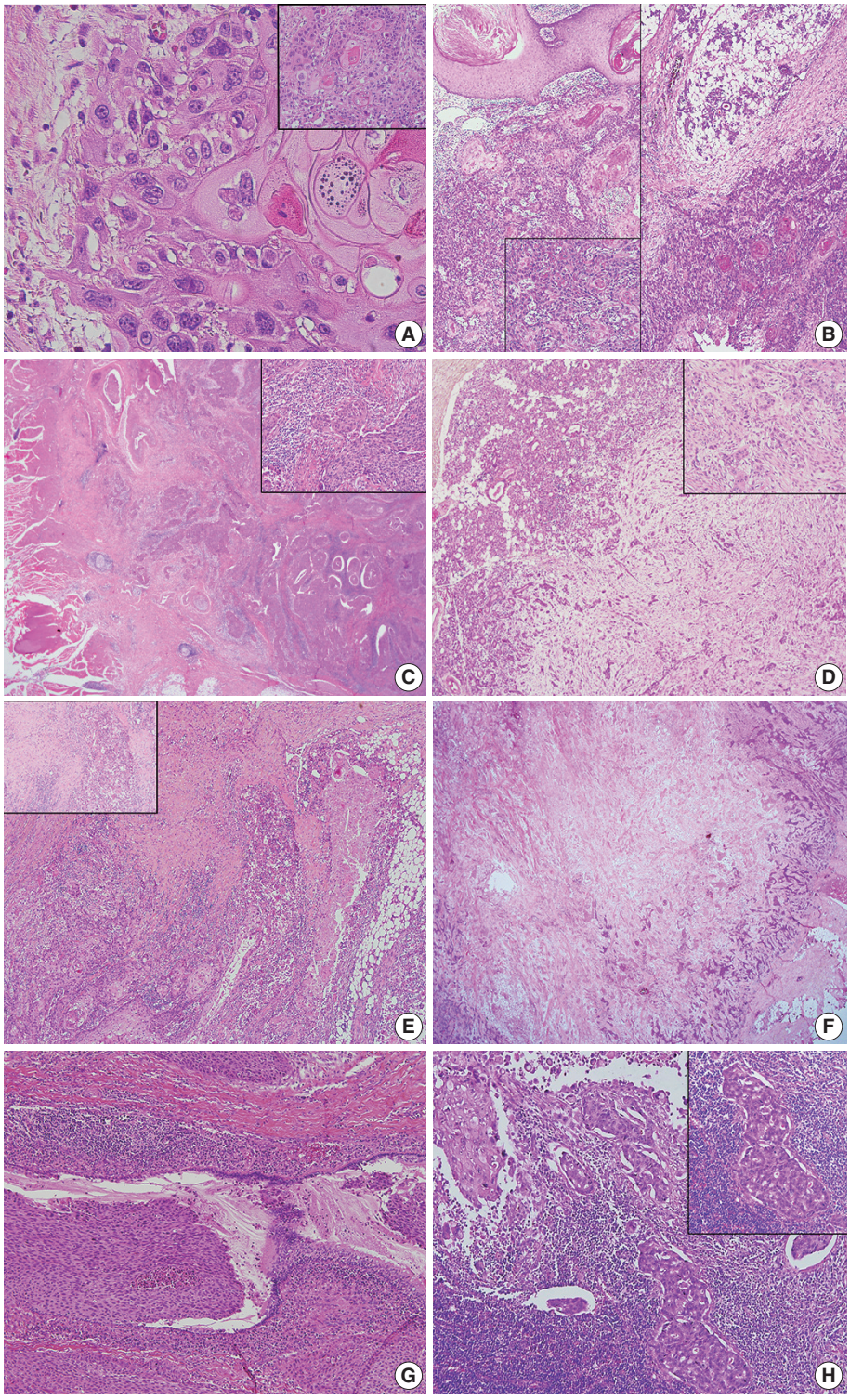

Fig. 1. Histologic features of primary squamous cell carcinoma (SCC) and metastatic SCC of the salivary gland. (A, B) Keratinization, keratin pearls, and intercellular bridges are observed in primary SCC (A, case #8; inset, ×100) and metastatic SCC (B, case #15; left, original SCC; right, metastatic SCC). (C, D) Representative tumor border and tumoral microenvironment in primary and metastatic SCC. Primary SCC shows serrated sharp borders (C, case #5; inset, peritumoral inflammation and desmoplasia), while metastatic SCC shows a bosselated smooth boundary (D, case #14; inset, ×200). (E, F) Tumor necrosis is irregularly distributed in primary SCC (E, case #8; inset, ×200) and centrally located in metastatic SCC (case #16). (G) Primary SCC continuing to transitional or pseudostratified ductal epithelium (case #5). (H) The transitional area of salivary duct carcinoma in SCC is observed in a metastatic lymph node (case #7).

https://doi.org/10.4132/jptm.2020.07.19

The clinical characteristics of the patients diagnosed with metastatic SCC are summarized in Table 2. There were four men and four women aged 45–85 years, with all cases involving the parotid glands. Metastatic SCCs were identified by a palpable mass or on CT imaging during follow-up after initial diagnosis of SCC. Resected tumors measured 0.6–3 cm in the greatest dimension. Three patients had synchronous lymph node metastasis at the time of detection of metastatic SCC in the parotid gland.

Histologic features

Representative histological features of primary and metastatic SCC of the salivary gland are summarized in Table 3. The same general histologic features of SCC were observed in the primary and metastatic groups including keratinization, keratin pearls, intercellular bridges, and large nuclei with eosinophilic cytoplasm (Fig. 1A). Metastatic SCC tended to resemble primary SCC (Fig. 1B). The frequency of keratinization and keratin pearl formation was similar between the primary and metastatic groups. Extraparenchymal extension was present in eight and six cases of primary and metastatic SCC, respectively, and different growth patterns were observed at the tumor boundary. Primary SCC was characterized by significant desmoplastic reactions and lymphoplasma cell infiltration resulting in serrated pointed borders (Fig. 1C). Metastatic SCC exhibited less desmoplasia and inflammatory reactions and possessed bosselated smooth borders (Fig. 1D). Necrosis patterns also differed between the groups, showing spotty necrosis in primary SCC and a central pattern in metastatic SCC (Fig. 1E, F). Two cases (cases #5 and #7) in the primary group showed involvement of large ducts, continuing to the transitional or pseudostratified ductal epithelium (Fig. 1G), thought to be a metaplastic step. Case #7 also exhibited the coexistence of squamous and ductal carcinomas in the metastatic lymph nodes (Fig. 1H). Lymphovascular invasion and regional lymph node metastasis were observed in both groups. The frequency of lymphovascular invasion, lymph node metastasis, and bilateral lymph node metastasis was slightly higher in primary SCC (Table 3).

IHC findings

The IHC staining results for primary and metastatic SCC of the salivary gland are shown in Table 4. The expression rates of p53, p16, and GCDFP-15 did not differ significantly between the two groups, except for a slightly higher rate of p53 positivity in the primary SCC group. Mucicarmine staining was negative in all 16 cases, excluding high-grade mucoepidermoid carcinoma. One primary SCC (case #5) (13%) was positive for c-erbB2 (Fig. 2A). An immunopositive response for AR was observed in two primary SCCs (25%), of which one (case #6) exhibited AR expression within the primary tumor (Fig. 2B), while one (case #7) showed AR expression at ductal differentiation in lymph node metastasis (Fig. 2C). This case also demonstrated focal GCDFP-15 positivity (Fig. 2D).

Table 4. Results of immunohistochemical and histochemical stains

	Primary SCC of salivary gland	Metastatic SCC of salivary gland
Staining		
Expression	8 (100)	8 (100)
p53		
Positive	7 (88)	5 (63)
Negative	1 (12)	3 (37)
p16		
Positive	5 (63)	6 (75)
Negative	3 (37)	2 (25)
Androgen receptor		
Positive	2 (25)[a]	0
Negative	6 (75)	8 (100)
GCDFP-15		
Positive	1 (12)	0
Negative	7 (88)	8 (100)
c-erb B2		
Positive	1 (12)	0
Negative	7 (88)	8 (100)
Mucicarmine		
Positive	0	0
Negative	8 (100)	8 (100)

Values are presented as number (%).
SCC, squamous cell carcinoma; GCDFP-15, gross cystic disease fluid protein 15.
[a]One of two cases expressing androgen receptor was found in metastatic tumors of primary SCC in lymph nodes.

Survival analysis

Overall survival (OS) was analyzed for primary and metastatic SCCs and compared with p16, p53, and AR IHC staining statuses of primary SCCs. Primary SCC did not exhibit significant differences in OS compared to metastatic SCCs ($p = .992$) (Supplementary Fig. S1A). When restricting the analysis to primary SCC only ($n = 8$), there were no statistically significant differences in survival according to p16, p53, and AR statuses (Supplementary Fig. S1B-D). The p53-positive group exhibited a tendency toward shorter OS ($p = .384$) (Supplementary Fig. S1B).

DISCUSSION

SCC of the salivary gland is an uncommon occurrence, and most cases represent metastases from other head and neck sites

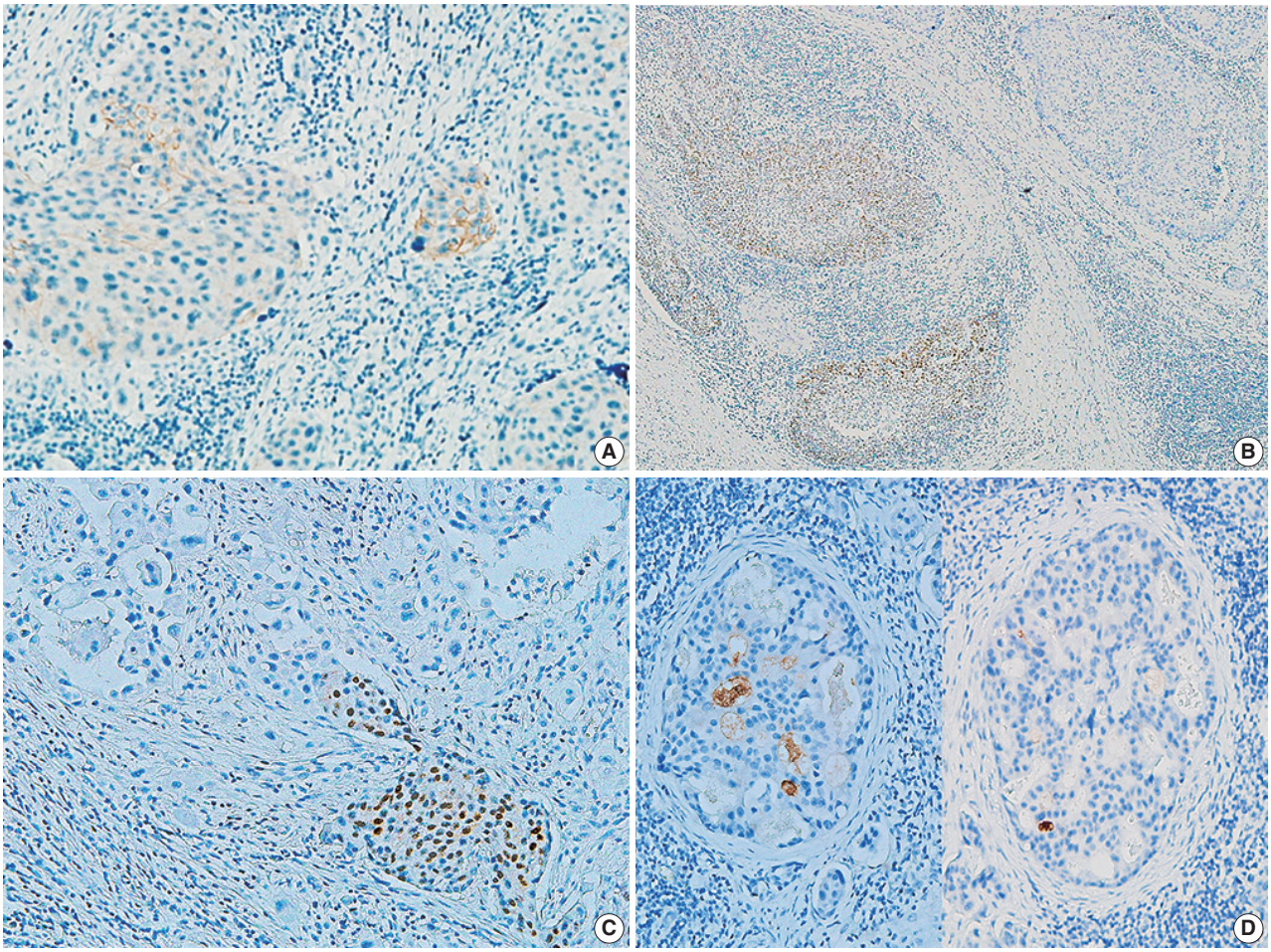

Fig. 2. Results of immunohistochemical staining in primary squamous cell carcinoma (SCC) and metastatic SCC. (A) Immunopositive reaction to c-erbB2 in primary SCC (case #5). (B, C) Immunopositive response to androgen receptor staining in the salivary duct carcinoma component of the primary tumor (B, case #6) and metastatic tumor (case #7) in primary SCC. (D) Focal positivity for gross cystic disease fluid protein 15 in a metastatic tumor of primary SCC in a lymph node (case #7).

[1,3,14]. There are few studies on primary SCC of the salivary gland [3,6,14], and a histologic comparison of primary and metastatic SCC has not been reported. The purpose of this study was to share helpful histologic features and diagnostic challenges between primary SCC and metastatic SCC of the salivary gland. Though previous studies researched variable kinds of salivary gland tumors including primary and metastatic tumors, the present series studied only SCCs of the salivary gland [6,14-16]. Therefore, primary SCCs of this study comprised a higher proportion (8 of 16 cases, 50%) among the total SCCs of the salivary gland retrieved over a 19-year period at one institution (Tables 1, 2). The histology of primary and metastatic SCCs was comparable even though some differences were observed. Primary SCCs exhibited a considerable desmoplastic reaction and peritumoral inflammation compared to metastatic SCCs, as well as a serrated margin and less central necrosis. However, these findings were non-specific, and distinguishing between the two groups was difficult based on histology alone.

Salivary duct involvement was observed in two primary SCCs, supporting the possible ductal origin of primary SCC of the salivary gland. Consistently, SCCs in situ arising from salivary ductal epithelium have been reported [6,13]. Flynn et al. [3] reported presence of squamous metaplasia within the ductal epithelium adjacent to invasive carcinoma in a fraction of primary SCC cases. One case in the present series exhibited a new finding of coexisting ductal and squamous carcinomas in a metastatic lymph node even though this phenomenon was not observed in the primary tumor. This ductal component was positive for AR and GCDFP-15 on IHC, consistent with salivary duct carcinoma, a predominantly apocrine tumor [7,17]. Although the other AR-positive case was pure SCC, AR-expressing areas contained lobules of non-keratinizing uniform cells, which is different from

https://doi.org/10.4132/jptm.2020.07.19

conventional SCC. AR expression in salivary SCC has not been reported [18-21]. These findings suggest a possible relationship between salivary duct carcinoma and SCC. A subset of primary SCCs of the salivary gland may be derived from extensive squamous differentiation of salivary duct carcinomas, whereas other cases may arise from squamous metaplasia of the salivary duct epithelium. While all metastatic SCCs involved the parotid gland, primary SCCs affected both parotid and submandibular glands. The parotid gland is the most commonly involved major gland in primary SCC [1,3,14], although many isolated cases of submandibular gland origin have been reported [4,5,16,22,23]. The location of primary SCC as well as the age and sex of the patients were similar to those reported for salivary duct carcinomas.

Previous radiation injury is a risk factor for salivary SCC development [4,5]. However, none of our patients had a history of radiation. Smoking is a risk factor for SCC of the head and neck. Six of the eight primary SCC patients were moderate smokers, supporting the role of smoking as a risk factor. The pathogenesis of primary SCC of the salivary gland remains to be determined.

An important issue in diagnosis of primary SCC of the salivary gland is exclusion of high-grade MEC. Mucin production suggests MEC or adenosquamous carcinoma arising in the salivary glands rather than primary SCC of the salivary gland. Taxy et al. [6] published controversial results regarding mucicarmine positivity in metastatic SCC of the submandibular gland and in one case of intraductal in situ SCC. The former case may have been metastatic MEC, while the latter case may have corresponded to early MEC. None of the primary or metastatic SCCs in this study exhibited intracytoplasmic mucin based on mucicarmine staining.

Primary SCC is a high-grade malignancy of the salivary gland that may require extensive excision with neck dissection and adjuvant radiotherapy [3]. A large series from the Surveillance, Epidemiology, and End Results database including 2,104 patients (not designated as primary) aged > 85 years with a tumor size ≥4 cm identified extraparenchymal extension, cervical metastasis, and distant metastasis as independent prognostic factors [2]. Surgery resulted in better 5-year disease-specific survival rates compared to no surgery or radiation alone. In the present series, all patients were younger than 85 years, and survival outcomes after surgery with or without radiotherapy were variable. The small sample size was a limitation of our study, and no prognostic factors were determined from the IHC results. However, with respect to treatment, effects of anti-AR therapy in primary SCCs of the salivary gland are anticipated [19,23].

To accurately diagnose primary SCCs of the salivary gland, metastatic disease and high-grade MEC must be excluded through careful evaluation of relevant patient history and special staining. Although the pathogenesis of salivary SCC remains unknown, the present histology and IHC results suggest a possible association with salivary duct carcinoma.

Supplementary Information

The Data Supplement is available with this article at https://doi.org/10.4132/jptm.2020.07.19.

Ethics Statement

All procedures performed for the current study were approved by the Institutional Review Board (IRB) of Asan Medical Center (Approval No. 2020-0746) in accordance with the 1964 Helsinki Declaration and its later amendments. Formal written informed consent was waived by the IRB.

ORCID

Uiree Jo https://orcid.org/0000-0001-6783-4016
Joon Seon Song https://orcid.org/0000-0002-7429-4254
Seung-Ho Choi https://orcid.org/0000-0001-9109-9621
Soon Yuhl Nam https://orcid.org/0000-0002-8299-3573
Sang Yoon Kim https://orcid.org/0000-0002-2162-7983
Kyung-Ja Cho https://orcid.org/0000-0002-4911-7774

Author Contributions

Conceptualization: KJC. Data curation: KJC, UJ, JSS. Formal Analysis: UJ. Investigation: UJ, KJC. Methodology: KJC. Project administration: UJ, JSS, KJC. Resources: UJ, JSS, KJC, SHC, SYN, SYK. Software: UJ. Supervision: KJC. Validation: KJC. Visualization: UJ. Writing—original draft: UJ. Writing—review & editing: KJC. Approval of final manuscript: all authors.

Conflicts of Interest

J.S.S., a contributing editor of the *Journal of Pathology and Translational Medicine*, was not involved in the editorial evaluation or decision to publish this article. All remaining authors have declared no conflicts of interest

Funding Statement

No funding to declare.

References

1. Batsakis JG. Primary squamous cell carcinomas of major salivary glands. Ann Otol Rhinol Laryngol 1983; 92(1 Pt 1): 97-8.
2. Chen MM, Roman SA, Sosa JA, Judson BL. Prognostic factors for squamous cell cancer of the parotid gland: an analysis of 2104 patients. Head Neck 2015; 37: 1-7.
3. Flynn MB, Maguire S, Martinez S, Tesmer T. Primary squamous cell carcinoma of the parotid gland: the importance of correct histological diagnosis. Ann Surg Oncol 1999; 6: 768-70.
4. Manvikar V, Ramulu S, Ravishanker ST, Chakravarthy C. Squamous cell carcinoma of submandibular salivary gland: a rare case report. J Oral Maxillofac Pathol 2014; 18: 299-302.
5. Panchbhai AS. Primary squamous cell carcinoma of salivary gland: report of a rare case. J Cancer Res Ther 2015; 11: 664.
6. Taxy JB. Squamous carcinoma in a major salivary gland: a review of the diagnostic considerations. Arch Pathol Lab Med 2001; 125: 740-5.
7. Williams L, Thompson LD, Seethala RR, et al. Salivary duct carcinoma: the predominance of apocrine morphology, prevalence of histologic variants, and androgen receptor expression. Am J Surg

Pathol 2015; 39: 705-13.
8. Alsahafi E, Begg K, Amelio I, et al. Clinical update on head and neck cancer: molecular biology and ongoing challenges. Cell Death Dis 2019; 10: 540.
9. Zhou G, Liu Z, Myers JN. *TP53* mutations in head and neck squamous cell carcinoma and their impact on disease progression and treatment response. J Cell Biochem 2016; 117: 2682-92.
10. Wolff AC, Hammond ME, Allison KH, Harvey BE, McShane LM, Dowsett M. HER2 testing in breast cancer: American Society of Clinical Oncology/College of American Pathologists clinical practice guideline focused update summary. J Oncol Pract 2018; 14: 437-41.
11. Glisson B, Colevas AD, Haddad R, et al. HER2 expression in salivary gland carcinomas: dependence on histological subtype. Clin Cancer Res 2004; 10: 944-6.
12. Xu B, Wang L, Borsu L, et al. A proportion of primary squamous cell carcinomas of the parotid gland harbour high-risk human papillomavirus. Histopathology 2016; 69: 921-9.
13. Gallego L, Junquera L, Calvo N, Fuente E, Rosado P. Bilateral carcinoma in situ of Wharton's duct after chronic obstructive sialadenitis: inflammation as the cause of malignancy? Ann Otol Rhinol Laryngol 2012; 121: 296-300.
14. Franzen A, Lieder A, Guenzel T, Buchali A. The heterogenicity of parotid gland squamous cell carcinoma: a study of 49 patients. In Vivo 2019; 33: 2001-6.
15. Bron LP, Traynor SJ, McNeil EB, O'Brien CJ. Primary and metastatic cancer of the parotid: comparison of clinical behavior in 232 cases. Laryngoscope 2003; 113: 1070-5.
16. Kulkarni AA, Thakur SS. Primary squamous cell carcinoma of submandibular salivary gland with sialo-cutaneous fistula: a rare case report. J Clin Diagn Res 2015; 9: PD03-5.
17. Kapadia SB, Barnes L. Expression of androgen receptor, gross cystic disease fluid protein, and CD44 in salivary duct carcinoma. Mod Pathol 1998; 11: 1033-8.
18. Can NT, Lingen MW, Mashek H, et al. Expression of hormone receptors and HER-2 in benign and malignant salivary gland tumors. Head Neck Pathol 2018; 12: 95-104.
19. Dalin MG, Watson PA, Ho AL, Morris LG. Androgen receptor signaling in salivary gland cancer. Cancers (Basel) 2017; 9: 17.
20. Nasser SM, Faquin WC, Dayal Y. Expression of androgen, estrogen, and progesterone receptors in salivary gland tumors: frequent expression of androgen receptor in a subset of malignant salivary gland tumors. Am J Clin Pathol 2003; 119: 801-6.
21. Udager AM, Chiosea SI. Salivary duct carcinoma: an update on morphologic mimics and diagnostic use of androgen receptor immunohistochemistry. Head Neck Pathol 2017; 11: 288-94.
22. Agarwal M, Agarwal L, Saxena R. Primary squamous cell carcinoma of submandibular salivary gland: a case report. J Clin Diagn Res 2017; 11: XD01-2.
23. Gaikwad RV, Kumaraswamy SV, Keerthi R. Primary squamous cell carcinoma of the submandibular salivary gland: a rare entity. J Maxillofac Oral Surg 2015; 14(Suppl 1): 57-9.

 https://doi.org/10.4132/jptm.2020.07.19

JPTM
Journal of Pathology and Translational Medicine 2020; 54: 497-503
https://doi.org/10.4132/jptm.2020.09.14

ORIGINAL ARTICLE

Can BAP1 expression loss in mesothelial cells be an indicator of malignancy?

Hanife Gulnihal Ozdemir[1], Sermin Coban Kokten[2], Nagehan Ozdemir Barisik[2]

[1]Department of Pathology, Osmaniye Public Hospital, Osmaniye; [2]University of Health Sciences Kartal Dr Lutfi Kırdar Training and Research Hospital, Istanbul, Turkey

Background: Malignant mesothelioma is a highly aggressive tumor that can be confused with a benign mesothelial lesion, especially cytomorphologic lesions. BRCA1-associated protein 1 (BAP1) acts as a tumor suppressor. In this study, we aim to investigate the value of BAP1 staining of malignant mesothelioma cases with expression loss and diagnosis in cell block and biopsy tissue. **Methods:** Between January 2009 and March 2017, 64 mesotheliomas, 117 reactive mesothelial hyperplasias, and 20 fibrinous pleuritis/pericarditis were diagnosed with morphologic and immunohistochemical findings in our pathology clinic and were included in the study. Formalin-fixed, paraffin-embedded tissues were immunohistochemically examined for BAP1. Inflammatory and stromal cells were used as positive internal controls. BAP1 was assessed for nuclear staining in mesothelial cells. **Results:** Examinations of the relationship between patient diagnosis and BAP1 biopsy status showed that the BAP1 loss rate (76.6%) was significantly higher in malignant mesothelioma cases than in other benign diseases (0%) ($p < .001$). Sensitivity and specificity were 76.56% and 100%, respectively, for biopsy tissue from malignant mesothelioma. Sensitivity and specificity were both 100% for BAP1 test on cell block tissue. Furthermore, the consistency between BAP1 cell block and biopsy results was excellent ($\kappa = 0.90$) and the correlation was significant ($p < .001$). **Conclusions:** This study shows that BAP1 expression loss in both cytology and biopsy tissue in biopsy-confirmed malignant mesothelioma cases is an essential parameter for malignant mesothelioma diagnosis.

Key Words: Asbestosis; BAP1; Immunohistochemistry; Malignant mesothelioma; Pleura

Received: May 26, 2020 **Revised:** August 22, 2020 **Accepted:** September 14, 2020
Corresponding Author: Hanife Gulnihal Ozdemir, MD, Department of Pathology, Osmaniye Public Hospital, Akyar Central Location Hospital Street Osmaniye/Center 80010, Turkey
Tel: +90-5547884275, E-mail: dr.gulnihalzdmr@gmail.com

Malignant mesothelioma (MM) is an aggressive tumor originating from serosal surfaces, mostly pleura [1]. Exposure to some carcinogens, especially asbestos, is a strong risk for MM development [2,3]. MM has an inadequate response to treatment because in most patients diagnosis is delayed. However, prognosis is better if recognized earlier. Therefore, it is crucial to diagnose MM early [4-6].

About 80% of MM cases are associated with asbestos exposure. MM incidence is high in Turkey, especially the Cappadocia region, where environmental asbestos is widely distributed [7]. It is thought that 20 years or more of asbestos exposure can increase the risk of MM development.

Malignant mesothelioma, benign mesothelial neoplasia, and reactive mesothelial proliferation are lesions that are difficult to diagnose because they mimic each other cytomorphologically. Although the features supporting malignancy include clear cytological atypia, dense cell clusters, and necrosis, the most reliable diagnostic criterion is the presence of deep-tissue invasion [8]. MM diagnosis in cytologic materials is even more difficult because invasion is the only reliable standard.

To date, an immunohistochemical marker that can reliably differentiate a reactive process from neoplastic mesothelioma does not exist [9,10]. Various immunohistochemical markers (epithelial membrane antigen, p53, p100, p-glycoprotein, desmin, etc.) are used together to reach a final decision [11-13].

BRCA1-associated protein 1 (BAP1) acts as a tumor suppressor and belongs to the family of high-risk cancer-related genes located at 3p21.1. It is associated with a high-risk cancer syndrome that includes malignancies such as malignant mesothelioma, uveal melanoma, cutaneous melanoma, atypical melanocytic tumor, and renal cell carcinoma (especially clear-cell type). BAP1 expression loss may be an indicator of malignancy in mesotheli-

pISSN 2383-7837
eISSN 2383-7845

omas [4,14,15]. BAP1 is not yet routinely used as an immunohistochemical marker but may soon be preferred for diagnosis and targeted treatment [16,17].

This study aims to investigate the efficacy of immunohistochemically stained BAP1 antibodies for differential diagnosis of MM, reactive mesothelial hyperplasia (RMH), and fibrinous pleuritis/pericarditis (FP).

MATERIALS AND METHODS

Case selection

Sixty-four patients with mesothelioma, 117 patients with reactive mesothelial hyperplasia, and 20 patients with FP who were diagnosed at our pathology clinic between January 2009 and March 2017 were included in the study. Diagnosis of the MM cases was made according to presence of deep-tissue invasion composed of mesothelial cells using immunohistochemically applied calretinin, WT1, and D2.40 stains of biopsy tissue. The cell blocks obtained from cytological material taken during biopsy were evaluated for the presence of mesothelial cells. The cell blocks, which were also stained with the same immunohistochemical markers, were also analyzed for this study.

We examined slides, paraffin blocks, and report archives of all the study cases where available. Cell blocks of cytological material and biopsy tissue were evaluated for suitability for immunohistochemical examination. Both cell blocks and tissue blocks that had sufficient mesothelial cells (≥ 20 cells) were immunohistochemically stained with BAP1 antibodies. For cases that did not have cell blocks or that had insufficient mesothelial cells in cell blocks, only tissue blocks were stained. Two pathologists, blinded from the diagnosis, evaluated results on light microscopy.

Immunohistochemical procedure

For immunohistochemical examination, 4-μm-thick sections prepared from formalin-fixed and paraffin-embedded tissues were used. Tissue sections were taken into electrostatically charged slides (Isotherm) and dried at 70°C for at least 1 hour. The whole immunohistochemical staining process, including deparaffinization and antigen release, was performed on a fully automated immunohistochemistry staining device (Ventana BenchMark XT, Ventana Medical Systems, Tucson, AZ, USA). We used a ready-made kit that is biotin-free, based on an horseradish peroxidase (HRP) multimer, and contains hydrogen peroxide substrate and 3,3'-diaminobenzidine tetrahydrochloride (DAB) chromogen (Catalog number 760-500, ultraView Universal DAB Detection Kit, Ventana Medical Systems) for this process. BAP1 antibody (1:100, Thermo Fisher Scientific, Rockford, IL, USA) was administered. Contrast staining with hemotoxylin and bluing solution was performed with a staining device; the procedure was completed manually with dehydration, transparency with xylene, and closure of the sections with lamel.

Inflammatory and stromal cells in the cell block of cytologic materials and biopsy materials were used as a positive internal control for BAP1 antibody. Mesothelial cells were evaluated via nuclear staining with BAP1 antibodies. Detection of nuclear staining was interpreted as "BAP1 normal expression" (Fig. 1A–D) and lack of staining as "loss of BAP1 expression" (Fig. 2A–D). Cytoplasmic staining, observed in some cases, was evaluated as nonspecific, and we took into account only nuclear staining.

Statistical analyses

Statistical analyses were performed using SPSS ver. 16.0 software (SPSS Inc., Chicago, IL, USA). Variables were evaluated for normality both visually (histogram and probability graphs) and statistically (Kolmogorov-Smirnov/Shapiro-Wilk tests). Descriptive analyses were performed using mean and standard deviations for normally distributed variables. In cases where the data were not normally distributed, the Mann-Whitney U test was used to compare two groups and the Kruskal-Wallis test was used to compare more than two groups. The chi-square and Fisher exact tests were used to compare nominal variables, e.g., biopsy results. Patient age was recategorized into ordinal groups and trend analysis was performed with meaningful parameters. Also, we used the Kappa test to determine the consistency of biopsy results with each other. A p-value < .05 was considered statistically significant.

RESULTS

Of 64 MM cases, 40 (62.5%) were male and 24 (37.5%) were female. The median age at diagnosis was 61 (± 12.26) years, and 56.3% of the patients were between 40–64 years old. While 57 of the 64 cases (89.1%) originated in the pleura, six (9.4%) were from the peritoneum and one (1.5%) from the pericardium. In histological subtypes, 54 cases (84.4%) were epithelioid type, five cases (5.2%) sarcomatoid type, and 5 cases (5.2%) biphasic type. Asbestos exposure was detected in 35.9% of our MM cases.

Seventy-four of 117 RMH cases (63.2%) and 15 of 20 FP cases (75%) were male, with median ages of 45 (± 19.36) years and 59.5 (± 16.07) years, respectively. Of the 137 non-MM cases (117 RMH and 20 FP), 103 biopsy specimens (75.1%) were taken from the pleura, 31 (22.6%) from the peritoneum, and 3

 https://doi.org/10.4132/jptm.2020.09.14

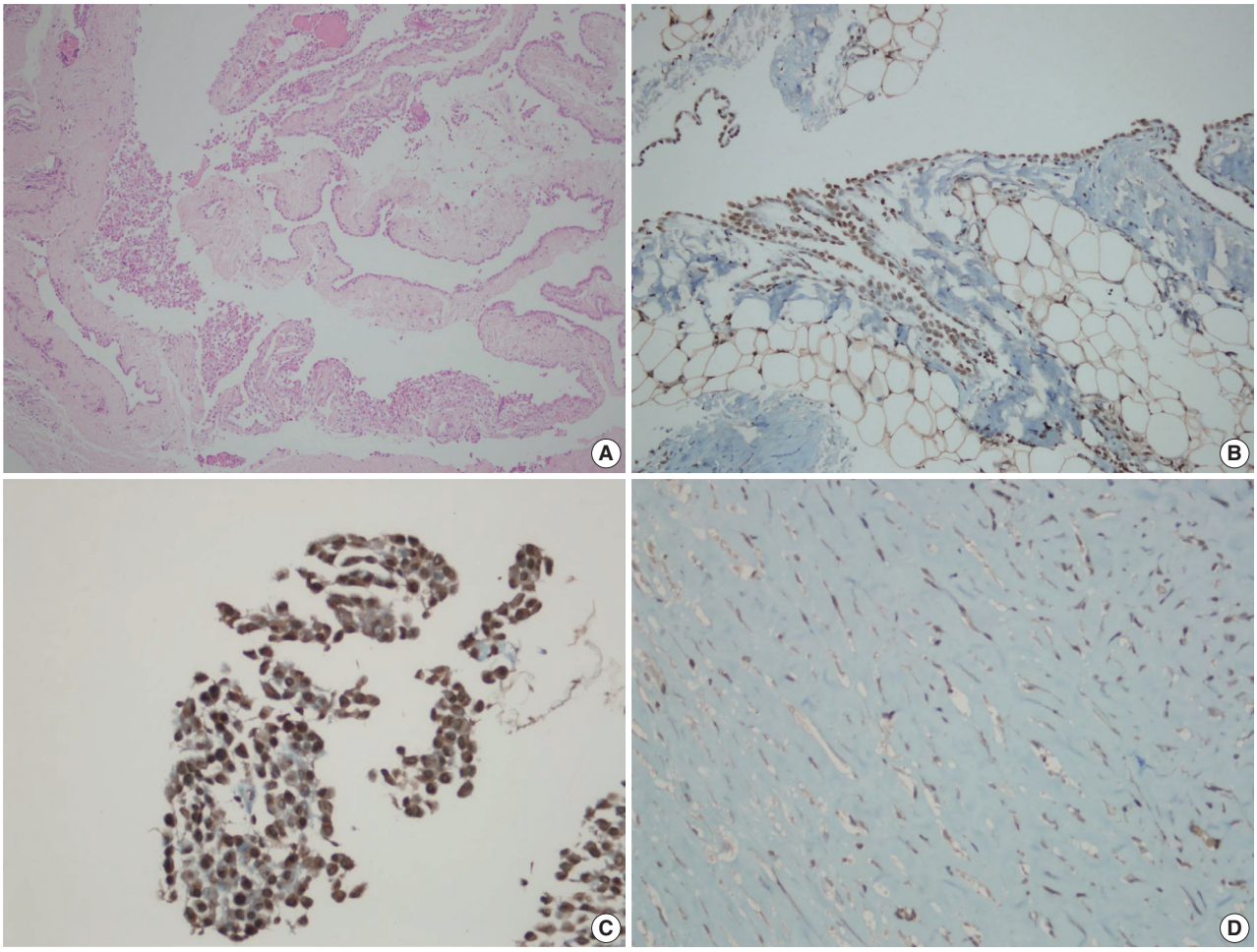

Fig. 1. BRCA1-associated protein 1 (BAP1) immunohistochemistry results in reactive mesothelial hyperplasia. Biopsy material with hematoxylin and eosin staining (A) and BAP1 immunohistochemistry (B) with strong nuclear staining. Cell block material with BAP1 immunohistochemistry staining. (C) Note the strong nuclear and weak nonspecific cytoplasmic staining. (D) An example of a fibrinous pleuritis case with BAP1 staining.

(2.3%) from the pericardium.

According to biopsy status, the BAP1 expression loss rate (76.6%) in patients diagnosed with MM was significantly higher than among other benign diseases (0%; $p < .001$). When MM cases were evaluated by histological subtype, the BAP1 expression loss rate was 81.5% in epithelioid-type MM cases, whereas no BAP1 expression loss was observed among sarcomatoid-type MM cases. BAP1 expression loss was observed in all five biphasic cases, but all expression loss was found in the epithelioid components, and no loss was found in the sarcomatoid components (Table 1). For MM diagnosis, the sensitivity and specificity of BAP1 expression loss in tissue biopsies were 76.56% and 100%, respectively.

Only the epithelioid histological subtype of malignant mesothelioma cases had sufficient cell block material. According to cell block status, expression loss was observed in all malignant mesothelioma cases ($n = 11$), while there was no expression loss in any of the benign processes (8 RMH and 1 FP cases). The sensitivity and specificity of the BAP1 test were both 100% for cell block (Table 2).

When the consistency between cell block and tissue biopsy results for BAP1 expression status was examined, a high consistency ($\kappa = 0.90$) and significant correlation were obtained ($p < .001$). Accordingly, 10 of the 11 patients (90.9%) who were found to have BAP1 expression loss in cell block also showed expression loss in biopsy, while all nine patients (100%) who did not show expression loss in cell block also showed no loss in biopsy (Table 3).

MM cases were evaluated in terms of BAP1 expression loss according to age, gender, asbestos exposure, additional cancer, and localization, and no significant differences were found (all $p > .05$) (Table 4).

DISCUSSION

Due to high tumor aggressiveness, distinguishing MM cases from reactive processes and diagnosing accurately as early as possible is of great importance [4-6]. However, the only reliable criterion for histopathological diagnosis is detection of fatty tissue invasion [8]. Unfortunately, these criteria cannot be evaluated in cytological materials. For this reason, numerous studies have been conducted to find an immunohistochemical marker that might aid MM diagnosis or even offer a definitive diagnosis.

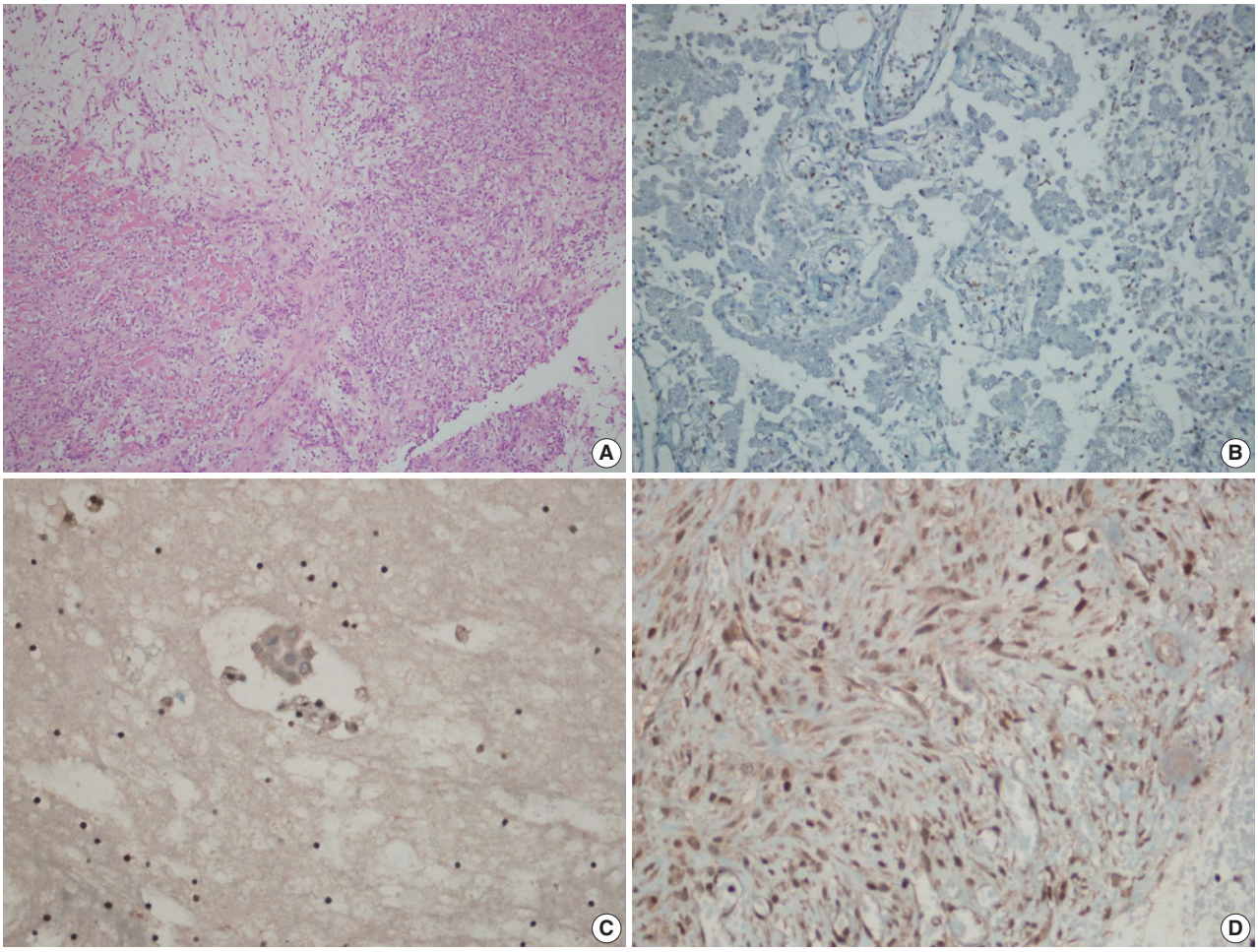

Fig. 2. BRCA1-associated protein 1 (BAP1) immunohistochemistry results in malignant mesothelioma. Biopsy material with hematoxylin and eosin staining (A) and loss of BAP1 expression (B) with inflammatory cells as a positive internal control in epithelioid mesothelioma. Cell block material with BAP1 staining (C). BAP1 normal expression in sarcomatoid mesothelioma (D).

Table 1. BAP1 expression status according to biopsy diagnosis

	Loss of BAP1 expression (n=49)	BAP1 normal expression (n=152)	p-value
Histologic type (n=201)			<.001
Malignant mesothelioma	49 (76.6)	15 (23.4)	
Reactive mesothelial hyperplasia	0	117 (100)	
Fibrinous pleuritis/Pericarditis	0	20 (100)	
Histologic subtype of MM (n=64)			<.001
Epithelioid type	44 (81.5)	10 (18.5)	
Sarcomatoid type	0	5 (100)	
Biphasic type	5 (100)	0	

BAP1, BRCA1-associated protein 1; MM, malignant mesothelioma.

Table 2. BAP1 expression status according to cell block diagnosis

	Loss of BAP1 expression (n=11)	BAP1 normal expression (n=9)	p-value
Histologic type (n=20)			<.001
Malignant mesothelioma	11 (100)	0	
Reactive mesothelial hyperplasia	0	8 (100)	
Fibrinous pleuritis/pericarditis	0	1 (100)	
Histologic subtype of MM (n=11)			<.001
Epithelioid type	11 (100)	0	
Sarcomatoid type	0	0	
Biphasic type	0	0	

BAP1, BRCA1-associated protein 1; MM, malignant mesothelioma.

https://doi.org/10.4132/jptm.2020.09.14

Table 3. Consistency between BAP1 expression status in cell block and biopsy

BAP1 expression status in cellblock	BAP1 expression status in biopsy		Total
	Loss of BAP1 expression	BAP1 normal expression	
Loss of BAP1 expression	10 (90.9)	1 (9.1)	11 (100)
BAP1 normal expression	0	9 (100)	9 (100)
Total	10 (50.0)	10 (50.0)	20 (100)

Values are presented as number (%).
BAP1, BRCA1-associated protein 1.
$p < .001$; $\kappa = 0.90$.

Table 4. BAP1 expression status according to age, sex, asbestos exposure, neoplastic transformation, and localization in MM cases

	Loss of BAP1 expression	BAP1 normal expression	p-value
Age (yr)	60.0 (49.0–68.0)	62.0 (58.0–75.0)	.084
Sex			
Male	29 (72.5)	11 (27.5)	.322
Female	20 (83.3)	4 (16.7)	
Asbestos exposure			
No	32 (78.0)	9 (22.0)	.708
Yes	17 (73.9)	6 (26.1)	
Neoplastic transformation			
No	47 (75.8)	15 (24.2)	.427
Yes	2 (100)	0	
Localisation			
Pleura	43 (75.4)	14 (24.6)	.545
Periton and pericard	6 (85.7)	1 (14.3)	

Values are presented as median (percentile 25–percentile 75) or number (%).
BAP1, BRCA1-associated protein 1; MM, malignant mesothelioma.

Various studies have demonstrated that immunohistochemical evidence of BAP1 expression loss in mesothelial cells may be a clue to malignancy. Cozzi et al. [18] reported that BAP1 expression loss in cell blocks obtained from effusions had a sensitivity of 76% for MM diagnosis, and that BAP1 expression loss in biopsy samples had 48.7% sensitivity. Meanwhile, Cigognetti et al. [19] and Walts et al. [20] estimated 100% specificity for BAP1 expression loss. In our study, we estimated 76% sensitivity and 100% specificity from biopsy tissue, but 100% sensitivity and specificity from cell blocks obtained from effusion.

Cozzi et al. [18], who investigated the role of BAP1 expression loss in effusion diagnosis for MM, found that BAP1 expression loss was 76.5% prevalent in mesothelioma cases, while it was 11.7% in mesothelial hyperplasia cases. In the same study, looking at biopsy diagnosis, BAP1 expression loss was 47.5% prevalent in patients diagnosed with mesothelioma, but no BAP1 expression loss was observed in any cases diagnosed with mesothelial hyperplasia. In our study, BAP1 expression loss was 76.6% prevalent in biopsy materials and 100% in cell blocks. Furthermore, no BAP1 expression loss was observed in either cell block or biopsy materials in our mesothelial hyperplasia cases.

There are some differences between MM subtypes in terms of nuclear BAP1 expression loss. Wu et al. [21] grouped 38 pleural MM cases as 29 biphasic and nine epithelioid types and then compared their BAP1 expression loss status and subtypes. In this study, we observed BAP1 expression loss in five of eight epithelioid-type MM cases (62.5%), while also observing loss in both sarcomatoid and epithelioid components in five of 13 biphasic-type MM cases (38.5%). Shinozaki-Ushiku et al. [17] studied 32 MM cases and found BAP1 expression loss in 53% (17/32), among which 14 were epithelioid and 3 were biphasic. Furthermore, two biphasic-type cases showed expression loss in both epithelioid and sarcomatoid components, while only 1 showed BAP1 expression persistence in the sarcomatoid component. In our study, BAP1 expression loss was observed in 81.5% of 54 epithelioid-type MM cases, whereas it was observed in all five biphasic-type MM cases (100%), all of which were detected in the epithelioid component. Moreover, no loss of BAP1 expression was observed in any of our five sarcomatoid-type MM cases.

Massive and recurrent effusions occur in the early stages of MM. Therefore, initial diagnosis is mostly based on cytological samples, especially in the epithelioid type [22]. However, in some cases, effusion material alone is not sufficient to diagnose MM. In such cases, diagnosis requires biopsy tissue from the patients. Although the diagnostic power of biopsies have been demonstrated by numerous studies, less invasive methods are preferred by both patients and surgeons.

Pulford et al. [14] included both cytological and biopsy materials of 83 MM cases and 18 cases with malignant pleural effusion due to metastatic adenocarcinoma. In addition to the diagnostic value and prognostic significance of BAP1 expression loss, they also measured the agreement of cytological and biopsy materials with the Kappa test. Pulford et al. [14] reported that BAP1 expression loss was observed in 59% of MM cases and the Kappa value was 0.85. Similarly, we applied BAP1 antibodies to the biopsies of cases with cytological samples and we calculated agreement with the Kappa test. Accordingly, the agreement between cytological and histological specimens for BAP1 expression loss was excellent ($\kappa = 0.90$), and the correlation was significant ($p < .001$).

Environmental exposure to asbestos, especially for regions with abundant white soil, like some provinces of Turkey, is of great importance in MM development. Onder et al. [23] evaluated 88 MM cases from central Ankara, which is the nearest city to Cappadocia; they reported that 95% of the cases had been exposed

to asbestos and no significant relationship was found between asbestos exposure and BAP1 expression loss. In our study, only 35.9% of MM cases were exposed to asbestos. We attribute this difference to the fact that the city where we work is far from Cappadocia, and we could not find as significant a relationship as Onder et al. [23] did.

There were some limitations to our work. Primarily, because of the retrospective nature of our study, it was not possible to obtain all of the cytological specimens from the biopsy materials analyzed by immunohistochemistry for BAP1 expression.

In conclusion, BAP1 expression loss was found in all the cytological materials of the cases whose diagnoses were confirmed by tissue biopsy, and the results were replicated for each case when BAP1 antibodies were applied to biopsy materials. This suggests that BAP1 expression loss is a robust criterion in achieving MM diagnosis from cytological materials. Effusion in the serosal cavity is a common early finding for MM. Furthermore, because cytologic examination is less invasive and easy to perform, it is likely to be the preferred diagnostic method, especially given the results reported here. In patients with only serous effusion and no radiological suspicion of MM but who show evidence of BAP1 expression loss by immunohistochemical analysis of cell blocks, we suggest that invasive MM may develop in the near future and, thus, these patients need strict clinical follow-up.

Ethics Statement

Approval was obtained from the Ethics Committee on May 30, 2017 (protocol number: 2017/514/108/8). Informed consent was obtained from all participants included in the study.

ORCID

Hanife Gulnihal Ozdemir https://orcid.org/0000-0003-1405-3886
Sermin Coban Kokten https://orcid.org/0000-0003-1780-2942
Nagehan Ozdemir Barisik https://orcid.org/0000-0002-6606-1848

Author Contributions

Conceptualization: HGO, SCK. Data curation: HGO, SCK, NOB. Formal analysis: HGO. Funding acquisition: HGO, SCK, NOB. Investigation: HGO. Methodology: HGO, SCK. Supervision: HGO. Validation: HGO, NOB. Writing—original Draft: HGO, NOB. Writing—review & editing: HGO. Approval of final manuscript: all authors.

Conflicts of Interest

The authors declare that they have no potential conflicts of interest.

Funding Statement

No funding to declare.

References

1. Cagle PT, Allen TC. Pathology of the pleura: what the pulmonologists need to know. Respirology 2011; 16: 430-8.
2. Carbone M, Bedrossian CW. The pathogenesis of mesothelioma. Semin Diagn Pathol 2006; 23: 56-60.
3. Hicks J. Biologic, cytogenetic, and molecular factors in mesothelial proliferations. Ultrastruct Pathol 2006; 30: 19-30.
4. Hida T, Hamasaki M, Matsumoto S, et al. Immunohistochemical detection of MTAP and BAP1 protein loss for mesothelioma diagnosis: comparison with 9p21 FISH and BAP1 immunohistochemistry. Lung Cancer 2017; 104: 98-105.
5. Kushitani K, Amatya VJ, Mawas AS, et al. Utility of survivin, BAP1, and Ki-67 immunohistochemistry in distinguishing epithelioid mesothelioma from reactive mesothelial hyperplasia. Oncol Lett 2018; 15: 3540-7.
6. Lee HE, Molina JR, Sukov WR, Roden AC, Yi ES. BAP1 loss is unusual in well-differentiated papillary mesothelioma and may predict development of malignant mesothelioma. Hum Pathol 2018; 79: 168-76.
7. Baris YI, Artvinli M, Sahin AA. Environmental mesothelioma in Turkey. Ann N Y Acad Sci 1979; 330: 423-32.
8. Cagle PT, Churg A. Differential diagnosis of benign and malignant mesothelial proliferations on pleural biopsies. Arch Pathol Lab Med 2005; 129: 1421-7.
9. King J, Thatcher N, Pickering C, Hasleton P. Sensitivity and specificity of immunohistochemical antibodies used to distinguish between benign and malignant pleural disease: a systematic review of published reports. Histopathology 2006; 49: 561-8.
10. Kradin RL, Mark EJ. Distinguishing benign mesothelial hyperplasia from neoplasia: a practical approach. Semin Diagn Pathol 2006; 23: 4-14.
11. Attanoos RL, Griffin A, Gibbs AR. The use of immunohistochemistry in distinguishing reactive from neoplastic mesothelium: a novel use for desmin and comparative evaluation with epithelial membrane antigen, p53, platelet-derived growth factor-receptor, P-glycoprotein and Bcl-2. Histopathology 2003; 43: 231-8.
12. Mayall FG, Goddard H, Gibbs AR. The frequency of p53 immunostaining in asbestos-associated mesotheliomas and non-asbestos-associated mesotheliomas. Histopathology 1993; 22: 383-6.
13. Taheri ZM, Mehrafza M, Mohammadi F, Khoddami M, Bahadori M, Masjedi MR. The diagnostic value of Ki-67 and repp86 in distinguishing between benign and malignant mesothelial proliferations. Arch Pathol Lab Med 2008; 132: 694-7.
14. Pulford E, Huilgol K, Moffat D, Henderson DW, Klebe S. Malignant mesothelioma, BAP1 immunohistochemistry, and VEGFA: does BAP1 have potential for early diagnosis and assessment of prognosis? Dis Markers 2017; 2017: 1310478.
15. McGregor SM, McElherne J, Minor A, et al. BAP1 immunohistochemistry has limited prognostic utility as a complement of CDKN2A (p16) fluorescence in situ hybridization in malignant pleural mesothelioma. Hum Pathol 2017; 60: 86-94.
16. LaFave LM, Beguelin W, Koche R, et al. Loss of BAP1 function leads to EZH2-dependent transformation. Nat Med 2015; 21: 1344-9.
17. Shinozaki-Ushiku A, Ushiku T, Morita S, Anraku M, Nakajima J, Fukayama M. Diagnostic utility of BAP1 and EZH2 expression in malignant mesothelioma. Histopathology 2017; 70: 722-33.
18. Cozzi I, Oprescu FA, Rullo E, Ascoli V. Loss of BRCA1-associated protein 1 (BAP1) expression is useful in diagnostic cytopathology of malignant mesothelioma in effusions. Diagn Cytopathol 2018; 46: 9-14.
19. Cigognetti M, Lonardi S, Fisogni S, et al. BAP1 (BRCA1-associated

protein 1) is a highly specific marker for differentiating mesothelioma from reactive mesothelial proliferations. Mod Pathol 2015; 28: 1043-57.
20. Walts AE, Hiroshima K, McGregor SM, Wu D, Husain AN, Marchevsky AM. BAP1 Immunostain and CDKN2A (p16) FISH analysis: clinical applicability for the diagnosis of malignant mesothelioma in effusions. Diagn Cytopathol 2016; 44: 599-606.
21. Wu D, Hiroshima K, Yusa T, et al. Usefulness of p16/CDKN2A fluorescence in situ hybridization and BAP1 immunohistochemistry for the diagnosis of biphasic mesothelioma. Ann Diagn Pathol 2017; 26: 31-7.
22. Hjerpe A, Ascoli V, Bedrossian CW, et al. Guidelines for the cytopathologic diagnosis of epithelioid and mixed-type malignant mesothelioma: a secondary publication. Cytopathology 2015; 26: 142-56.
23. Onder S, Ozogul E, Koksal D, Sarinc Ulasli S, Firat P, Emri S. Diagnostic value of BRCA1-associated protein-1, glucose transporter-1 and desmin expression in the discrimination between reactive mesothelial proliferation and malignant mesothelioma in tissues and effusions. Cytopathology 2019; 30: 592-600.

JPTM
Journal of Pathology and Translational Medicine 2020; 54: 504-507
https://doi.org/10.4132/jptm.2020.09.18

CASE STUDY

A case of monoclonal gammopathy of renal significance presenting as atypical amyloidosis with IgA lambda paraproteinemia

Chankyung Kim[1], John Brealey[1], Anjelo Jobert[2], James Nolan[1]

[1]Department of Anatomical Pathology, SA Pathology, Adelaide;
[2]Central and Northern Adelaide Renal Transplantation Services, Royal Adelaide Hospital, Adelaide, Australia

Monoclonal gammopathy of renal significance is defined as any B cell or plasma cell clonal lymphoproliferation which neither causes tumor complications nor meets any current hematological criteria for specific therapy, with one or more kidney lesions related to the produced monoclonal immunoglobulin, such as amyloidosis. A 50-year-old male presented with heavy proteinuria and blood tests showing IgA and Lambda paraproteinemia. Light microscopy showed mesangial eosinophilic ground substance extending into the capillary loops, and positive staining within the glomeruli and vessel walls for amyloid P immunohistochemistry was also noted. Immunofluorescence showed positive staining for IgA and Lambda in the mesangia and capillary loops. Electron microscopy exhibited organized fibrils measuring 4–5 nm in diameter in the mesangia, glomerular basement membranes and vessel walls. We interpreted the overall findings as atypical renal amyloidosis with IgA and Lambda deposition on immunofluorescence. Further amyloid typing using laser microdissection-liquid chromatography and mass spectrometry will be useful.

Key Words: Monoclonal gammopathy of renal significance; AHL amyloidosis; Immunoglobulin A; Atypical amyloidosis

Received: June 18, 2020 **Revised:** August 12, 2020 **Accepted:** September 18, 2020
Corresponding Author: James Nolan, MBBS, FRCPA, Department of Anatomical Pathology, SA Pathology, Royal Adelaide Hospital, Port Rd, Adelaide SA 5000, Australia
Tel: +61-8-7074-1181, Fax: +61-8-7074-6148, E-mail: James.Nolan@sa.gov.au

Amyloid is a material that is deposited in vivo that displays a characteristic fibrillary electron microscopic appearance and an affinity for Congo red stain, with green birefringence on polarized light microscopy [1]. Amyloidosis is a disease secondary to amyloid deposition. There are a range of amyloid proteins among which monoclonal kappa/lambda immunoglobulin light chain (AL) and AA are commonly associated with renal involvement. Moreover, other amyloid proteins have been reported to involve the kidney, including TR, AAPO A1, AAPO A2, Afib, ALys, AGel, ACysC and ALECT2 [2].

The International Kidney and Monoclonal Gammopathy Research Group (IKMG) defines monoclonal gammopathy of renal significance (MGRS) as any B cell or plasma cell clonal lymphoproliferation with both of the following characteristics: (1) one or more kidney lesions that are related to the produced monoclonal immunoglobulin and (2) the underlying B cell or plasma cell clone does not cause tumor complications or meet any current hematological criteria for specific therapy [3]. There are various renal diseases associated with MGRS, and they are now known as MGRS-associated lesions, conditions or disorders [3].

CASE REPORT

A 50-year-old male was evaluated by a renal physician due to the clinical features of nephrotic syndrome including heavy proteinuria and edema. A native kidney biopsy was sent to our laboratory for light microscopy, fresh frozen immunofluorescence and electron microscopy. Blood tests showed albumin of 17 g/L (normal range, 34 to 48 g/L) and creatinine of 99 μmol/L (normal range, 60 to 110 μmol/L), and the 24-hour urine protein was 8,596 mg/24 hr. The serum free kappa/lambda light chain ratio measured 0.09 (kappa light chain = 24.03 mg/L [normal range, 3.00 to 19.00 mg/L], lambda light chain = 276.87 mg/L [normal range, 6.00 to 26.00 mg/L]). The serum electrophoresis detected 5 g/L of paraprotein of IgA lambda and free lambda types.

A bone marrow biopsy showed the following: mildly increased plasma cells, less than 5%; phenotype: $CD38^+$, $CD138^+$, $CD19^-$,

pISSN 2383-7837
eISSN 2383-7845

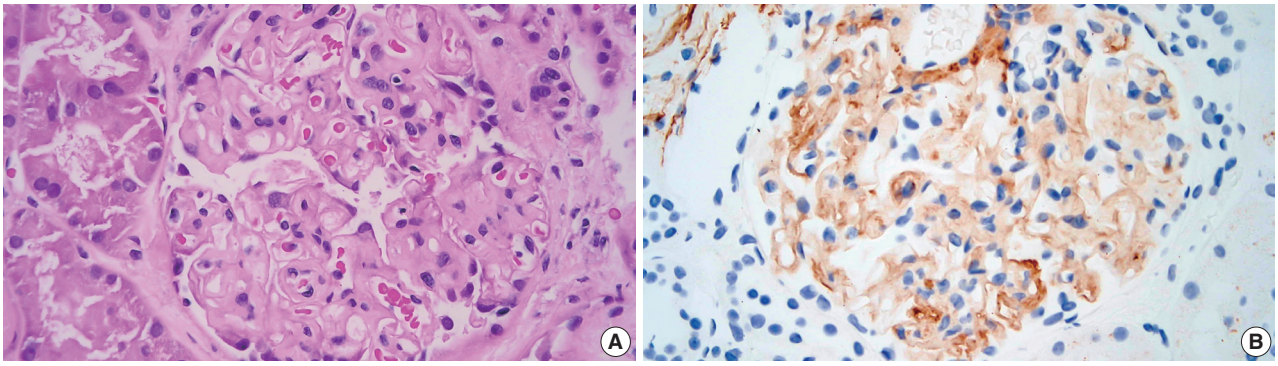

Fig. 1. Hematoxylin and eosin stain and Amyloid P immunohistochemistry. (A) The glomerulus shows mesangial eosinophilic ground substance which extends into the capillary loops. (B) Positive staining is seen within the glomerulus with amyloid P immunohistochemistry.

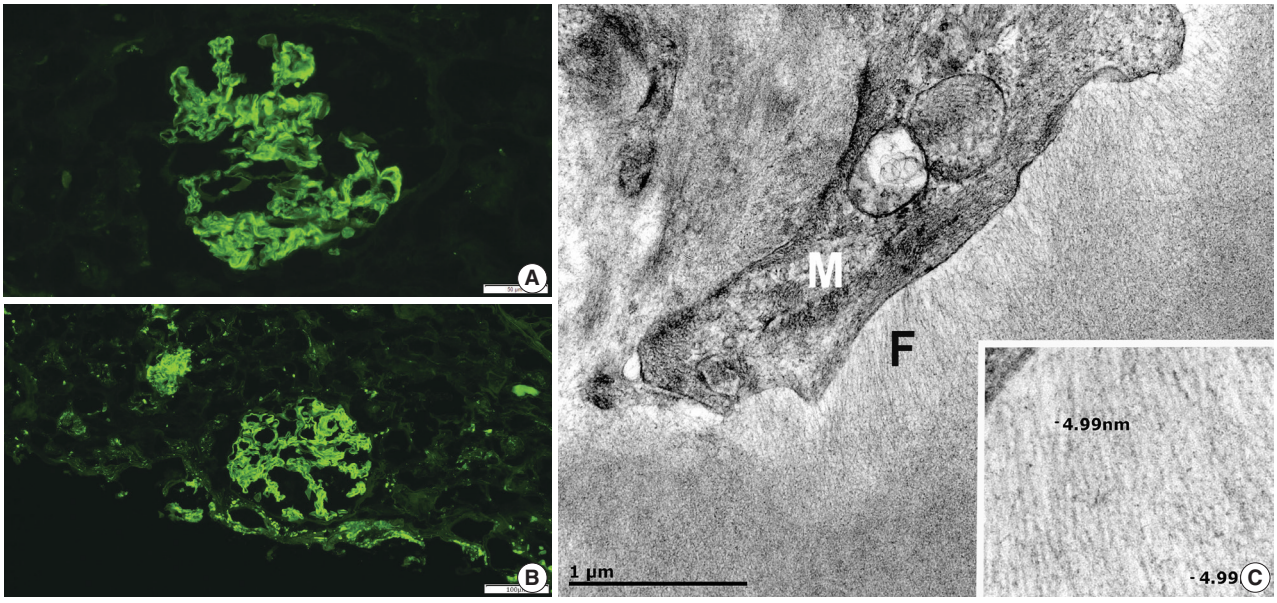

Fig. 2. Immunofluorescence and electron microscopy. (A) Positive mesangial and capillary loop staining with IgA on immunofluorescence. (B) Positive mesangial and capillary loops staining with Lambda on immunofluorescence. (C) The fine fibrillary material (F) is present adjacent to the mesangial cell (M) (×40,000). The inset shows amyloid-like fibrils measuring approximately 5 nm in diameter (×120,000).

$CD20^-$, $CD56^-$, $CD28^+$, $CD117^-$; and cytoplasmic lambda light chain restriction. This was consistent with monoclonal gammopathy of undetermined significance (MGUS).

A percutaneous core renal biopsy was performed, and the following tissues were submitted: formalin-fixed tissue for histology, fresh tissue for immunofluorescence and glutaraldehyde-fixed tissue for electron microscopy.

Light microscopy showed mesangial eosinophilic ground substance extending into the capillary loops (Fig. 1A). Positive staining within the glomeruli and vessel walls was identified for amyloid P immunohistochemistry (Fig. 1B). The Congo red stain demonstrated faint non-specific staining of the glomeruli in which no green birefringence was seen on polarized light microscopy. Immunofluorescence showed positive staining for IgA (Fig. 2A) and Lambda (Fig. 2B) in the mesangia and capillary loops. Electron microscopy exhibited fibrils measuring 4–5 nm in diameter in the mesangia, glomerular basement membranes and vessel walls (Fig. 2C).

DISCUSSION

We interpret this case as an unusual form of amyloidosis in a patient with a clinical presentation of heavy proteinuria in the setting of MGUS. The overall findings fit with a recently described diagnostic entity known as MGRS. Deposition of fibrillary eosinophilic material that show positive labelling with amyloid P im-

munohistochemistry in the mesangia, glomerular basement membranes and blood vessels supports the diagnosis of amyloidosis. On the other hand, there were two factors that are unusual for typical amyloidosis. First, the fibrils in this case only measured 4–5 nm in thickness, whereas amyloid fibrils typically measure 7–12 nm [4]. The absence of green birefringence or anomalous colors on polarized microscopy was the second unusual finding.

The weak non-specific staining of glomeruli with Congo red without green birefringence on polarized microscopy observed in this case could be secondary to the properties of the amyloid protein. A study by Suhr et al. [5] revealed that different types of transthyretin (TTR) amyloid fibrils can exhibit altered affinity for Congo red stain and birefringence. For example, type A, which consists of carboxy-terminal TTR-related amyloidosis (ATTR) fragments and full-length TTR, displayed strong affinity for Congo red stain, whereas type B, which consists only of full-length TTR, showed weak affinity for Congo red stain and absence of glittering birefringence. Thus, amyloids may demonstrate a variable affinity for Congo red and variable birefringence.

The immunofluorescence staining suggests that the amyloid is of IgA lambda origin, and hence, a diagnosis of IgA-lambda type renal heavy- and light-chain amyloidosis (AHL amyloidosis) is being considered. However, there is a case report from Japan which described AL amyloidosis in a patient with lymphoplasmacytic lymphoma secreting IgM-kappa chains [6]. In this case, the origin of the amyloid was initially thought to be from both IgM heavy and kappa light chain as suggested by renal immunofluorescence and laser microdissection–liquid chromatography and mass spectrometry (LMD-LC-MS). However, LMD-LC-MS of the amyloid fibrils after the amyloid purification method suggested that the heavy chain identified was actually from the non-specific co-deposition of monoclonal IgM-kappa, which demonstrated that the amyloid was only of light chain origin. Therefore, it would be imprudent to diagnose the present case as AHL amyloidosis until we obtain the LMD-LC-MS results.

According to the study published by Nasr et al. [7], among 16 heavy-chain (AH) and heavy- and light-chain renal amyloidosis cases, five showed detection of IgA, and one showed both IgA and lambda positivity on laser microdissection and mass spectrometry (LMD-MS). There were 202 cases of AL renal amyloidosis during the same time period, with AH/AHL renal amyloidosis cases accounting for 7.3% of the entire cohort and IgA and lambda positive AH/AHL occupying only less than 0.01% of the entire cohort. Interestingly, there was a case in which immunofluorescence was positive for both IgA and lambda, but only IgA was found on LMD-MS. This again demonstrates the difficulty in accurate typing of AH/AHL solely by immunofluorescence.

Given the unusual findings for typical amyloidosis in the present case, other possible diagnoses were considered. Negative staining with Congo red suggested monoclonal immunoglobulin deposition disease (MIDD) as an alternate diagnosis, especially when amyloid P immunohistochemistry can sometimes show non-specific staining (from our experiences). However, electron microscopy showed organized fibrils rather than the non-fibrillar "powdery" electron dense deposits which are typically seen in MIDD [8]. This made the diagnosis of MIDD less likely. Positive IgA staining on immunofluorescence is unusual for amyloidosis and raised the possibility of IgA nephropathy, but no mesangial or endocapillary hypercellularity was present, C3 was negative, and most importantly, the clinical presentation did not fit with IgA nephropathy. Hence, this was disregarded from our diagnostic work-up.

As mentioned, further renal amyloid typing can be performed by LMD-LC-MS [3]. Vrana et al. [9] reported that this method showed 100% specificity and 98% sensitivity in the identification of the types of amyloid protein. This may be indicated in our case due to the questionable Congo red staining and bright staining of IgA by immunofluorescence. Identification of the amyloid type is incredibly important as the disease management depends on the underlying cause of amyloidosis. In our case, further amyloid typing is being considered, and meanwhile, the patient will undergo autologous bone marrow transplantation for treatment.

Ethics Statement

Informed consent was obtained from the patient, and the study was approved by the Central Adelaide Local Health Network Human Research Ethics Committee (CALHN reference number: 13298, approved on 01/06/2020).

ORCID

Chankyung Kim https://orcid.org/0000-0001-6054-0605
James Nolan https://orcid.org/0000-0002-6034-7159

Author Contributions

Conceptualization: CK, JN. Data curation: CK. Formal analysis: CK, JB, JN. Investigation: CK, JN. Methodology: CK, JB, AJ, JN. Resources: JB, AJ, JN. Supervision: JN. Validation: JB, AJ, JN. Visualization: CK. Writing—original draft: CK. Writing—review & editing: CK, JB, AJ, JN. Approval of final manuscript: all authors.

Conflicts of Interest

The authors declare that they have no potential conflicts of interest.

Funding Statement

No funding to declare.

Acknowledgments

We would like to thank Associate Professor Sonja Klebe from anatomical pathology department of Flinders Medical Centre and Dr Sarita Prabhakaran from Flinders University for their assistance in photo editing and guidance in obtaining ethics approval.

References

1. Westermark P, Benson MD, Buxbaum JN, et al. A primer of amyloid nomenclature. Amyloid 2007; 14: 179-83.
2. Holanda DG, Acharya VK, Dogan A, Racusen LC, Atta MG. Atypical presentation of atypical amyloid. Nephrol Dial Transplant 2011; 26: 373-6.
3. Leung N, Bridoux F, Batuman V, et al. The evaluation of monoclonal gammopathy of renal significance: a consensus report of the International Kidney and Monoclonal Gammopathy Research Group. Nat Rev Nephrol 2019; 15: 45-59.
4. Leung N, Drosou ME, Nasr SH. Dysproteinemias and glomerular disease. Clin J Am Soc Nephrol 2018; 13: 128-39.
5. Suhr OB, Lundgren E, Westermark P. One mutation, two distinct disease variants: unravelling the impact of transthyretin amyloid fibril composition. J Intern Med 2017; 281: 337-47.
6. Manabe S, Iwasaki C, Hatano M, et al. AL amyloidosis with non-amyloid forming monoclonal immunoglobulin deposition: a case mimicking AHL amyloidosis. BMC Nephrol 2018; 19: 337.
7. Nasr SH, Said SM, Valeri AM, et al. The diagnosis and characteristics of renal heavy-chain and heavy/light-chain amyloidosis and their comparison with renal light-chain amyloidosis. Kidney Int 2013; 83: 463-70.
8. Nasr SH, Valeri AM, Cornell LD, et al. Renal monoclonal immunoglobulin deposition disease: a report of 64 patients from a single institution. Clin J Am Soc Nephrol 2012; 7: 231-9.
9. Vrana JA, Gamez JD, Madden BJ, Theis JD, Bergen HR 3rd, Dogan A. Classification of amyloidosis by laser microdissection and mass spectrometry-based proteomic analysis in clinical biopsy specimens. Blood 2009; 114: 4957-9.

JPTM
Journal of Pathology and Translational Medicine 2020; 54: 508-512
https://doi.org/10.4132/jptm.2020.05.21

CASE STUDY

Intraoperative frozen cytology of intraosseous cystic meningioma in the sphenoid bone

Na Rae Kim[1], Gie-Taek Yie[2]

Departments of [1]Pathology and [2]Neurosurgery, Gil Medical Center, Gachon University College of Medicine, Incheon, Korea

Meningiomas in bone are rarely subjected to fine-needle aspiration diagnosis, and those arising in the skull bone with a cystic presentation are rare. A 24-year-old woman presented with subdural hemorrhage, and subsequent radiology depicted an osteolytic mass-like lesion in the sphenoid bone. Intraoperatively, a solid and cystic hemorrhagic lesion mimicking an aneurysmal bone cyst was observed in the sphenoid bone with dural tearing. Frozen cytology showed singly scattered or epithelioid clusters of round to elongated cells intermixed with many neutrophils. Tumor cells had bland-looking round nuclei with rare prominent nucleoli and nuclear inclusions and eosinophilic granular to globoid cytoplasm in capillary-rich fragments. Histology revealed intraosseous meningothelial and microcystic meningioma (World Health Organization grade 1) in right lesser wing of the sphenoid bone. Considering its unusual location and cytologic findings, differential diagnoses included chordoma, chondroma, chondrosarcoma, and aneurysmal bone cyst. The present case posed a diagnostic challenge due to possible confusion with these entities.

Key Words: Meningioma; Skull; Sphenoid bone; Osteolysis; Bone cysts, aneurysmal

Received: April 21, 2020 **Accepted:** May 21, 2020
Corresponding Author: Na Rae Kim, MD, Department of Pathology, Gil Medical Center, Gachon University College of Medicine, 21 Namdong-daero 774 beon-gil, Namdong-gu, Incheon 21565, Korea
Tel: +82-32-460-3073, Fax: +82-32-460-2394, E-mail: clara_nrk@gilhospital.com

Meningiomas are slow-growing mesenchymal neoplasms of the central nervous system and usually arise from the meningothelial cells of the arachnoid layer of meninges. Primary extradural meningioma constitutes 1% to 2% of all meningiomas [1]. Intraosseous meningioma is a rare form of bone tumor [2]. Cystic meningioma is uncommon [3], and intraosseous meningioma affecting the skull is also rare. Since the first report of intraosseous meningioma issued by Winkler in 1904, slightly more than 100 cases have been reported [4], and few of these cases concerned cystic osteolytic intraosseous meningioma in the skull [5]. Main differential diagnosis was aneurysmal bone cyst (ABC) that occupies only 2%–6% of the skull base [6].

We report a rare case of osteolytic intraosseous meningioma of the sphenoid bone in a 24-year-old woman, and describe intraoperative imprint smears produced using intraosseous samples and the clinicoradiologic resemblance of this disease entity with other intracranial lesions.

CASE REPORT

A previously healthy 24-year-old woman presented with a headache of two days duration. She was referred to the emergency room of our hospital because she had a history of slip-down in a bathroom two days previously. Precontrast brain computed tomography (CT) revealed a small amount of extra-axial hemorrhage at the right frontotemporal region (Fig. 1A). Skull magnetic resonance images showed a slightly rim-enhancing lesion invading right sphenoid bone. Differential diagnoses included vascular pathologies such as hemangioma and other tumorous conditions. The skull tumor was removed using a navigation system and cranioplasty of the right frontotemporal area was performed using bone cement. Inferolateral temporal dura over the lesion had been focally disrupted, but no gross leakage was observed. After exposing the right temporal fascia and muscle, the lateral wall of the right orbit, zygoma, and a thinned portion of the bone at the pterygoid process were drilled. Removal of the hematoma exposed a multiseptated cystic cavity (Fig. 1B).

pISSN 2383-7837
eISSN 2383-7845

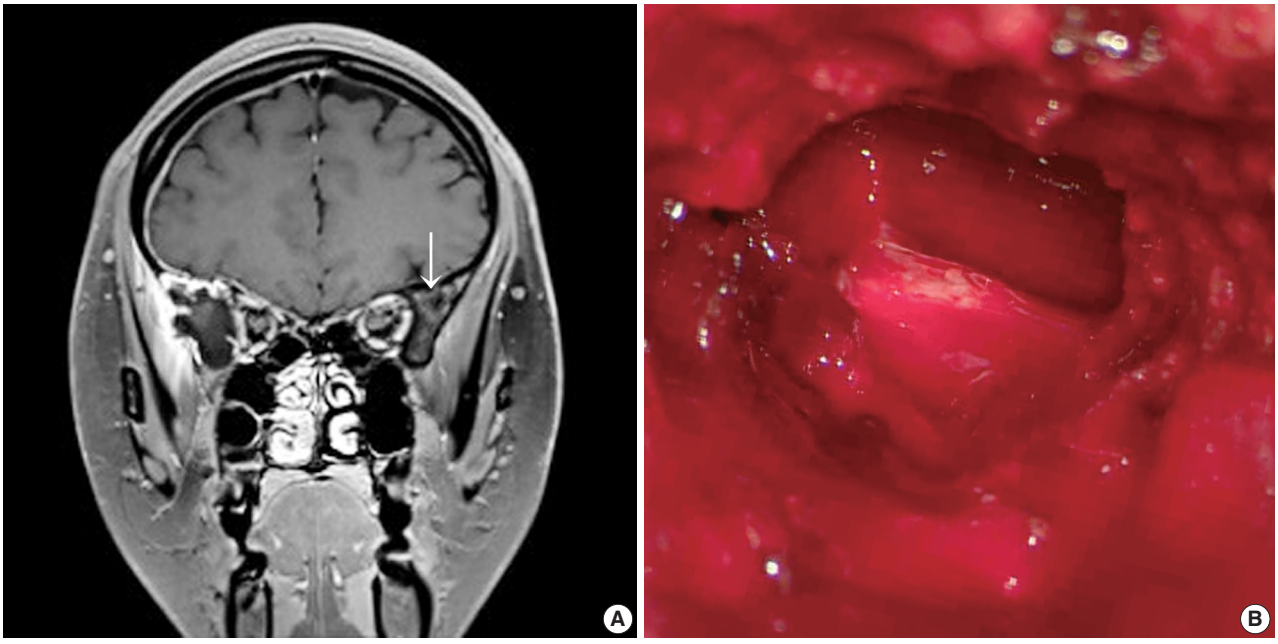

Fig. 1. (A) Brain magnetic resonance image shows a slightly enhanced lesion (arrow) at the right sphenoid bone. (B) Intraoperative gross examination of the lesion shows cystic spaces filled with blood and solid texture.

Intraoperative frozen biopsy was performed on the cystic portion of right sphenoid bone, and subsequent intraoperative squash cytology revealed moderate cellular smears composed of sheets or clusters of epithelioid cells in an inflammatory cell–rich background (Fig. 2A–D). Histologically, singly scattered or clusters of round-to-elongated tumor cells were found in sclerotic bone (Fig. 2E). Tumor cells with indistinct cell borders were observed in clusters forming meningothelial whorls and had centrally-placed small round and bland nuclei with or without nucleoli. Prominent hemorrhage was present. Individual tumor cells showed abundant eosinophilic cytoplasm with an occasional vacuolated appearance and cytoplasmic clearing resembling oligodendroglioma (Fig. 2F). Neutrophils were abundant (Fig. 2G, left). There was marked perivascular hyalinization and stromal sclerosis (Fig. 2G, right). Mitotic counts were up to 1 per 10 high power fields, necrosis was absent, and occasional atypia was observed. Tumor cells invaded the thick dura mater. They were positive for CD56 (1:100, CD564, Novocastra, Newcastle upon Tyne, UK), CD99 (prediluted, 12E7, Dako, Glostrup, Denmark), INI-1 (1:200, 25/BAF47, BD Bioscience, San Diego, CA, USA), vimentin (1:100, V9, Dako) (Fig. 2H, left), and progesterone receptor (1:200, 16, Novocastra). Tumor cells also displayed focally membranous positivity for epithelial membrane antigen (1:100, E29, Dako) (Fig. 2H, right). However, they were negative for glial fibrillary acidic protein (prediluted, Dako), S-100 protein (polyclonal, 1:600, Dako), smooth muscle actin (1:100, 1A4, Dako), synaptophysin (prediluted, DAK-SYNAP, Dako), chromogranin (1:100, DAK-A3, Dako), CD34 (1:100, QBEnd10, Dako), L1 cell adhesion molecule (1:200, polyclonal, Abcam, Cambridge, UK), OLIG2 (EP112; 1:500, Cell Marque, Rocklin, CA, USA), and STAT6 (S-20, sc-621, 1:150, Santa Cruz Biotechnology, Santa Cruz, CA, USA). The Ki-67 (MIB-1, 1:100, Dako) proliferation index was 3%. Intervening sclerosis stained with periodic acid-Schiff and Masson-trichrome.

Based on the above histology, notably, the clear cell morphology containing one mitosis, meningothelial whorls, and the lack of hypercellularity, macronuclei, small cell formation, or brain invasion, the tumor was determined to be an intraosseous meningioma of the microcystic and meningotheliomatous type (World Health Organization grade I). We diagnosed this case as intraosseous meningioma with dural involvement because the tumor was largely located within the sphenoid bone.

At 5 months of follow-up, the patient was healthy, asymptomatic, and scheduled for annual postoperative follow-ups.

DISCUSSION

Intraosseous occurrence of meningioma, especially in the skull, is uncommon [7]. Plausibly, this rare primary intraosseous meningioma may arise due to aberrant differentiation or localization of pluripotent embryonal precursor cells of the bone, or from misplaced or trapped arachnoid cells along the suture line dur-

ing molding of the head at birth and after differentiation into meningocytes or arachnoid cap cells [1]. Alternatively, it may arise from arachnoidal cells of blood vessels or nerves traversing the skull [8].

Intraosseous meningioma of the skull can be confused with primary calvarial bone tumors. On CT images, intraosseous me-

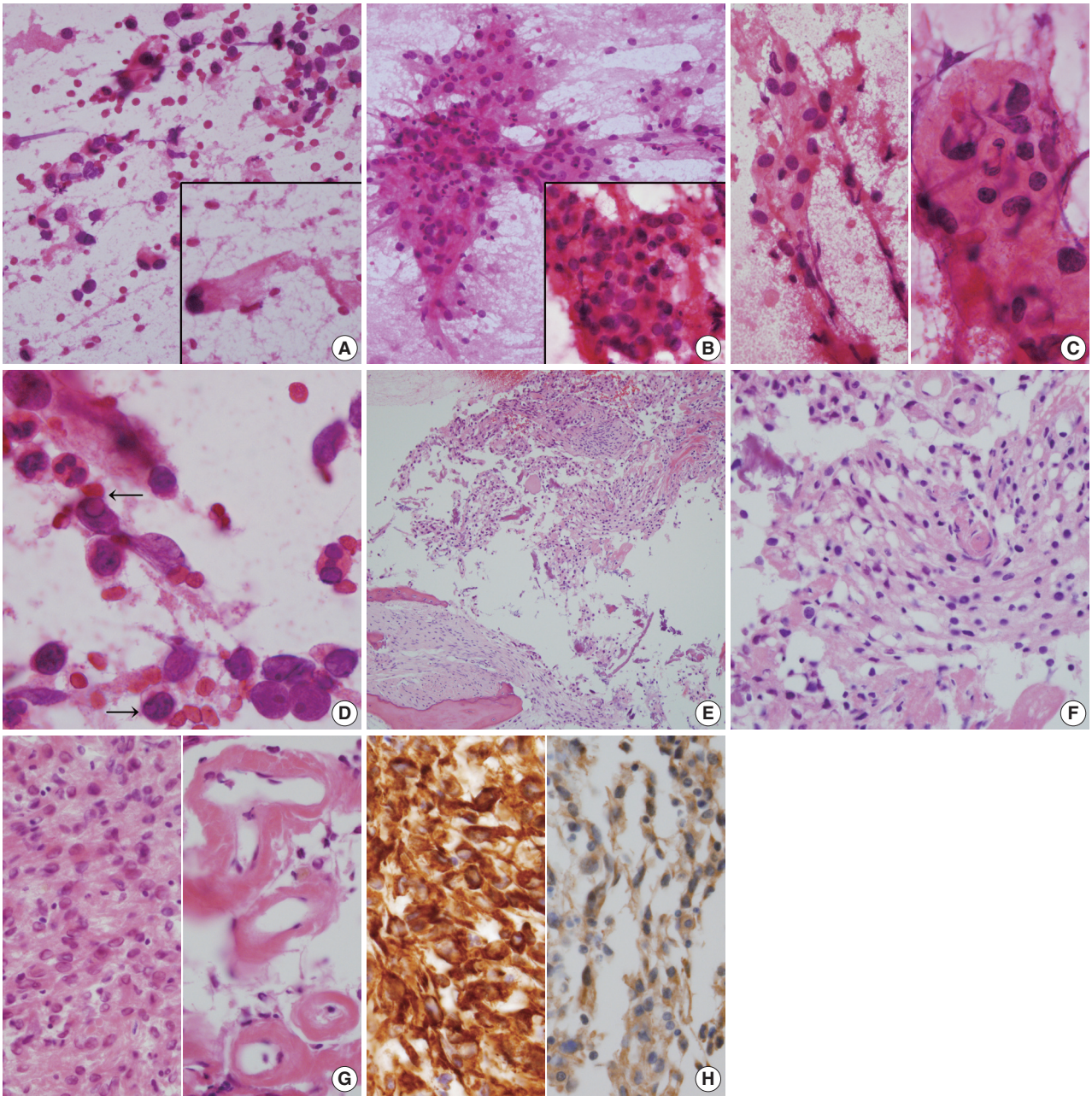

Fig. 2. (A–D) Frozen cytology. (A) The cystic portion of the right sphenoid bone shows singly scattered eosinophilic round to elongated cells with occasional nuclear hyperchromasia. Inset shows thick refractile collagenous cytoplasm with nuclear hyperchromasia. (B) Moderately cellular smears shows sheets of epithelioid cells in a bloody and inflammatory cell–rich background. Inset shows intermixed inflammatory cells in meningothelial whorls. (C) Cellular sheets of round-shaped epithelioid cells with moderate amounts of eosinophilic granular cytoplasm and euchromatic round nuclei, just apposed to the capillary (left). High magnification shows indistinct cell borders (right). (D) High power view shows occasional nuclear inclusions (arrows). (E–H) Histology. (E) Low power view shows sheets of spindle to round-shaped tumor cells, filling the bone. Note the lamellated bone and osteoblastic rimming. (F) Nests of meningothelial cells form microcystic cobweb-like arrangement. Note the microcystic and bubbly cytoplasm. (G) Sheets of spindle-shaped tumor cells are intermixed with inflammatory cells (left). Note the perivascular sclerosis (right). (H) The tumor cells are immunoreactive for vimentin (left) and epithelial membrane antigen (right).

https://doi.org/10.4132/jptm.2020.05.21

ningiomas appear as osteoblastic, osteolytic, or mixed patterns [3,9]. Skull lesions showing osteolytic lesions, as in our case, include epidermoid tumor, multiple myeloma, Langerhans cell histiocytosis, fibrous dysplasia, giant-cell tumor, Paget's disease, solitary fibrous tumor/hemangiopericytoma (SFT/HPC), hemangioma, osteosarcoma, and ABC [10]. In the present case, the lesion was located in the sphenoid bone and its preoperative radiologic and gross differential diagnoses included ABC, chordoma, chondrosarcoma, and vascular neoplasm [11]. ABC presenting as a locally destructive osteolytic lesion frequently involves the long bones of knee joints and vertebrae and is usually encountered in the first or second decades of life. When ABC occurs in the skull, it is usually located in the skull vault and only rarely in the skull base [11]. The preoperative diagnosis of an intraosseous lytic lesion like meningioma is challenging. The presence of an osteolytic extracranial soft tissue lesion usually raises the suspicion of malignancy [9]. Radiologic differential diagnosis of osteolytic intraosseous meningiomas of the skull should exclude other lytic lesions such as lytic metastasis, multiple myeloma, eosinophilic granuloma, fibrous dysplasia, Langerhans cell histiocytosis, giant-cell tumor, SFT/HPC, and hemangioma. Radiologically, intraosseous meningiomas present osteoblastic findings in about two-thirds of cases, an osteolytic pattern, in around a third, and a mixed osteoblastic-lytic lesion in only 6% of cases [2,9].

Evaluations of skull lesions by fine-needle aspiration are controversial. Cytologic findings of meningioma are diverse and heterogeneous [12], and notable features for differential diagnosis are as follows; cohesive syncytial meningothelial whorls, individual tumor cells showing nuclear inclusions or grooves and wispy collagenous, rather than fibrillary, cytoplasm with occasional short broad cell processes [13]. Tumor cells with indistinct cell borders and subsequent syncytial whorls are the most common. In meningothelial and microcystic type meningiomas, as in the present case, background collagenous sclerosis is observed in tumor cells with vacuolated cytoplasm mixed with scattered inflammatory cells [13]. Although the biologic roles of circulating neutrophils and intratumoral neutrophils in meningiomas remain unclear, the presence of many inflammatory cells including lymphocytes, plasma cells, natural killer cells, and macrophages is common [14]. A high concordance between frozen and permanent diagnoses (up to 99%) has been reported for meningeal tumors [12]. However, frozen cytologic diagnosis in the described case was difficult due to the presence of massive numbers of inflammatory cells, marked hemorrhage, and an unusual location. Scattered stellate, vacuolated cells, and foam cells may be found in regions of microcystic meningiomas [13]. Singly-scattered tumor cells with intracytoplasmic vacuoles in foci of microcystic meningioma resembling atypical chondrocytes of chondrosarcoma and lipoblasts of liposarcoma were occasionally found [15]. Cytologic findings of chondrosarcoma are moderately cellular with clusters of polygonal cells showing occasional binucleation and well-defined cytoplasm with rounded nuclei showing moderate nuclear pleomorphism embedded in a chondromyxoid background, suggestive of chondrosarcoma [15]. Cytologic findings of chordoma are characterized by mucoid and gelatinous fibromyxoid cellular smears and cords or clusters of round epithelioid cells with small round nuclei and scant basophilic cytoplasm and occasional large physaliphorous cells with central small round nuclei and bubbly cytoplasm [16]. Well differentiated chondrosarcoma arising in the sphenoid bone is another entity necessitating differential diagnosis; the findings of bland nuclei and refractile cytoplasmic processes and a lack of chondromyxoid matrix are useful diagnostic features of meningioma [12].

The most important macroscopic frozen differential diagnosis in the described case was ABC. Cytologic findings of ABC are dominated by blood; dispersed fibroblast-like histiocytes with occasional hemosiderin and multinucleated osteoclast-type giant cells containing fragments of collagen [17]. Osteoid and chondroid matrix material as well as woven bone may be present within aspirated or touch smears. Small fragments of bone may also be found. In hemorrhagic cases, as in our case, markedly vascular hemorrhagic SFT/HPC should be distinguished from meningioma. Cytologic findings of SFT/HPC are nonspecific and "patternless", i.e., heterogeneous, although naked stripped nuclei and scattered ropy collagen fragments are observed in an occasional pseudoalveolar pattern in a hemorrhagic bloody background [18]. The histologic diagnosis of intraosseous meningioma is not as difficult as that based on frozen cytology. One of the important histologic differential diagnoses of meningioma is SFT/HPC. Immunopositivity for both CD34 and STAT6 in SFT/HPC differentiate it from meningioma [19]. At a glance, clear cells mimicking oligodendroglial cells suggest oligodendroglioma [20]. However, oligodendroglioma and meningioma can be differentiated based on the presence of whorls and immunonegativity for OLIG2 in the meningioma. Histologically, ABC features fibroblastic proliferation and scattered giant cells with osteoid and blood-filled spaces lined by giant cells and hemosiderin laden macrophages [17].

Awareness of intraosseous cystic meningioma involving the skull may facilitate the intraoperative diagnosis of this rare condition. The present case cautions that the possibility of intraos-

seous meningioma should be kept in mind when is it is encountered in an unusual location.

Ethics Statement

An approval was obtained from our Institutional Review Board (No. GDIRB2020-122) for publication of this case report with a waiver of informed consent.

ORCID

Na Rae Kim https://orcid.org/0000-0003-2793-6856
Gie-Taek Yie https://orcid.org/0000-0002-8706-7253

Author Contributions

Conceptualization: NRK. Data curation: NRK. Investigation: GTY. Resources: GTY. Supervision: NRK. Validation: GTY. Visualization: GTY. Writing—original draft: NRK. Writing—review & editing: NRK. Approval of final manuscript: all authors.

Conflicts of Interest

The authors declare that they have no potential conflicts of interest.

Funding Statement

No funding to declare.

References

1. Lang FF, Macdonald OK, Fuller GN, DeMonte F. Primary extradural meningiomas: a report on nine cases and review of the literature from the era of computerized tomography scanning. J Neurosurg 2000; 93: 940-50.
2. Agrawal V, Ludwig N, Agrawal A, Bulsara KR. Intraosseous intracranial meningioma. AJNR Am J Neuroradiol 2007; 28: 314-5.
3. Rosahl SK, Mirzayan MJ, Samii M. Osteolytic intra-osseous meningiomas: illustrated review. Acta Neurochir (Wien) 2004; 146: 1245-9.
4. Butscheidt S, Ernst M, Rolvien T, et al. Primary intraosseous meningioma: clinical, histological, and differential diagnostic aspects. J Neurosurg 2019 Jun 21 [Epub]. https://doi.org/10.3171/2019.3.JNS182968.
5. Caruso R, Fini G, Pesce A, et al. A primary intraosseous cystic meningioma: case report. Int J Surg Case Rep 2017; 37: 189-92.
6. Aghaghazvini L, Sedighi N, Karami P, Yeganeh O. Skull base aneurysmal bone cyst presented with foramen jugular syndrome and multi-osseous involvement. Iran J Radiol 2012; 9: 157-60.
7. Ilica AT, Mossa-Basha M, Zan E, et al. Cranial intraosseous meningioma: spectrum of neuroimaging findings with respect to histopathological grades in 65 patients. Clin Imaging 2014; 38: 599-604.
8. Turner OA, Laird AT. Meningioma with traumatic etiology: report of a case. J Neurosurg 1966; 24: 96-8.
9. Tokgoz N, Oner YA, Kaymaz M, Ucar M, Yilmaz G, Tali TE. Primary intraosseous meningioma: CT and MRI appearance. AJNR Am J Neuroradiol 2005; 26: 2053-6.
10. Kee TP, Liauw L, Sathiyamoorthy S, Lee HY, Tan GSL, Yu WY. Large solitary lytic skull vault lesions in adults: radiological review with pathological correlation. Clin Imaging 2020; 59: 129-43.
11. Ustabasioglu FE, Samanci C, Asik M, et al. Aneurysmal bone cyst of sphenoid bone and clivus misdiagnosed as chordoma: a case report. Brain Tumor Res Treat 2015; 3: 115-7.
12. Kang M, Chung DH, Kim NR, et al. Intraoperative frozen cytology of central nervous system neoplasms: an ancillary tool for frozen diagnosis. J Pathol Transl Med 2019; 53: 104-11.
13. Seok JY, Kim NR, Cho HY, Chung DH, Yee GT, Kim EY. Crush cytology of microcystic meningioma with extensive sclerosis. Korean J Pathol 2014; 48: 77-80.
14. Pinton L, Solito S, Masetto E, et al. Immunosuppressive activity of tumor-infiltrating myeloid cells in patients with meningioma. Oncoimmunology 2018; 7: e1440931.
15. Lee S, Kim NR, Chung DH, Yee GT, Cho HY. Squash cytology of a dural-based high-grade chondrosarcoma may mimic that of glioblastoma in the central nervous system. Acta Cytol 2015; 59: 219-24.
16. Nijhawan VS, Rajwanshi A, Das A, Jayaram N, Gupta SK. Fine-needle aspiration cytology of sacrococcygeal chordoma. Diagn Cytopathol 1989; 5: 404-7.
17. Creager AJ, Madden CR, Bergman S, Geisinger KR. Aneurysmal bone cyst: fine-needle aspiration findings in 23 patients with clinical and radiologic correlation. Am J Clin Pathol 2007; 128: 740-5.
18. Kang M, Kim NR, Chung DH, Yie GT. Frozen cytology of meningeal malignant solitary fibrous tumor/hemangiopericytoma. J Pathol Transl Med 2019; 53: 192-7.
19. Fritchie K, Jensch K, Moskalev EA, et al. The impact of histopathology and NAB2-STAT6 fusion subtype in classification and grading of meningeal solitary fibrous tumor/hemangiopericytoma. Acta Neuropathol 2019; 137: 307-19.
20. Ligon KL, Alberta JA, Kho AT, et al. The oligodendroglial lineage marker OLIG2 is universally expressed in diffuse gliomas. J Neuropathol Exp Neurol 2004; 63: 499-509.

JPTM
Journal of Pathology and Translational Medicine 2020; 54: 513-516
https://doi.org/10.4132/jptm.2020.08.18

BRIEF CASE REPORT

Xanthogranulomatous endometritis: a report of two Korean cases with cytologic findings

Ji Min Na[1], Min Hye Kim[1], Gyung Hyuck Ko[1,2,3], Jeong Kyu Shin[2,3,4]

[1]Department of Pathology, Gyeongsang National University Hospital, Jinju; [2]Gyeongsang National University College of Medicine, Jinju; [3]Gyeongsang Institute of Health Science, Jinju; [4]Department of Obstetrics and Gynecology, Gyeongsang National University Hospital, Jinju, Korea

Xanthogranulomatous inflammation is a form of chronic inflammation characterized by aggregation of lipid-laden foamy histiocytes that occurs most commonly in the kidney and gallbladder. Xanthogranulomatous endometritis (XGE) is rare—less than 30 cases have been reported worldwide [1-10], and none were in Korea. We report here two cases of XGE in Korea along with its cytologic findings, which have not been described previously.

CASE REPORT

Case 1

A 78-year-old woman presented with a chief complaint of yellow pus-like vaginal discharge for 15 days. She had a history of hypertension for 10 years and was on medication for heart failure. On ultrasonography, her uterus was found to be enlarged, and fluid collection was observed in the endometrial cavity. Cytologic examination of the endometrial fluid was negative for malignancy but revealed many neutrophils with scattered foamy histiocytes (Fig. 1A). Chronic active endometritis with xanthomatous inflammation was diagnosed on examination of the endometrial curettage specimen. Antibiotics were prescribed with a follow-up appointment.

Two months later, the patient presented with abdominal pain, chills, and vaginal bleeding. The patient showed signs of systemic inflammation and septic shock, with a blood neutrophil count of 25,020/mm^3 (95.7%) and blood pressure of 60/40 mm Hg. Culture of an endometrial curettage specimen showed no bacterial growth, but blood culture produced *Escherichia coli* growth. Antibiotics were administered, and after the patient's neutrophil count and vital signs normalized, hysterectomy with right salpingo-oophorectomy was performed.

On gross examination, the endometrial cavity was filled with blood clots and most of the endometrium was bright yellow (Fig. 1B). Microscopic examination of the endometrium showed a massive aggregation of foamy histiocytes admixed with lymphocytes, neutrophils, and plasma cells (Fig. 1C). No complications related to XGE have been noted in the 4 years since surgery.

Case 2

A high-grade squamous intraepithelial lesion was detected on the cervicovaginal smear of a 72-year-old woman. Ultrasound scanning revealed intrauterine fluid accumulation, and pyometra was suspected. Cytologic examination of the endometrial washing specimen revealed many neutrophils with scattered foamy histiocytes, and a few atypical cells, probably from the uterine cervix (Fig. 2A). Blood neutrophil count was 9,840/mm^3 (81.8%). Endometrial fluid culture produced *Pseudomonas aeruginosa* growth. Hysterectomy with bilateral salpingo-oophorectomy was performed.

On gross examination, the endometrium was thickened and yellow in many areas (Fig. 2B). There was a 5.2-cm-sized fibroma in the right ovary. Microscopic examination showed massive aggregation of foamy histiocytes and lymphocytes in the endometrium (Fig. 2C). Early invasive squamous carcinoma was noted in the uterine cervix. The patient has been healthy for the 23 months since surgery.

Received: June 22, 2020 **Accepted:** August 18, 2020

Corresponding Author: Min Hye Kim, MD
Department of Pathology, Gyeongsang National University Hospital, 79 Gangnam-ro, Jinju 52727, Korea
Tel: +82-55-772-8061, Fax: +82-55-759-7952, E-mail: joymine86@naver.com

pISSN 2383-7837
eISSN 2383-7845

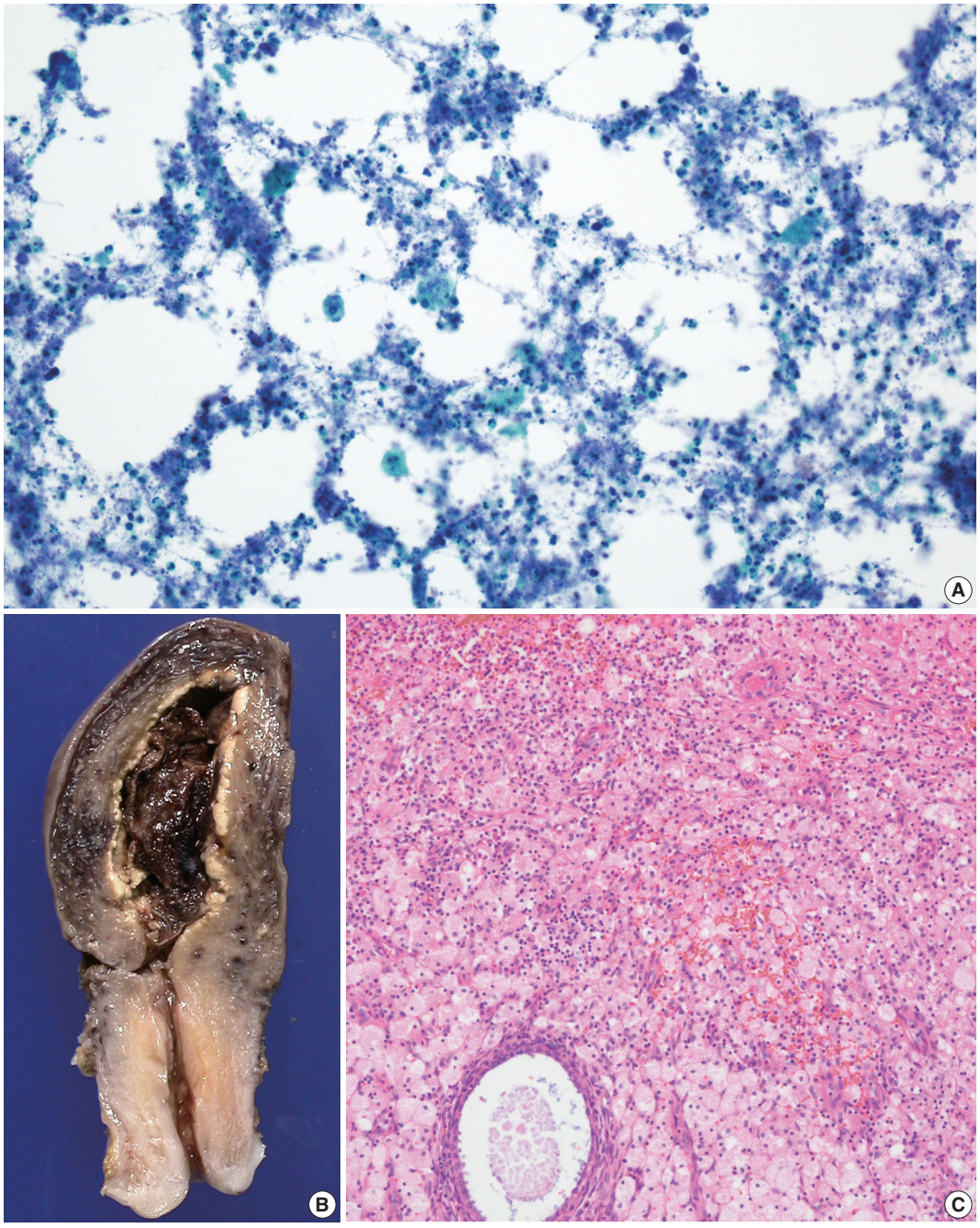

Fig. 1. (A) Aspiration cytology of endometrium showing many neutrophils with scattered foamy histiocytes. (B) Gross examination of the uterus shows bright yellow endometrium. (C) Microscopic examination of the endometrium shows aggregation of foamy histiocytes admixed with lymphocytes, neutrophils, and plasma cells.

DISCUSSION

XGE occurs mostly in postmenopausal women and is frequently associated with hematometra or pyometra. It can also occur after radiotherapy-induced endometrial or cervical tumor necrosis [1]. Cervical stenosis is presumed to contribute to the retention of hemorrhage or necrotic tissue [2].

The characteristic histological finding of XGE is the replacement of the endometrium by thick sheets of lipid-laden foamy histiocytes, although other inflammatory cells can also be present. In both of our cases, cytologic evaluation revealed many neutrophils with scattered foamy histiocytes, as seen on the microscopic findings of curettage and surgical specimens. Bacteria may or may not be isolated, but when related to bacterial infection, the

https://doi.org/10.4132/jptm.2020.08.18

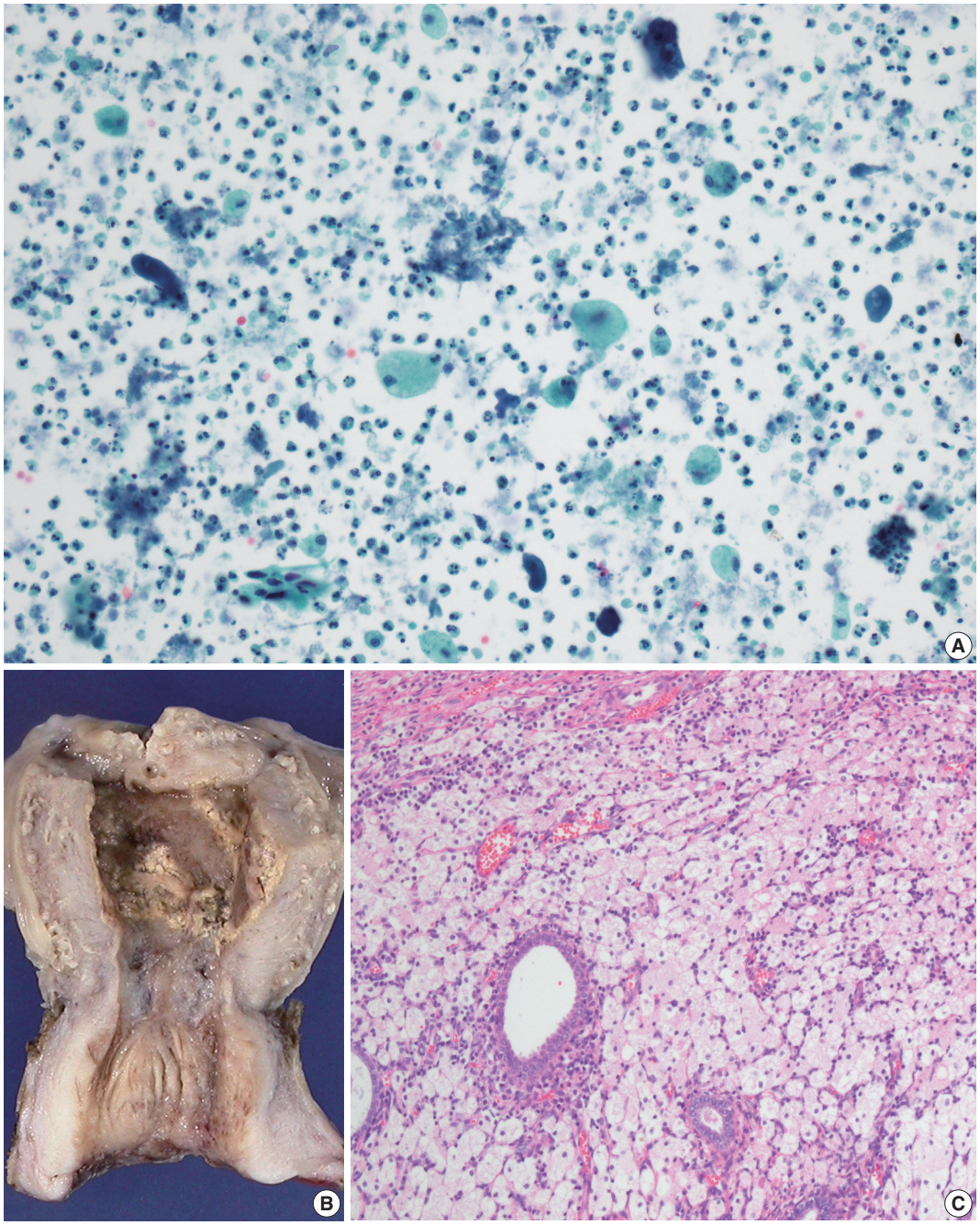

Fig. 2. (A) Endometrial washing cytology showing many neutrophils with scattered foamy histiocytes. (B) Gross examination of the uterus shows thickened and partly yellow endometrium. (C) Microscopic examination of the endometrium shows aggregation of foamy histiocytes and lymphocytes.

involved organisms include *Escherichia coli*, *Proteus vulgaris*, *Peptostreptococcus magnus*, or *Enterococcus* spp. [3,4].

While cases of XGE might resolve spontaneously or with antibiotic treatment, progression to peritonitis or sepsis can lead to a poor prognosis. Systemic inflammation originating from endometritis resulted in septic shock in our 78-year-old patient. Noack et al. [4] reported a case of XGE that led to a fatal outcome because of transmural extension of inflammation.

Differential diagnoses of XGE include malakoplakia, also a rare entity of the female reproductive tract. The absence of pathognomonic Michaelis-Gutmann bodies can exclude a diagnosis of malakoplakia [5]. On radiologic imaging, XGE can mimic malignant neoplasia of the endometrium, with findings such as endometrial thickening or mass formation [6]. However, the pres-

ence of XGE does not exclude the possibility of co-existing malignancies [7]; therefore, extensive sectioning and thorough microscopic examination of the whole endometrium is recommended.

In conclusion, XGE is a rare but clinically important entity because of its capacity to mimic endometrial malignancy. Cytological evaluation can be useful in cases with unclear clinical presentations. XGE can be diagnosed in the absence of cells that are definite or suspicious for malignancy and in the presence of lipid-laden histiocytes and inflammatory cells such as neutrophils.

Ethics Statement

This study was approved by the Institutional Review Board of Gyeongsang National University Hospital and waived the need for informed consent (IRB No. GNUH 2020-06-001).

ORCID

Ji Min Na https://orcid.org/0000-0003-4330-6598
Min Hye Kim https://orcid.org/0000-0002-8631-5104
Gyung-Hyuck Ko https://orcid.org/0000-0002-6721-1828
Jeong Kyu Shin https://orcid.org/0000-0001-9050-0874

Author Contributions

Conceptualization: MHK, GHK. Data curation: JMN, GHK. Investigation: GHK, JKS. Resources: GHK, JKS. Supervision: GHK. Visualization: JMN, GHK. Writing—original draft: JMN, GHK. Writing—review & editing: MHK, GHK.

Conflicts of Interest

The authors declare that they have no potential conflicts of interest to disclose.

Funding Statement

No funding to declare.

References

1. Russack V, Lammers RJ. Xanthogranulomatous endometritis: report of six cases and a proposed mechanism of development. Arch Pathol Lab Med 1990; 114: 929-32.
2. Ladefoged C, Lorentzen M. Xanthogranulomatous inflammation of the female genital tract. Histopathology 1988; 13: 541-51.
3. Barua R, Kirkland JA, Petrucco OM. Xanthogranulomatous endometritis: case report. Pathology 1978; 10: 161-4.
4. Noack F, Briese J, Stellmacher F, Hornung D, Horny HP. Lethal outcome in xanthogranulomatous endometritis. APMIS 2006; 114: 386-8.
5. Pounder DJ, Iyer PV. Xanthogranulomatous endometritis associated with endometrial carcinoma. Arch Pathol Lab Med 1985; 109: 73-5.
6. Dogan-Ekici AI, Usubutun A, Kucukali T, Ayhan A. Xanthogranulomatous endometritis: a challenging imitator of endometrial carcinoma. Infect Dis Obstet Gynecol 2007; 2007: 34763.
7. Gupta P, Dhingra KK, Roy S, Khurana N, Azad M. Xanthogranulomatous endometritis coexisting with carcinoma cervix. ANZ J Surg 2009; 79: 498-9.
8. Makkar M, Gill M, Singh D. Xanthogranulomatous endometritis: an unusual pathological entity mimicking endometrial carcinoma. Ann Med Health Sci Res 2013; 3(Suppl 1): S48-9.
9. Malik CA, Dudani S, Mani BN. Xanthogranulomatous endometritis presenting as pyometra and mimicking carcinoma on imaging. J Midlife Health 2016; 7: 88-90.
10. Du XZ, Lu M, Safneck J, Baker P, Dean E, Mottola J. Xanthogranulomatous endometritis mimicking endometrial carcinoma: A case report and review of literature. Radiol Case Rep 2019; 14: 121-5.


JPTM
Journal of Pathology and
Translational Medicine